THE PHOTOLYSIS AND RADIOLYSIS OF BARIUM AZIDE, WITH SOME OBSERVATIONS ON THE PHOTOLYSIS AND RADIOLYSIS OF LITHIUM AZIDE.

by

W.G.SEARS B.Sc.(Hons),(Cape Town)

A thesis submitted to the University of Cape Town in fulfilment of the requirements for the Degree of Doctor of Philosophy.

Department of Chemistry,
University of Cape Town,
Rondebosch, Cape,
South Africa.

APRIL 1972.

CONTENTS

relative positions of the potential energy curves, for the ground and excited states. If the respective curves intersect and the excited state has a minimum lying inside the ground state curve, then on optical transition to the excited state will be followed by a radiationless transition to the point where the excited and ground state curves intersect. If, however, the minimum in the potential energy curve lies outside the potential energy of the ground state, an electron could remain in the excited state until a radiationless transition occurs. This would then correspond to a metastable state.

Taking into consideration that an exciton is able to move with the speed of a thermal electron, it will interact with the vibrational modes of the lattice. This results in considerable scattering and loss of kinetic energy. The life time of an exciton is usually less than 10^{-8} seconds, provided that it is not trapped in some metastable state. Seitz[2] believes that mobile excitons may also transfer their energy to imperfections, since at least 10^{7} ions are passed over in 10^{-8} seconds.

Although thermal dissipation to the lattice is the main way in which energy absorbed during optical excitation of a crystal is utilised, an electron can only revert to the ground state by re-emission of radiation if the potential energy curves for the ground and excited state do not overlap. The emitted radiation must necessarily be of longer wavelength than the absorbed radiation owing to some thermal dissipation to the lattice in the excited state.

The emitted radiation is classified as fluorescence if it is emitted during irradiation, and phosphorescence if emitted after irradiation. Phosphorescence of longer duration than 10^{-4} sec. can only occur if the excited electron is transferred to a metastable state, from which a direct transition to the ground state cannot occur. For most phosphors, the characteristic property of luminescence depends on impurities called activators, usually present in very small amounts. X-rays, electrons and

positive ions have also been effective in producing luminescence, although optical means are by far the most common method, and the region of wavelength within which a particular phosphor can be excited optically, usually consists of a series of broad bands, which can depend on the presence of the activation.

When ionic solids, in particular the alkali halides are exposed to ultraviolet light, electron bombardment or X-radiation, they exhibit a colouration characteristic of the salt. This colouration will fade gradually with time, heating the substance accelerating the bleaching process.

Pohl[3] showed that this colouration was owing to a bell-shaped absorption band at about 400-800 mu, and he called the centres responsible for absorption, F-centres. De Boer's[4] suggestion that the F-centres are electrons trapped at vacant anion sites, has found general acceptance, the anion vacancy being considered as an effective unit positive charge. This model of the F-centres is supported by the production of paramagnetism, indicating unpaired electrons in the lattice. Spin resonance absorption lines in coloured alkali halides seem to confirm this. Since F-centres represent trapped electrons excited from the full band, their formation must be accompanied by positive hole formation in the full band. In an analogous manner, it is to be expected that these positive holes could be trapped by vacant cation sites, giving rise to a different type of absorbing centre. Mollwo[5] has demonstrated the presence of a series of absorption bands, called V-bands, associated with the interaction of positive holes with cation vacancies. Those same bands have been observed in X-irradiated KCl and NaCl crystals at low temperatures.

Crystals containing F-centres display photoconductivity when irradiated with light of wavelength within the F-band, suggesting that the excited state is sufficiently close to the conduction band for electrons to be

ionised thermally. These free electrons then wander through the crystal until retrapped. The effective distance travelled by electrons before retrapping occurs, has been found in KCl at -100°C to be inversely proportional to the F-centre concentration, indicating that the trapping centres are themselves F-centres. This indicates that an anion vacancy is able to trap two electrons.

This is confirmed by optical measurements, which show that during irradiation in the F-band the band is bleached and at low temperatures, in additively coloured salts (e.g. heating of ionic solids in presence of the vapour of its electropositive constituent) a broad band called the F^1-band appears on the long wavelength side of the F-band. If the crystal is now irradiated in the F^1-band, the F-band is regenerated, the quantum yield being 2, i.e. each quantum liberates an electron from an F-centre, and on combining with an anion vacancy, forms a second F-centre, according to the equations :

$$F^1 \xrightarrow{h\nu} F + e^-$$

$$e^- + \square \longrightarrow F$$

where $\square$ denotes a vacant anion site.

Perturbations caused to the first excited anion levels (exciton levels) by a neighbouring anion vacancy, lead to exciton levels somewhat lower than the normal exciton levels, and a new absorption band, called the α-band appears superimposed on the normal lattice absorption edge.

When anion vacancies form F-centres in irradiated alkali halides the perturbation effect of vacancies on adjacent exciton levels is reduced, and so a new band, the β-band, occurs between the α-band and the main lattice exciton band.

Thus irradiations in the F-band bleach F-centres, producing anion vacancies and F^1-centres. Perturbations on ions adjacent to these bleached F-centres (i.e. anion vacancies) are now enhanced and exciton formation occurs in the α-band instead of the β-band. Absorption within the

α-band is accompanied by fluorescence, indicating that the exciton formed is trapped by the anion vacancy and the resulting complex does not dissociate into an F-centre and a free positive hole.

Irradiation with light and X-rays within the F-band at room temperatures, produces a different series of bands on the long wavelength side of the F-bands. These have been called R_1, R_2, M and N bands. The M-centre is formed by the association of an F-centre with an anion-cation vacancy pair. During irradiation in the F-band, anion vacancies and free electrons are produced. If an M-centre now captures a second electron, it will become unstable and decompose into a R_2-centre (F-centre pair) and a cation vacancy.

Anion vacancies, M-centres or a vacancy pair may trap one of the electrons of an R_2-centre by the tunnel effect, producing an R_1-centre consisting of an F-centre associated with an anion vacancy. The above bands occur in KCl irradiated at room temperatures. When KCl is irradiated within the F-band at even higher temperatures (100°C) a broad band called the R^1-band appears on the long wavelength side of the F-band. This band is not resolved on cooling to 78°K, so that it must be made up of a large number of components. Increased vacancy mobility at 100°C result in electrons combining with groups of vacancies, including R_1, R_2 and M-centres. R-centre formation from F-centres increases with temperatures up to about 500°C, whereupon dissociation of R^1-centres to F-centres occurs.

Alkali halides irradiated within the F-band also show some bleaching of the V-bands. When crystals are X-irradiated at liquid air temperatures, the most prominent band produced is the V_1- band. Warming of the crystal causes a disappearance of the V_1-band and the F-band is markedly diminished. This bleaching results in photoconductance and luminescence, supporting the model of a positive hole trapped by a cation vacancy for the V_1-centre.

photolysis of silver bromide, postulates that the absorption of energy occurs principally within the volume elements of the sub-structure of the silver bromide crystal and that it results in the formation of either:

(a) excitons or

(b) pairs of electrons and positive holes.

Although the energy is absorbed within the volume elements of the sub-structure, the consequent photo-chemical changes are produced by secondary processes on their surfaces.

If the excitons interact with phonons and dissociate, then alternative (b) would apply. When excitons are formed, it is assumed that they can transfer their energy at room temperature to bromide ions occupying:

(i) kink sites on the free surfaces of the crystal.

(ii) jogs along edge dislocation lines on kink sites associated with internal surfaces, to eject electrons from them.

In both cases a bromine atom would be formed and an adjacent silver ion would then represent a localised excess positive charge with which the electron might ultimately, on account of its small range, combine to produce a silver atom.

By applying the Franck-Condon principle to the process, it may be deduced that electrons are unlikely to be trapped immediately by bromine atoms or silver ions which are absorbed at the surfaces, so that an interval will be available, during which the silver ion can diffuse away from the bromine atom, most probably into and along an adjacent sub-boundary. It may then combine with the electron to form a silver atom.

If bromide ions associated with jogs along the dislocation lines of internal surfaces interact with excitons, the same discussion will apply. The process can, however, not lead to the separation of a silver atom unless the bromine atom can diffuse to the surface and

escape, without combining with a previously separated silver atom.

Precisely the same changes would result if electrons and positive holes were created directly by the absorption of energy in the crystal and the holes were trapped before the electrons, by bromide ions on the free surface or on internal surfaces. Atoms of bromine would again be produced, together with excess silver ions which would combine with the electrons.

Thus the following possibilities might exist when silver halides are U.V. irradiated.

1. Production of excitons

2. Liberation of pairs of electrons and positive holes.

The excitons represent excited states of the crystal in which electrons are bound in the electrostatic field associated with positive holes. They should therefore be mobile and able either

(i) to decay, transferring their energy to lattice vibrations,

(ii) to interact with phonons and dissociate into a free electron and positive hole, or

(iii) to interact with atoms, ions or molecules on the bounding surfaces of the volume elements of the substructure of the silver halide crystal and so produce photochemical changes.

With (ii) it is virtually impossible to distinguish experimentally between excitation and ionization.

With (iii) photochemical changes might result from excitation processes, followed by rearrangements or from ionization processes.

In the latter case it seems likely that electrons alone would be liberated, the compensating positive charge remaining as an ionic charge on the surface. Photoconductivity studies should then reveal the absence of any photocurrent which could be attributed to positive holes.

The kinetics of gas evolution from anhydrous silver perchlorate using the low pressure mercury arc, has been studied by Verneker and Maycock[19]. Depending on the age of the sample, an initial accelerating rate or decelerating period is followed by a constant rate period. The rate of evolution of O_2 during photolysis was found to be directly proportional to the intensity. Doping experiments to produce increased concentration of anion vacancies lead to enhancement of the maximum rate with respect to an undoped sample. For the initial accelerating period, the following mechanism was postulated.

$$ClO_4^- + \boxminus \xrightarrow{h\nu} ClO_4^{\cdot} + e \quad \ldots\ldots\ldots 1$$

$$ClO_4^{\cdot} \longrightarrow \text{products} + \boxminus \quad \ldots\ldots\ldots 2$$

$$Ag^+ + e \longrightarrow Ag^{\circ} + \boxminus \quad \ldots\ldots\ldots 3$$

For the decelerating region, a mechanism involving consumable trapping centres was postulated, and from the doping experiments it appeared that the trapping centres were anion vacancies. Since the rate did not proceed to zero, after prolonged irradiation, a new mechanism must have come into operation, which did not involve consumable trapping centres. The new mechanism presumably continues to operate until the crystal is consumed, the rate of gas evolution being proportional to the first power of the intensity. The activation energy was found to be about 4.5 KCals/mole.

Presumably silver metal formed as a result of the tepetition of reactions (1) and (3) acts as a reaction initiation by photo-emitting an electron

$$Ag^{\circ}_M \xrightarrow{h\nu} Ag^{+}_M + \bar{e} \quad \ldots\ldots\ldots 4$$

$$Ag^+ + ClO_4^- \longrightarrow Ag^{\circ}_M + ClO_4^{\cdot} \quad \ldots\ldots\ldots 5$$

$$ClO_4^{\cdot} \longrightarrow \text{products} \quad \ldots\ldots\ldots 6$$

$$Ag^{\circ}_M + Ag^+ + \bar{e} \longrightarrow Ag^{\circ}_{M+1} \quad \ldots\ldots\ldots 7$$

where Ag°_{M+1} represents the growth of colloid metal.

A possible reaction sequence could be as follows:

$$BrO_3^- \overset{h\upsilon}{\rightleftharpoons} BrO_3^{-*}$$

$$BrO_3^{-*} \overset{h\upsilon}{\rightleftharpoons} BrO_3^{-**}$$

or

$$BrO_3^{-*} + BrO_3^{-*} \rightleftharpoons BrO_3^{-**} + BrO_3^-$$

Once the doubly excited state is formed, it may generate a singly excited state,

$$BrO_3^{-**} + BrO_3^- \longrightarrow 2\,BrO_3^{-*}$$

or the doubly excited state may produce decomposition, e.g.

$$BrO_3^{-**} \longrightarrow BrO^- + O_2.$$

The generation of new decomposition sites from existing sites being similar to the process observed in the alkali halides for the generation of vacancies from centres that resume their initial characteristics after each additional vacancy is formed.

Photochemical Decomposition of Azides:

The simplest photolytic mechanism proposed for the azides (Gray [100]) has as its initial step exciton formation.

$$N_3^- \overset{h\upsilon}{\rightleftharpoons} N_3^{-*}$$

The exciton then decomposes thermally into an electron in the conduction band, leaving a positive hole (azide radical)

$$N_3^{-*} \longrightarrow \bar{e} + N_3$$

Two azide radicals may react at the surface, to form nitrogen gas, azide radicals formed internally, appearing at the surface by an electron transfer mechanism.

$$2\,N_3 \longrightarrow 3\,N_2$$

Metal is then formed by a mechanism suggested by Mitchell [15]

$$M_n + M^+ + \bar{e} \longrightarrow M_{n+1}$$

For barium azide, different but related mechanisms have been put forward [28,29,30,31,32]. According to these early mechanisms,

OBJECT OF THIS RESEARCH.

A detailed review of the work done on the photolysis of azides revealed that much confusion existed regarding the experimental evidence and postulated mechanisms. This state of affairs prompted a more detailed re-investigation into the photolysis of barium azide, working in a vacuum of 10^{-6} to 10^{-7} torr, with the employment of sensitive measuring devices such as ionization guages and a recently improved design of Pirani guage, capable of accurate measurement right down to 10^{-4} torr.

In particular, much attention has been given to the construction of the photolysis cell, so as not to include the use of greased joints and cements for attaching the quartz windows. Much evidence has been gathered in this work to show that these substances lead to significant gas evolution during the photolysis reaction.

The photolysis of lithium azide was also undertaken because this has not been reported previously and it was felt that such a study would be helpful in the formulation of reaction mechanisms for the photolysis of the ionic azides.

A detailed study of the X-radiolysis of lithium and barium azide was then undertaken, with the possibility of relating this to the photolytic mechanisms of the inorganic azides.

FIG. 1. VERY HIGH VACUUM LINE.

KEY : -

A. Liquid N_2 cold traps.

B. Mercury diffusion pumps.

C. McCloed gauge.

D. Backing reservoir .

E. Low pressure vacuum reservoir.

F. Liquid refrigerant storage dewar.

G. Ionization gauge head.

H. Pirani gauge head.

I. Extraction fan.

J. N_2 delivery tube.

K. Quartz photolysis cell.

L. N_2 vapour outlet.

M. Thermostating fluid (propanol or ethanol).

N. Stirrer.

O. Thermal insulation.

P. Bath. heater.

Q. U.V. arc.

R. Copper cooling coil.

were used for high intensity irradiation. These emitted a continuous spectrum with principal lines superimposed.

The X-ray generator employed for radiolysis was the Philips model PN 1009, employing tubes with copper and tungsten targets.

2.3. Photomicrography.

A Leitz microscope and heating stage (vacuum type) was used to follow some of the stages in the photolysis and radiolysis of barium azide. Photomicrographs were obtained, using a Leitz film holder and transport mechanism, coupled to the microscope with a Leitz micro-attachment with a central shutter. Magnifications of 65X and 110X were possible.

When photomicrographs had to be made, the vacuum-type hotstage was used as the decomposition cell, enabling every stage of a decomposition to be followed at temperatures right down to -20°C.

2.4. Grinding.

The azide material was powdered when desired, using a Wig-L-Bug grinding mill. Pellets of the azide were made using evacuable KBr dies (14 mm for radiolysis and 5 mm for photolysis) and a ten ton Apex type 341/4 hydraulic press was used to pellet the ground material.

2.5. Temperature Control.

Temperature control was achieved by designing and constructing a thermostat bath working over a very large temperature range (200 to -120°C). This is shown diagrammatically in Figure 2.

In the high temperature range 200 to -20°C a contact thermometer type Jumo MSD BP 568 was used as the sensing device while in the low temperature range -20 to -120°C a platinum resistance thermometer was coupled to a Wheatstone bridge device.

FIG. 2.

Key : -

a. Thermistor.

b. Liquid N_2 level sensor.

c. Contact Therm. (closed) for thermostat bath.

d. Sunvic master relay (de-energised).

e. L.T. transformer (de-energised).

f. Diode rectifier.

g. Solenoid ball valve.

h. Dewar heater.

i. Slave relay (de-energised).

j. Bleed heater.

k. L.T. transformer (permanently energised).

Operating Principle in the High Temperature Range.

The appropriate contact thermometer for the desired temperature range is set to the required temperature and immersed in the cooling fluid (iso-propanol, water or ethanol depending on the temperature range) contained in the dewar. If the temperature in the bath is too high, the circuit from the contact thermometer is made and this de-energises the Sunvic master relay and thus the slave relay. Contacts A and B close feeding current to the storage dewar heater and to the solenoid ball valve. The bleed heater is switched off at the same time as contacts C open. Owing to vapourization of the liquid nitrogen and the fact that the bleed is now closed, a pressure build up in the storage dewar forces liquid nitrogen along the thermally insulated delivery tube leading to the copper coil immersed in the thermostat dewar. A stirrer provides mixing to eliminate temperature gradients within this dewar.

The thermostating fluid is now rapidly cooled and at the set temperature, the contact thermometer open circuits and the Sunvic master relay is energised, and this in turn energises the slave relay. Contacts A and B now open while contacts C close, switching off the storage dewar heater and opening the solenoid ball valve of the bleed. The bleed heater is switched on to defrost the bleed system.

As soon as the temperature rises again, the cycle repeats itself.

Operating Principle in the Low Temperature Range.

When the temperature in the thermostat bath is too high, the platinum resistance thermometer in circuit with the Wheatstone bridge causes the bridge to be unbalanced and the small relay used in conjunction with the bridge closes, de-energising the Sunvic control relay and this has the effect of causing liquid nitrogen to be forced through the copper cooling coil.

For temperatures above room temperature, the bleed heater circuit is plugged into a bath heater P, while the dewar heater F (Fig. 3) is unplugged. In this way the bath fluid can be heated to the desired point. When the temperature rises above the set temperature the contact thermometer contacts close and this de-energises the Sunvic master relay which in turn de-energises the slave relay. This causes bath heater P to be open circuited and the temperature no longer rises.

Using the above systems, temperature control within $0,2^{o}C$ could be obtained.

2.6. Liquid nitrogen cold traps.

Employing an identical set up described above, but using a thermistor as a sensing device, to drive a relay which operates the Sunvic master relay, and leading the refrigerant delivery tube into the cold traps on the vacuum line, liquid nitrogen refrigerant level in these cold traps could be maintained to within 3 mm of the thermistor tip.

2.7. Photoconductivity.

Photoconductivity measurements were made using the circuit shown in Figure 4 in conjunction with the Vibron electrometer model 33 C.

2.8. Special Procedures.

A dry box shown in Figure 5 was used to transfer irradiated samples to evacuated dessicators to prevent atmospheric contamination of the radiation products.

FIG. 3. LIQUID REFRIGERANT STORAGE DEWAR.

KEY : -

A. Solenoid valve.

B. Bleed.

C. Bleed heater.

D. Delivery tube for liquid N_2.

E. Thermal insulation.

F. Dewar heater.

G. Filler.

H. Large reservoir dewar.

I. Liquid N_2.

FIG. 5. DRY BOX.

KEY : -

A. Flushing point inlet (dry nitrogen) and evacuating point for desicators.

B. Rubber gloves.

C. Flushing point outlet.

D. Outer door.

E. Double door entry chamber.

F. Flushing point and bleed.

G. Inner door.

H. Window.

I. Red light for illumination.

J. Removable hatch.

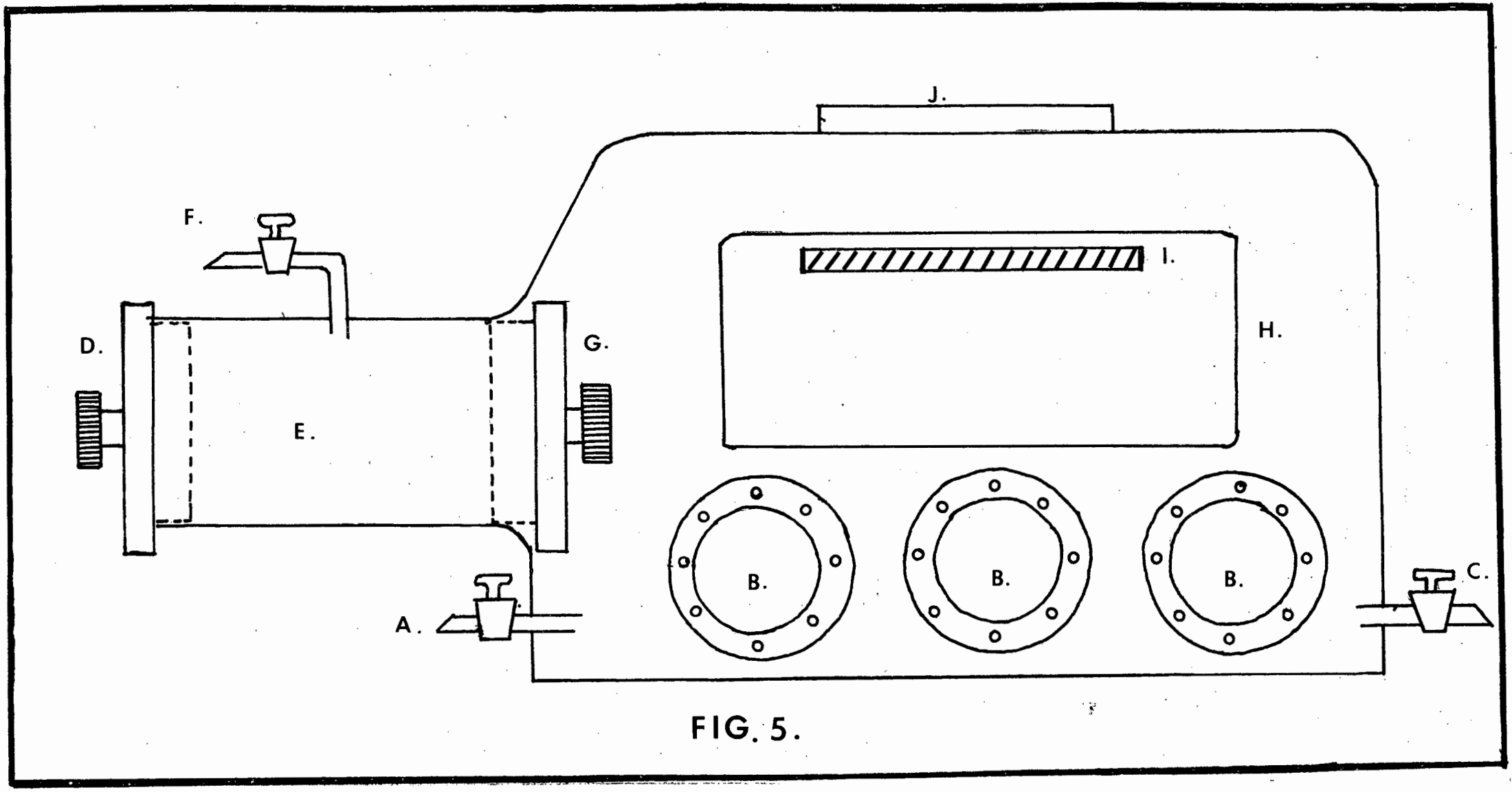

FIG. 5.

3. Preparation of Barium Azide Monohydrate and the Anhydrous form.

3.1. Preparation of the Monohydrate.

Pure barium azide (Light and Co.) with 15% alcohol added for safe handling and transporting, was dissolved in conductivity water (specific conductance of $2,0 \times 10^{-6}$ ohms^{-1} cms^{-1} at 20°C) at a temperature of 70°C. 3% hydrazoic acid solution was added to keep the solution acid in order to prevent hydrolysis of the barium azide to barium hydroxide.

Pure barium azide monohydrate was recrystallised from this acid solution and dried in a vacuum dessicator over P_2O_5. This removes water to produce an anhydrous powder.

3.2. Preparation of Anhydrous Barium Azide crystals.

Utilising the phase diagram put forward by Torkar [16] for the system barium azide-water, it is possible to recrystallise pure anhydrous barium azide from an aqueous solution by maintaining the temperature above 75°C. This was verified crystallographically and the cell parameters were obtained from Weissenberg photographs. These are as follows :

$$a = 9,46\ A^{\circ} \quad b = 4,55\ A^{\circ} \quad c = 5,30\ A^{\circ}$$

They are in good agreement with those obtained by Walitzi and Krishner [64] in 1969.

3.3. Preparation of Hydrazoic Acid.

The hydrozoic acid was prepared by an ion-exchange method, using "Analar" cationic resin in the H^+ form. A 10% solution of sodium azide (B.D.H.) was passed through the bed of the resin. The resulting 3% solution of hydrazoic acid was found to contain no iron or sodium ions as impurities. This was verified by the use of "Ferron" reagent and flamephotometry. Infrared spectra of both preparations showed that no water of crystallization was present.

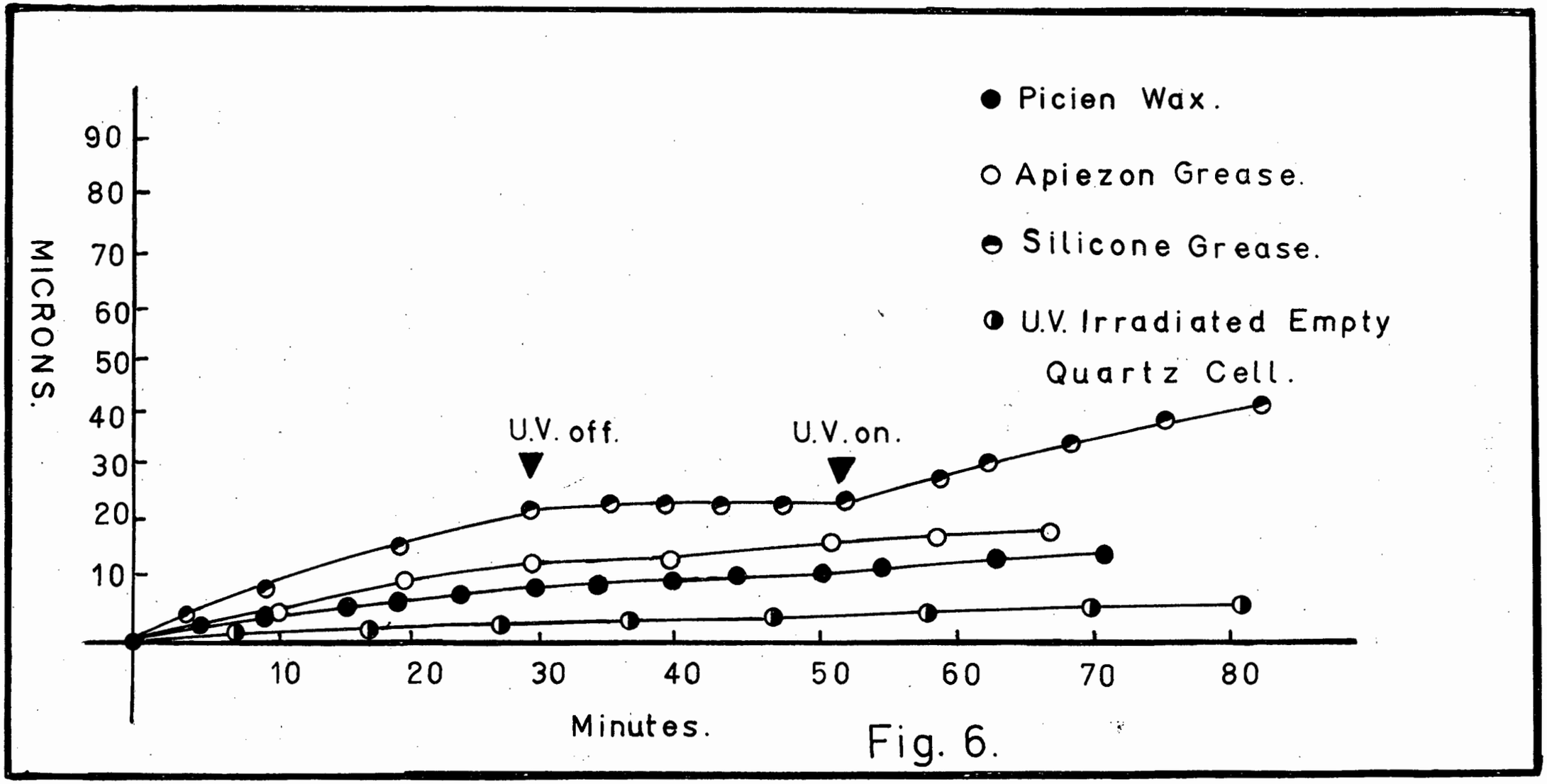
Picien Wax.
Apiezon Grease.
Silicone Grease.
U.V. Irradiated Empty Quartz Cell.
MICRONS.
90
80
70
60
50
40
30
20
10
U.V. off.
U.V. on.
10
20
30
40
50
60
70
80
Minutes.

Fig. 6.

PLATE I

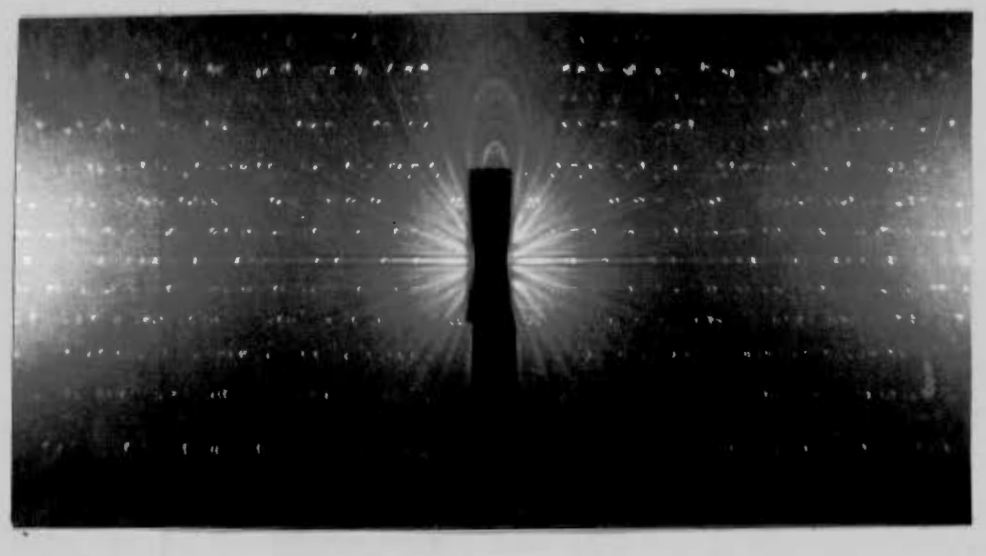

ROTATION - a AXIS -,

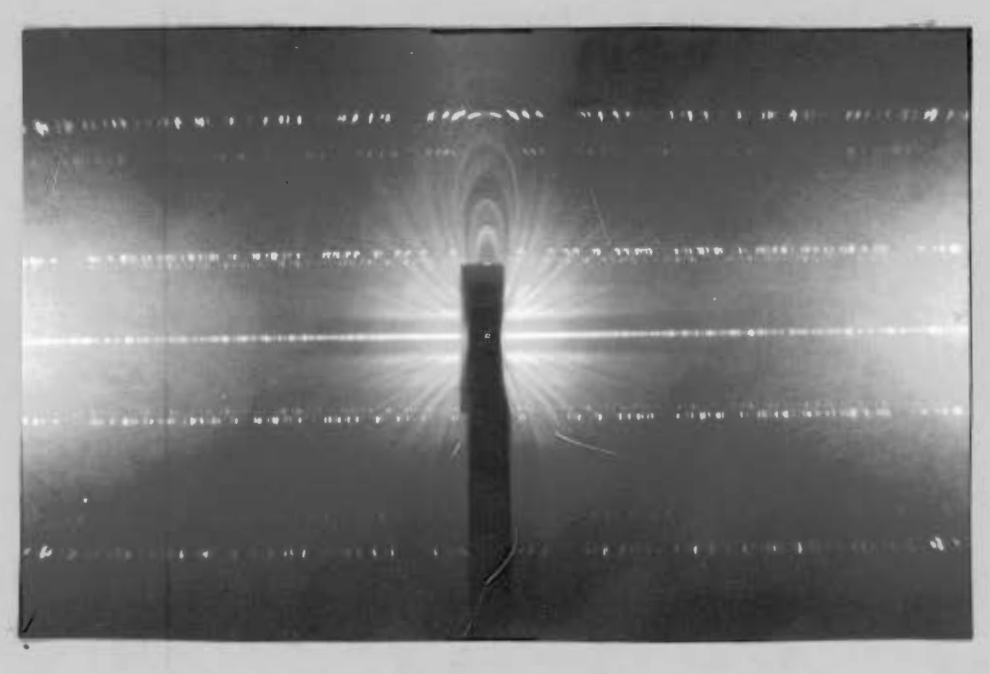

ROTATION - b AXIS -,

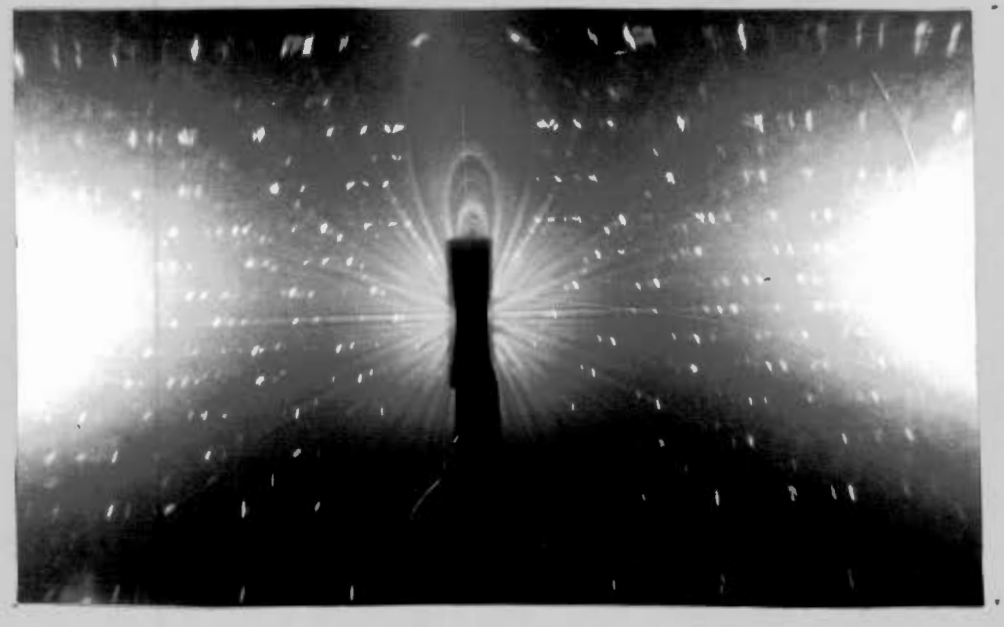

ROTATION - c AXIS -,

DOUBLE LAUE DIFFRACTION PHOTOGRAPH.

PLATE I (cont.)

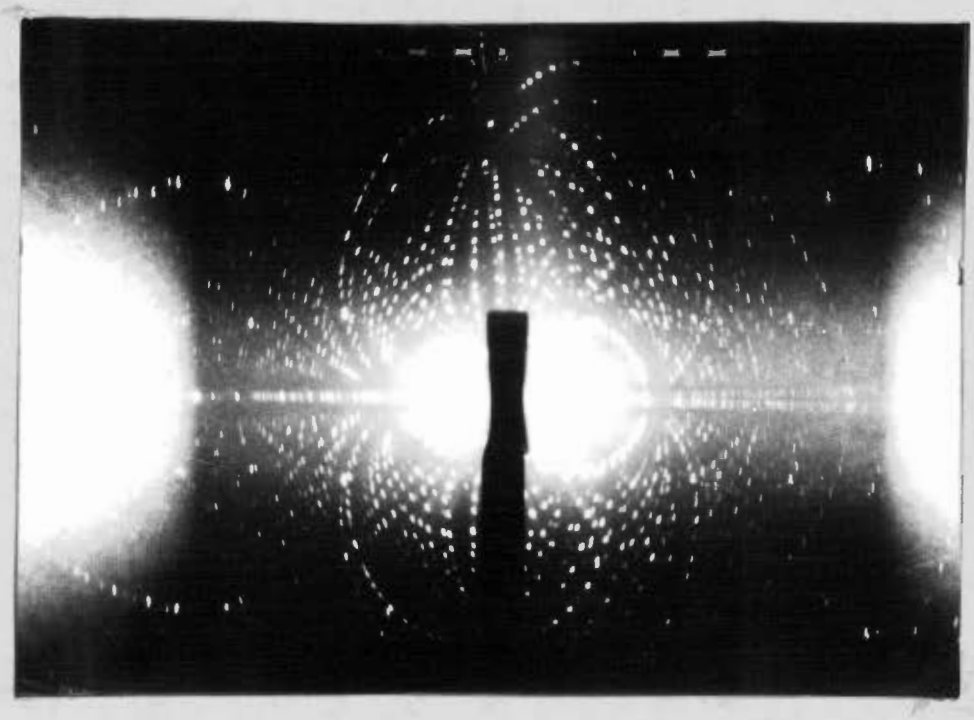

TABLE O.

Spot no.	x	y
1	0,18	0
2	0,34	0
3	0,50	0
4	0,67	0
5	0,83	0
6	1,00	0
7	1,16	0
8	1,48	0
9	1,63	0
10	1,75	0,27
11	1,58	0,28
12	1,43	0,29
13	1,27	0,29
14	1,11	0,29
15	1,05	0,29
16	0,94	0,29
17	0,78	0,29
18	0,72	0,29
19	0,62	0,30
20	0,56	0,30
21	0,46	0,30
22	0,40	0,30
23	0,29	0,30
24	0,23	0,30
25	0,10	0,30
26	0,00	0,30
27	-0,23	0,29
28	-0,40	0,28
29	-0,57	0,27
30	-0,72	0,27
31	-0,95	0,26
32	-1,05	0,25
33	-1,22	0,25
34	-1,38	0,24
35	-1,53	0,22
36	-1,69	0,20
37	-1,85	0,20
38	-1,74	0,50
39	-1,58	0,50
40	-1,43	0,51
41	-1,27	0,52
42	-1,10	0,53
43	-0,95	0,54
44	-0,78	0,55
45	-0,61	0,56
46	-0,45	0,57
47	-0,28	0,58
48	-0,11	0,59
49	0,06	0,58
50	0,23	0,59
51	0,40	0,58
52	0,56	0,58

PLATE I
(cont.)

WEISSENBERG - a AXIS -, (zero layer line)

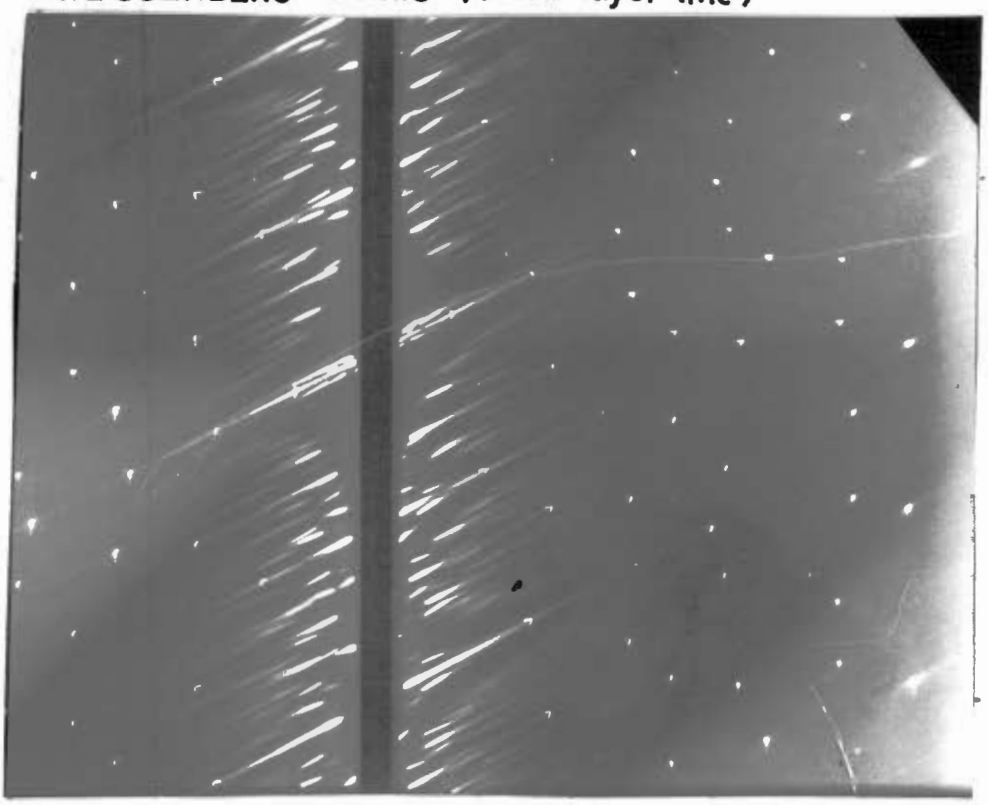

WEISSENBURG - b AXIS -, (z.l.l.)

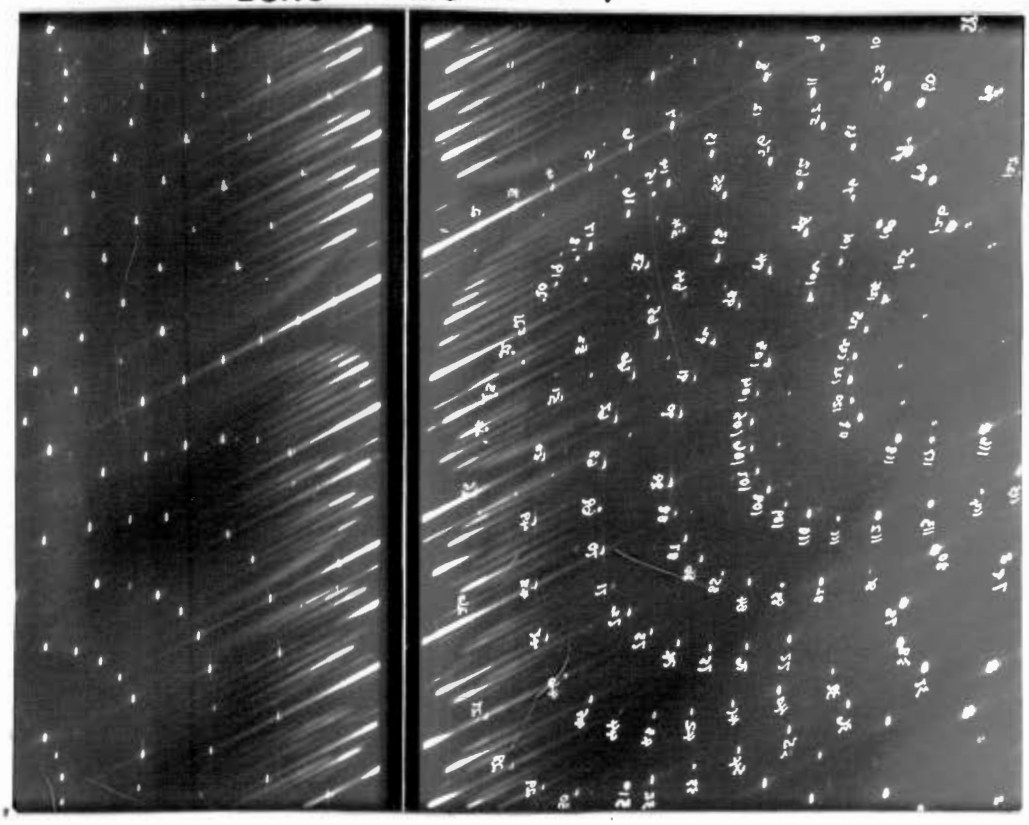

WEISSENBERG - c AXIS -, (z.l.l.)

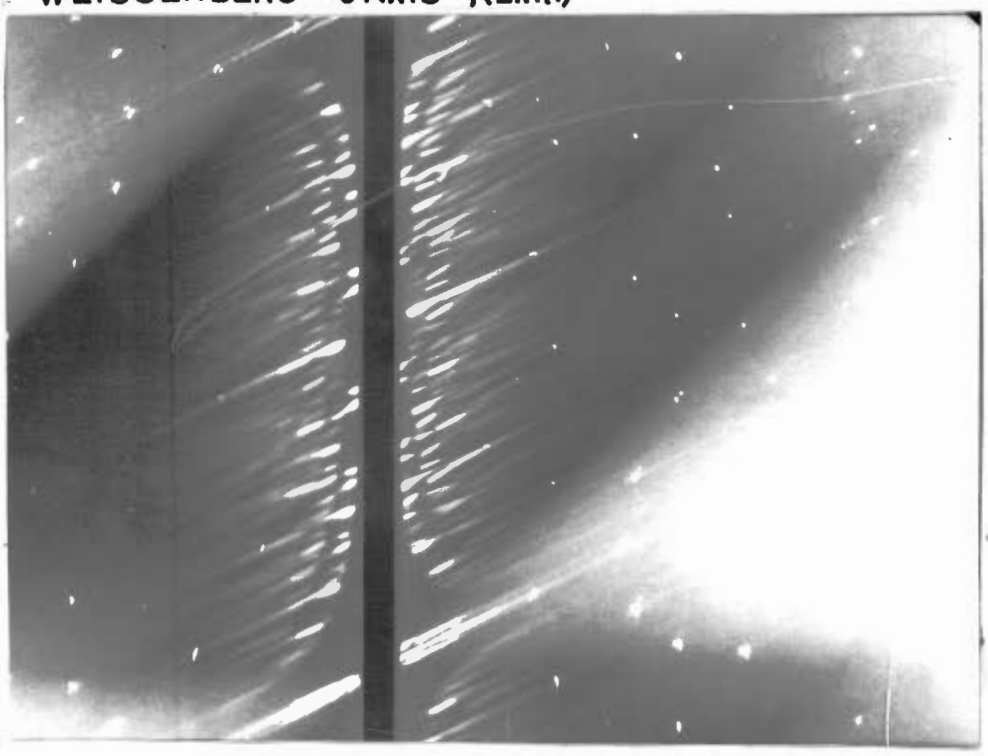

The angle β of the unit cell was calculated from the indexed Weissenberg (Zero layer line)

1. $99,5^{\circ}$
2. $97,0^{\circ}$
3. $98,0^{\circ}$
4. $98,5^{\circ}$
5. $99,0^{\circ}$
6. $96,0^{\circ}$
7. $100,0^{\circ}$
8. $100,0^{\circ}$
9. $99,5^{\circ}$
10. $100,0^{\circ}$

This yielded an average value of $98,75^{\circ}$ for β.

$a^* = 0,163$

Therefore, since $\lambda/a = a^*$

$$a = \lambda/a^*$$

where * refers to the reciprocal lattice parameter and λ= wavelength in Å,

and from this

$$a = 9,46 \text{ Å}$$

$$b = 4,55 \text{ Å}$$

$$c = 5,30 \text{ Å}$$

This agrees well with the values obtained by Walitzi and Krishner which are as follows:-

$$a = 9,63 \text{ Å}$$

$$b = 4,41 \text{ Å}$$

$$c = 5,43 \text{ Å}$$

with the value for $\beta = 99,5^{\circ}$.

Twelve photodecompositions of anhydrous crystals at 0°C showed the same characteristics as decompositions at 15°C. The use of a water filter, interposed between the cell and the U.V. arc produced no significant change in the shape of the pressure-time plots.

Fig. 8 shows the extent of irreproducibility obtained when crystals of anhydrous barium azide of fixed weight are used. Some curves deviated markedly from the basic type. For this reason only approximate activation could be obtained for this section. Fig. 9 shows a more typical pressure-time plot for the photolysis of a single anhydrous barium azide crystal.

An analysis of 12 curves yielded the following trends. The region AB showed a very slight decreasing of the initial rate for approximately 17 minutes. This was followed by an acceleratory period BCD lasting, on average, for 36 minutes. From D onwards, a decay commenced and lasted for periods greater than 600 minutes, punctuated throughout with linear rate regions. This type of curve is in fact sigmoid, without an induction period.

Activation energies, reflecting the critical increment for the photochemical processes involved in the photolysis of barium azide pellets, were obtained by applying the Arrhenius equation. The logarithm of rate (in any specified region of the decomposition curve) was plotted against 1/T, where T was the decomposition temperature in degrees absolute. The above plots were straight lines and the slopes were used to determine the activation energies by applying the Arrhenius equation. The error involved in these determinations was of the order of $\pm$ 200 cals.

Fig. 10 shows an activation energy plot obtained on the I.C.T. computer, with an average value of 2 k.cals/mole for eight runs, using the split run technique on each run, in the CDE region.

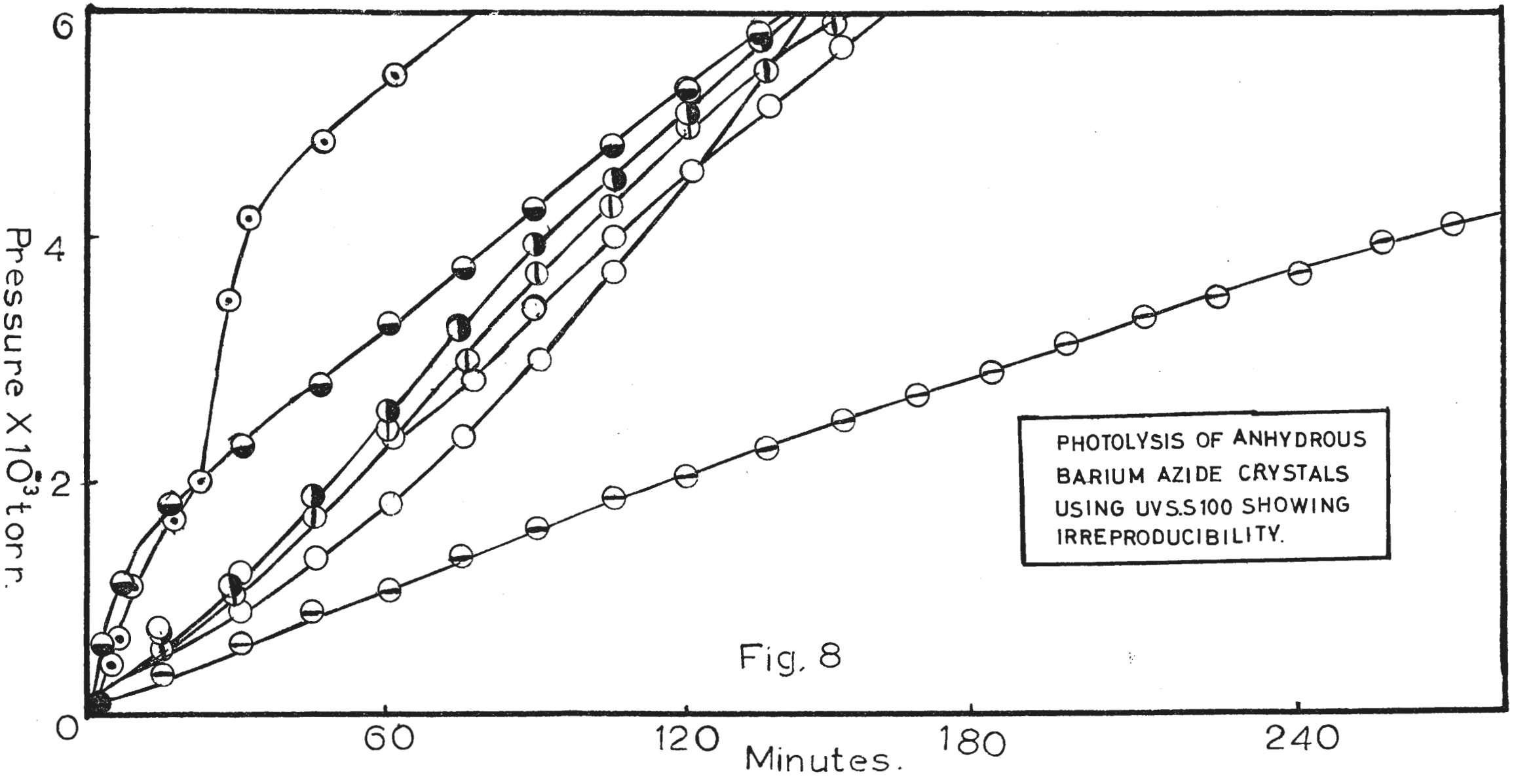
Pressure X 10^{-3} torr.
0
2
4
6
60
120
180
240
Minutes.
PHOTOLYSIS OF ANHYDROUS BARIUM AZIDE CRYSTALS USING UVS.S100 SHOWING IRREPRODUCIBILITY.

Fig. 8

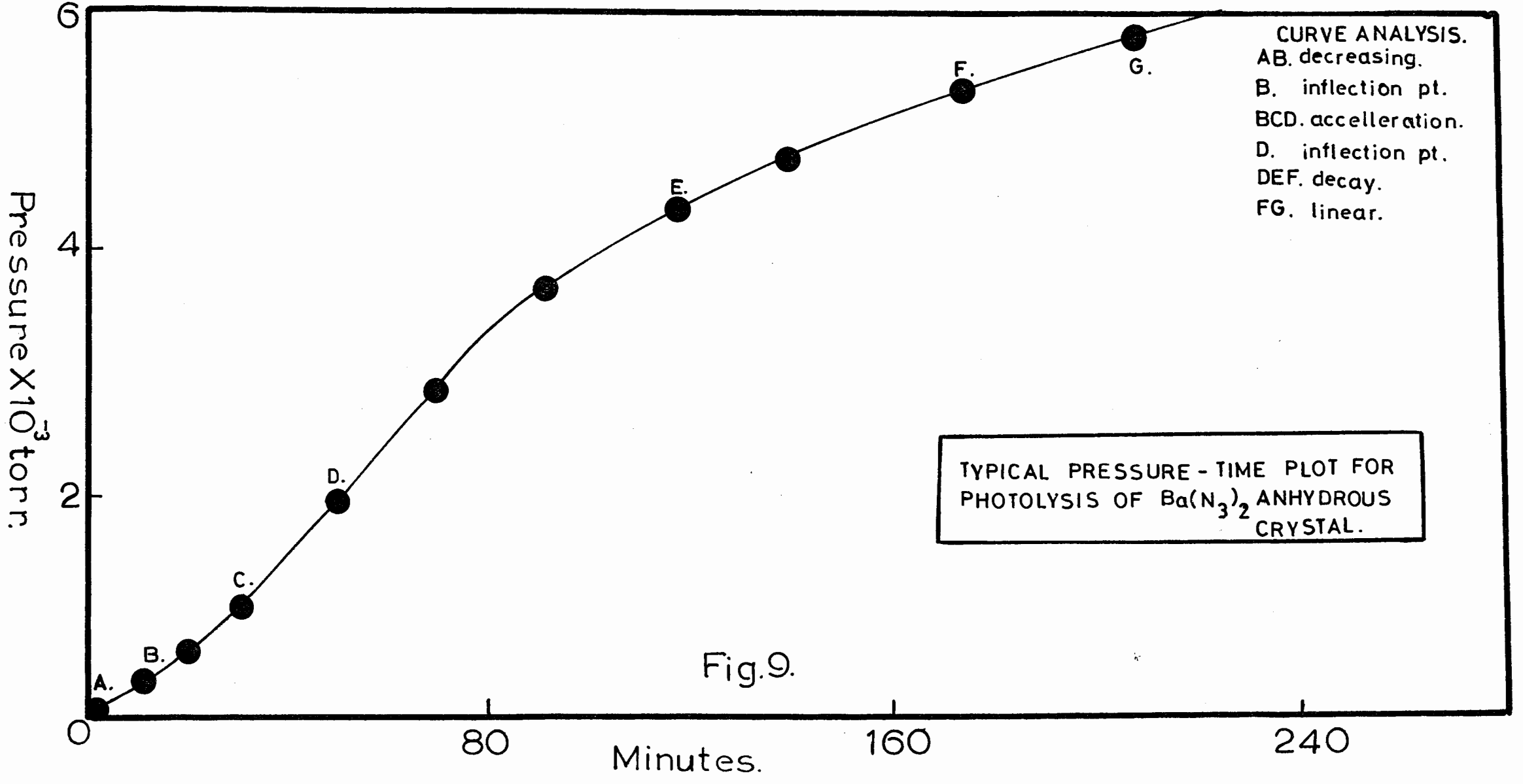
6
4
2
0
Pressure X 10^{-3} torr.
80
160
240
Minutes.
A.
B.
C.
D.
E.
F.
G.
CURVE ANALYSIS.
AB. decreasing.
B. inflection pt.
BCD. accelleration.
D. inflection pt.
DEF. decay.
FG. linear.
TYPICAL PRESSURE - TIME PLOT FOR PHOTOLYSIS OF $Ba(N_3)_2$ ANHYDROUS CRYSTAL.

Fig.9.

5.2. The photolysis of dehydrated barium azide monohydrate powder (ground 4 minutes).

8 mg. of powdered barium azide were weighed out in each case and transferred to the decomposition cell, which was carefully shaken to form a level surface of powder exposed to the ultraviolet arc (U.V.S. S100).

A 9 cm arc height and a temperature of 1°C were employed for the photolysis.

Although the basic curve shapes were similar (see fig. 11), large differences in photolytic rates and acceleratory periods were encountered. Since the weight of the powder was constant, as was the grinding time, these discrepancies can only be attributed to differences in surface area exposed to the ultraviolet arc.

Owing to the above difficulties, both in anhydrous crystals and in powder, it was decided to change to pelleted barium azide in order to eliminate large differences in surface area exposed to the U.V. radiation.

A weight for weight comparison of the photolysis of barium azide powder and pellets is shown in fig. 11a.

5.3. The photolysis of dehydrated barium azide monohydrate pellets.

IN THIS SECTION A GRINDING TIME OF 4 MINUTES WAS EMPLOYED UNLESS OTHERWISE STATED, AND THE 5 mm. 8 mg. PELLETS WERE PRESSED AT 2000 lbs/sq.inch UNLESS OTHERWISE STATED. ALL DECOMPOSITIONS WERE CARRIED OUT AT 1°C, EXCEPT WHERE ACTIVATION ENERGIES WERE DETERMINED, THE APPROPRIATE TEMPERATURES BEING CLEARLY INDICATED IN THE FIGURES AND TEXT. THE ULTRAVIOLET SOURCE (U.V.S.) EMPLOYED IN THIS SECTION WAS THE U.V.S. S100 125 Watt HANOVIA ARC.

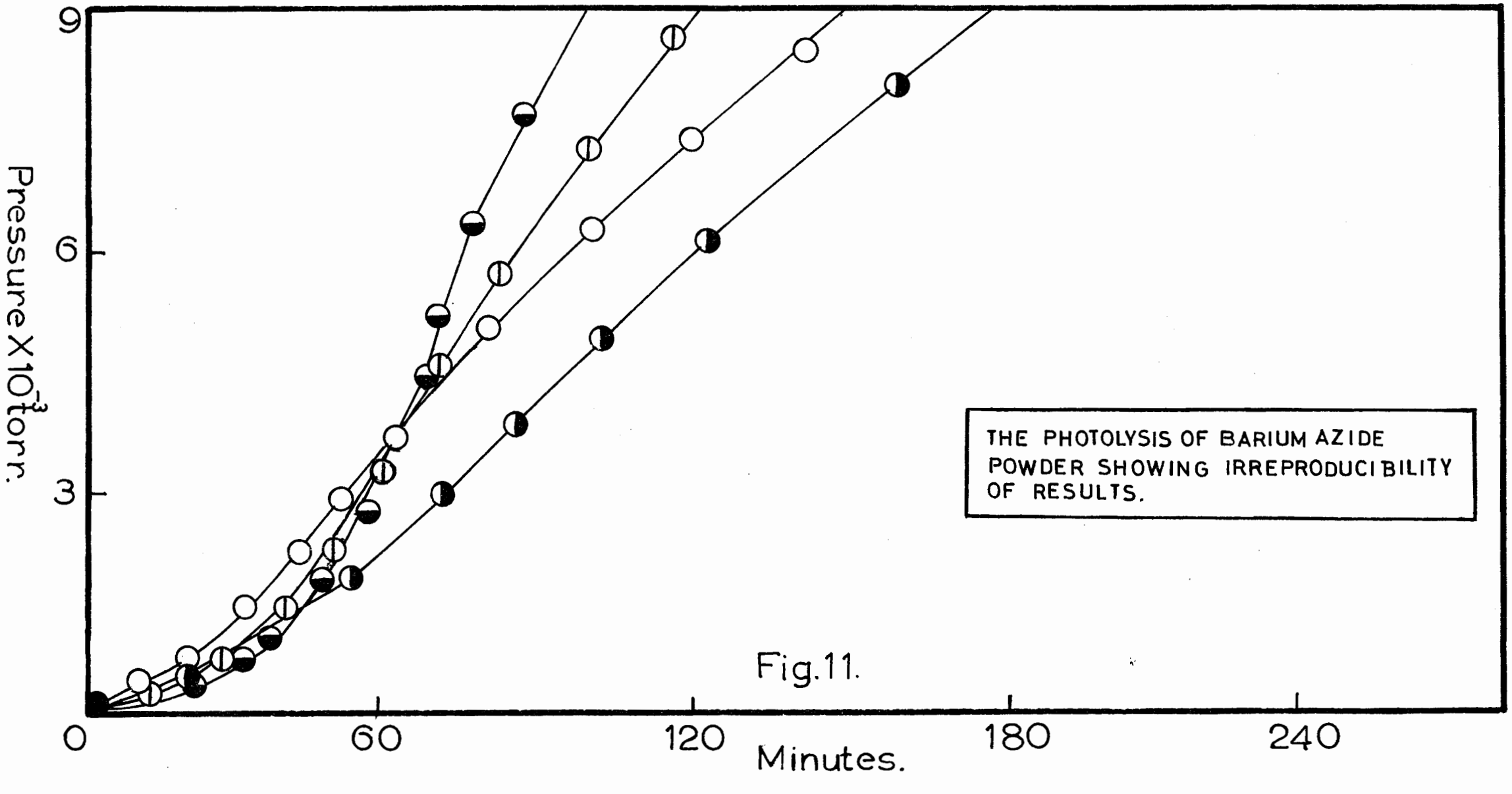
9
6
3
Pressure X 10^{-3} torr.
0
60
120
180
240
Minutes.
THE PHOTOLYSIS OF BARIUM AZIDE POWDER SHOWING IRREPRODUCIBILITY OF RESULTS.

Fig.11.

In order to obtain a high degree of reproducibility of the pressure-time plots, a standardised technique was employed in the following work and the effect of the following factors on the photolytic rates and shape of the pressure-time plots was investigated :

1. Evacuation time of the decomposition cell prior to photolysis.
2. Pelleting pressure.
3. Grinding time.
4. Water vapour.
5. Mercury vapour.
6. Ageing of sample.

IN THIS SECTION, UNLESS OTHERWISE INDICATED, BARIUM AZIDE PELLET WILL MEAN 5 mm DIAMETER 8 mg. PELLETS OF DEHYDRATED BARIUM AZIDE MONOHYDRATE GROUND FOR 4 MINUTES AND PELLETED AT 2000 lbs./sq.inch.

5.3.1. The prolonged photolysis of barium azide pellets.

In order to obtain the general characteristics of the pressure-time plot for the photolysis, pellets of barium azide as described above, were irradiated with the U.V. arc for periods in excess of 20 hrs.

Fig. 12 shows the resultant pressure-time plot. A total of five decompositions revealed the same general characteristics. After an initial acceleratory phase lasting on the average 30 minutes, a gradual deceleration occurred. The rate did not, however, proceed to zero, even after 20 hrs. irradiation.

5.3.2. The effect of the evacuation time on the photolysis of barium azide pellets.

For the sake of reproducibility of results, the outgassing rate of the photolysis cell after various evacuation times was investigated and its influence on the subsequent photolysis of barium azide pellets was studied.

A comparison between photolytic rates after 2-4 hrs. and

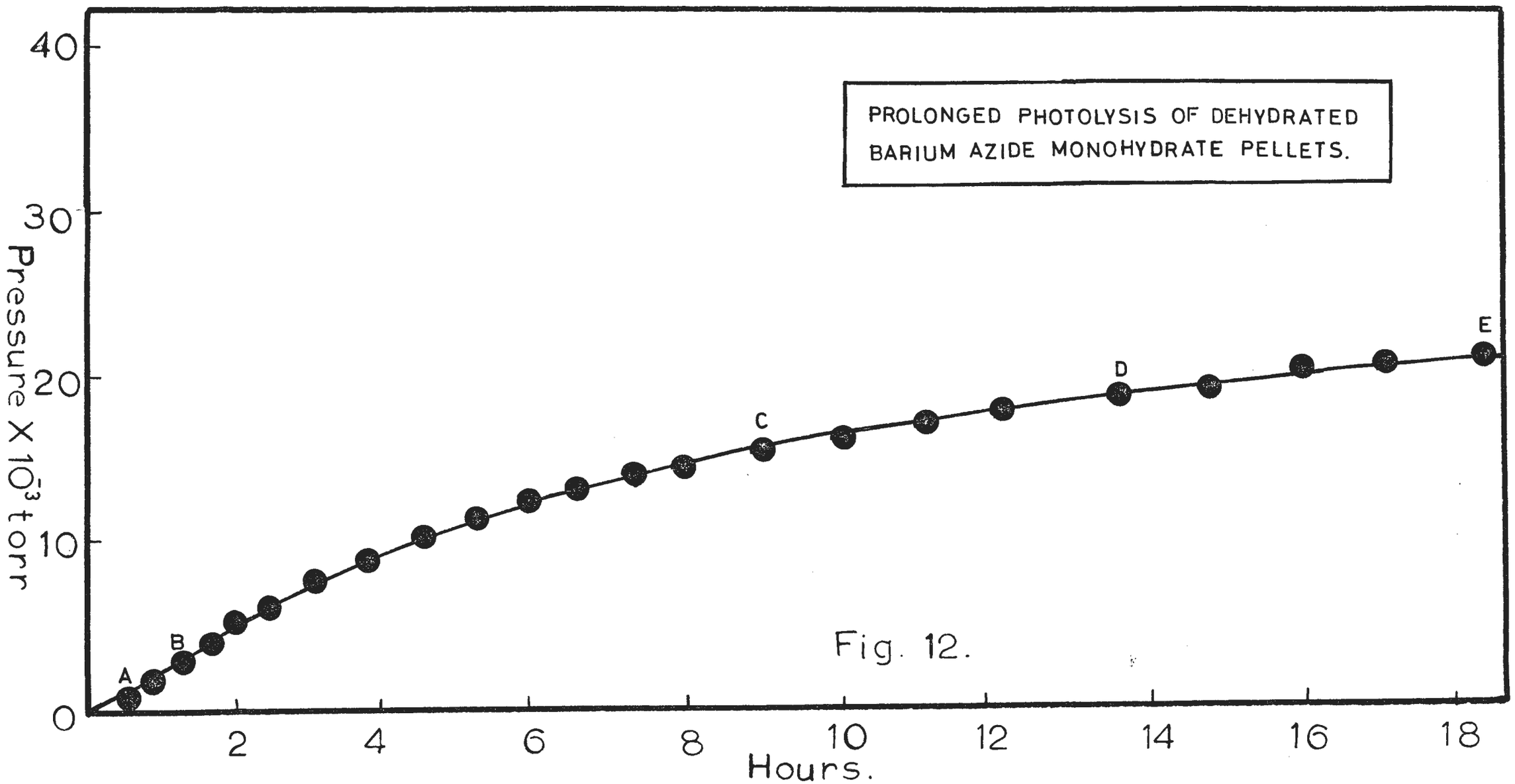
PROLONGED PHOTOLYSIS OF DEHYDRATED
BARIUM AZIDE MONOHYDRATE PELLETS.
Pressure X 10^{-3} torr
0
10
20
30
40
2
4
6
8
10
12
14
16
18
Hours.
A
B
C
D
E

Fig. 12.

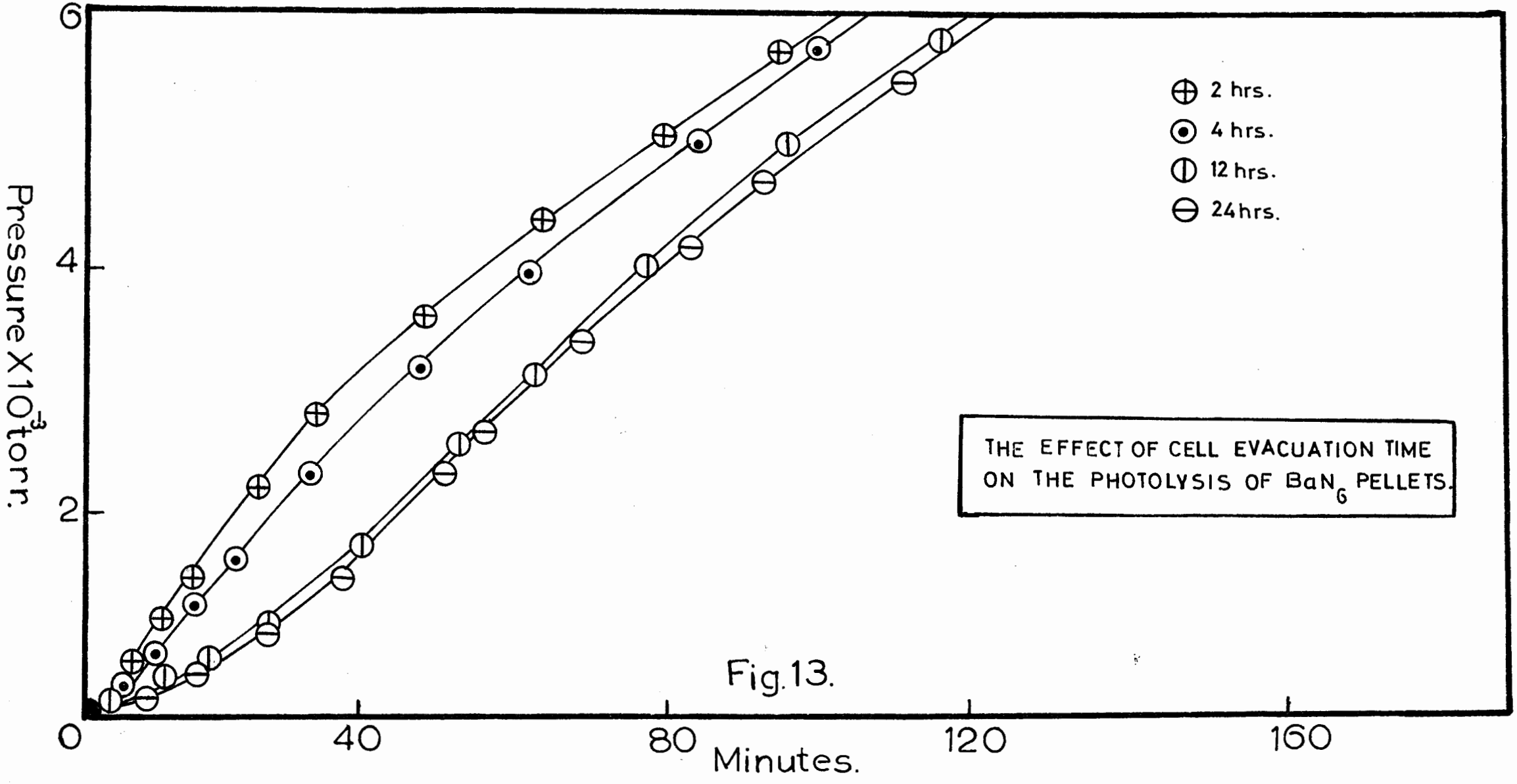
6
4
2
0
40
80
120
160
Minutes.
Pressure X10^{-3} torr.
2 hrs.
4 hrs.
12 hrs.
24 hrs.
THE EFFECT OF CELL EVACUATION TIME ON THE PHOTOLYSIS OF BaN_6 PELLETS.

Fig. 13.

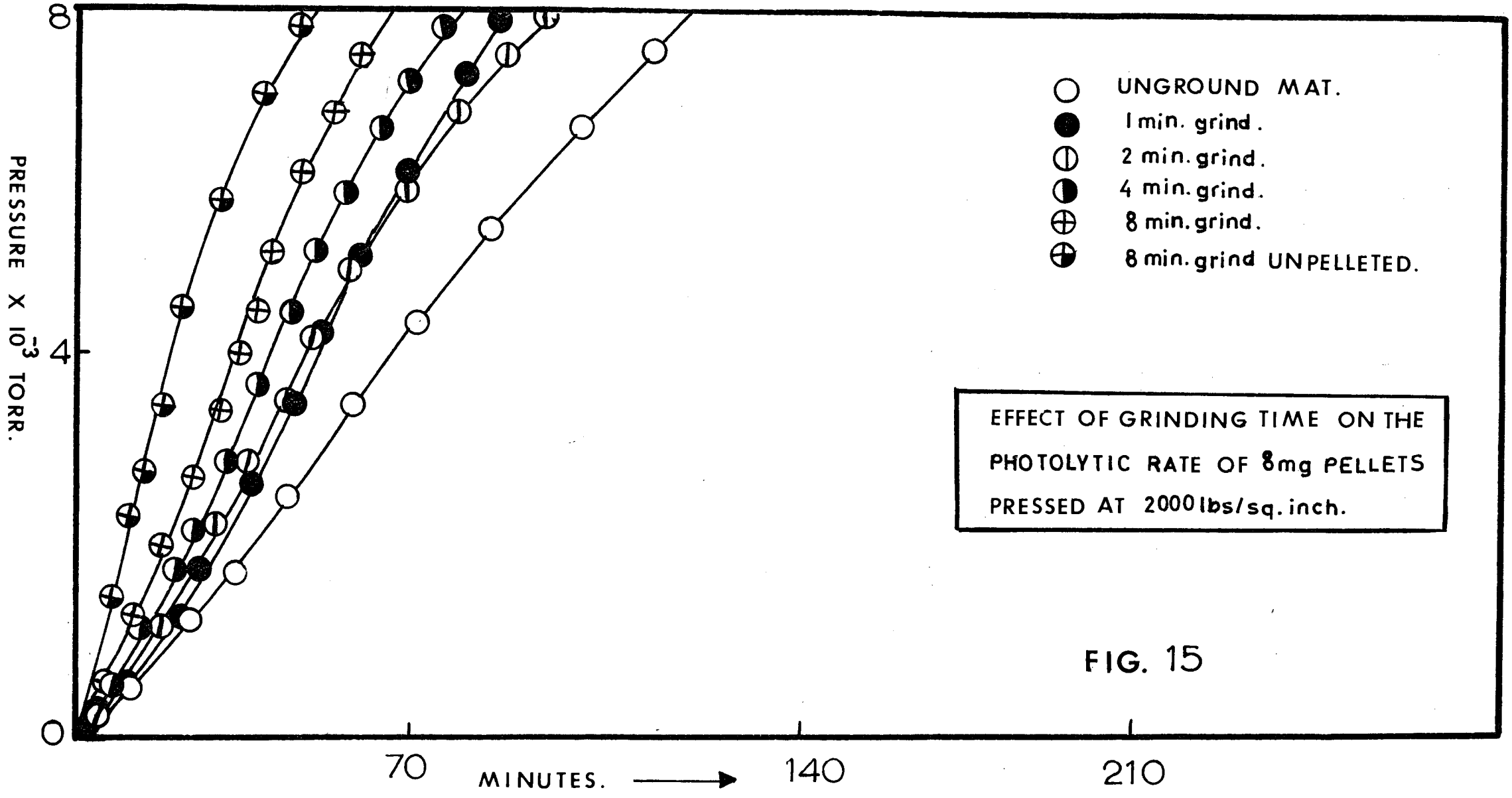
8
4
0
PRESSURE X 10^{-3} TORR.
70
MINUTES.
140
210
UNGROUND MAT.
1 min. grind.
2 min. grind.
4 min. grind.
8 min. grind.
8 min. grind UNPELLETED.
EFFECT OF GRINDING TIME ON THE PHOTOLYTIC RATE OF 8mg PELLETS PRESSED AT 2000 lbs/sq. inch.

FIG. 15

pelleted material, while curve ⊕ is for material ground 8 minutes, but not pelleted. From the above study a grinding time of 4 minutes was selected for further work on the photolysis of barium azide, because of the greater ease of pelleting and the greater extent of reproducibility of the pressure-time plots.

5.3.5. The effect of introducing water vapour into the decomposition cell prior to and during the photolysis of barium azide pellets.

Since barium azide hydrolysis fairly rapidly in moist air to form barium hydroxide, it was necessary to investigate the effect of water vapour introduced at various times before and during the U.V. photolysis of barium azide pellets in order to establish the effect on the photolytic rate.

Contamination by water vapour could occur in the transfer of pellets to the vacuum line if the humidity was high, and also water vapour in the cold traps could be liberated if the level of the liquid refrigerant fell too low in the trap dewars.

Fig. 16 shows the effect of introducing water vapour into the decomposition cell at $t = 0$ and various stages during the photolysis. It can be seen that in all cases the pressure-time plots are drastically reduced.

5.3.6. The effect of mercury vapour on the rate of photolysis of barium azide pellets.

Another source of contamination from the vacuum line itself is the presence of mercury vapour, both from the McCleod gauge and the mercury diffusion pump. Mercury vapour would have access to the decomposition cell if, for any reason, the liquid refrigerant level in the cold trap dewars were to fall too low. To test the effect of mercury vapour contamination, the dewar of the cold trap in the cell system (previously cleared of all water vapour and deliberately contaminated with mercury vapour) was lowered and the trap warmed to

60°C. The refrigerant dewar was then replaced after a few minutes.

Fig. 17 shows the effect of introducing mercury vapour into the decomposition cell. The effect of mercury vapour is even more drastic than that of the water vapour.

5.3.7. The effect of ageing on the photolysis of barium azide pellets.

In order to obtain a high degree of reproducibility of results for the photolysis of barium azide pellets, tests were conducted to determine whether storage time under vacuum would effect the rate and shape of the pressure-time plots.

Accordingly, samples of dehydrated barium azide monohydrate were stored in the dark in vacuo for various lengths of time and the rates of decomposition under ultra-violet light were compared with those of freshly prepared material. Fig. 18 illustrates a definite ageing effect for stored barium azide. Each curve in the figure represents an average of 4 determinations for each ageing period.

5.3.8. The effect of a water filter on the photolysis of barium azide pellets.

Owing to the considerable amounts of infrared generated by the ultraviolet arc, a water filter was employed to eliminate any infrared effect.

Fig. 19 illustrates the result of using such a filter. At the low temperatures employed in the photolysis, the effect of the water filter does not appear to be marked.

5.3.9. The reproducibility of results for the photolysis of barium azide pellets.

By rigidly controlling all the above factors which could contribute to errors in the photolytic rates, and by a careful standardisation of the experimental technique involved in the photodecompositions, good reproducibility of results was achieved.

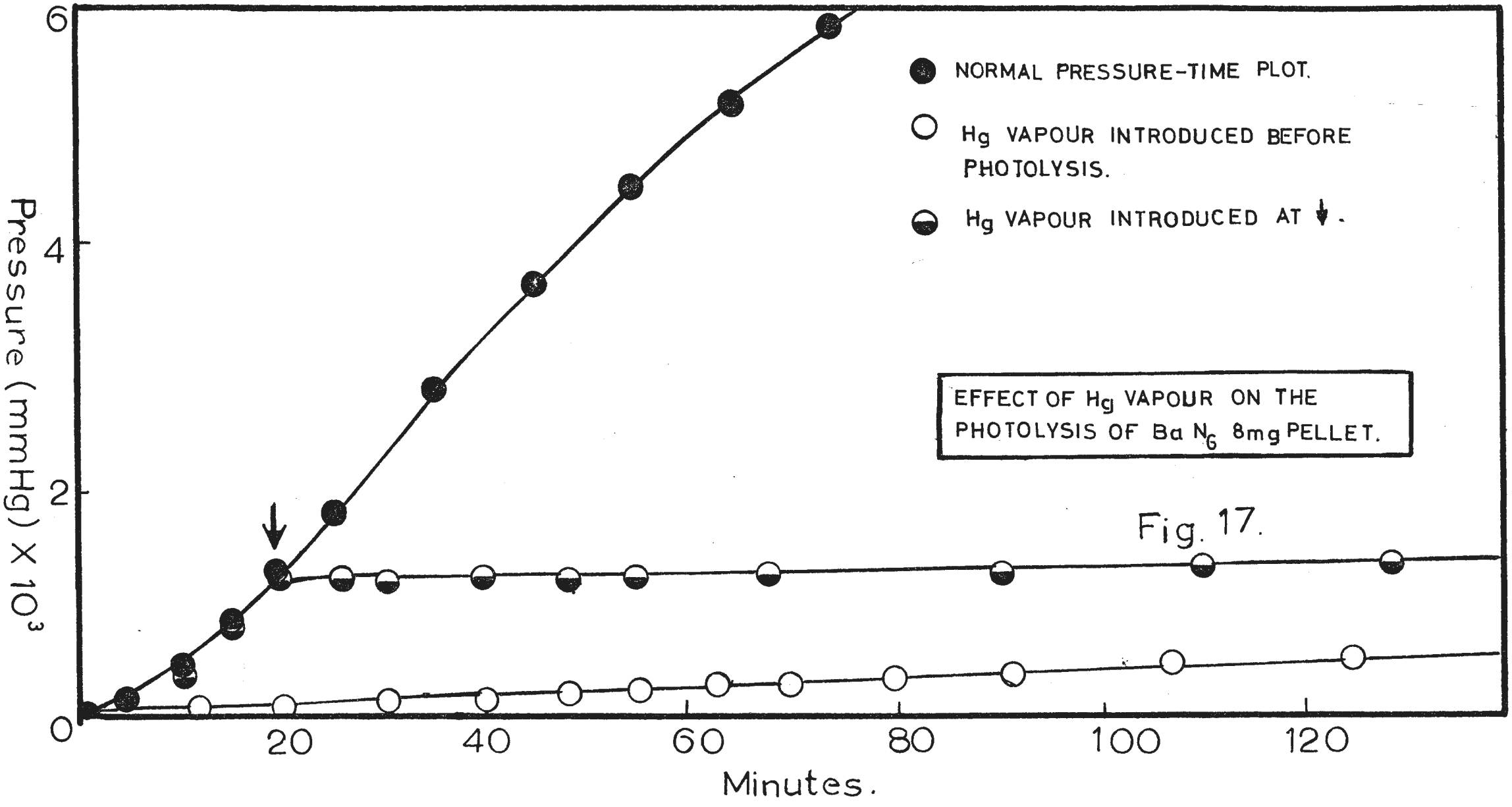
NORMAL PRESSURE-TIME PLOT.
Hg VAPOUR INTRODUCED BEFORE PHOTOLYSIS.
Hg VAPOUR INTRODUCED AT ↓.
EFFECT OF Hg VAPOUR ON THE PHOTOLYSIS OF Ba N6 8mg PELLET.
Pressure (mmHg) X 10³
0
2
4
6
20
40
60
80
100
120
Minutes.

Fig. 17.

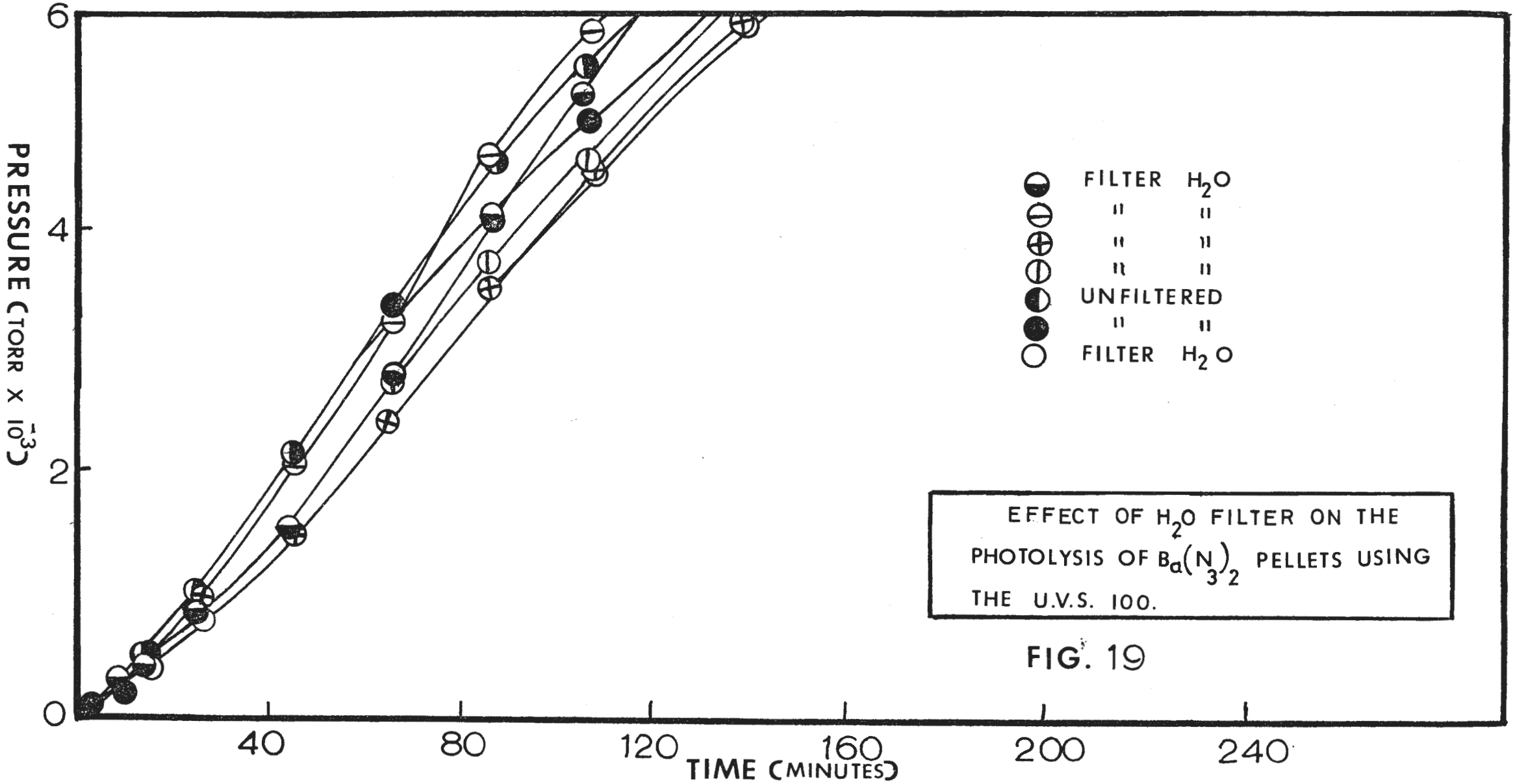

EFFECT OF H_2O FILTER ON THE PHOTOLYSIS OF $Ba(N_3)_2$ PELLETS USING THE U.V.S. 100.

FIG. 19

Fig. 20 illustrates the extent of reproducibility obtained for 7 decompositions under the same set of conditions.

5.4. Activation energies for the photolysis of barium azide pellets.

Fig. 21 depicts a typical pressure-time plot for the photo-decomposition, with labelled regions of the curve used in the determinations of activation energies.

As in the photolysis of the anhydrous crystals of barium azide, the Arrhenius equation was applied. The logarithm of rate k_1 (AB region) and rate k_2 (BC region) were plotted against I/T and the slope of the resultant linear plot was inserted into the above equation to give the activation energy (E_A) for each specific region indicated.

Three sets of activation energy determinations were performed for three different temperature ranges, as follows :

A. 0 to 22°C

B. -120 to 0°C

C. -197 to -120°C.

The split run technique (variation of the reaction temperature within the same decomposition) was employed in the activation energy determinations.

Table I shows the results obtained for the region AB of the photolysis curve.

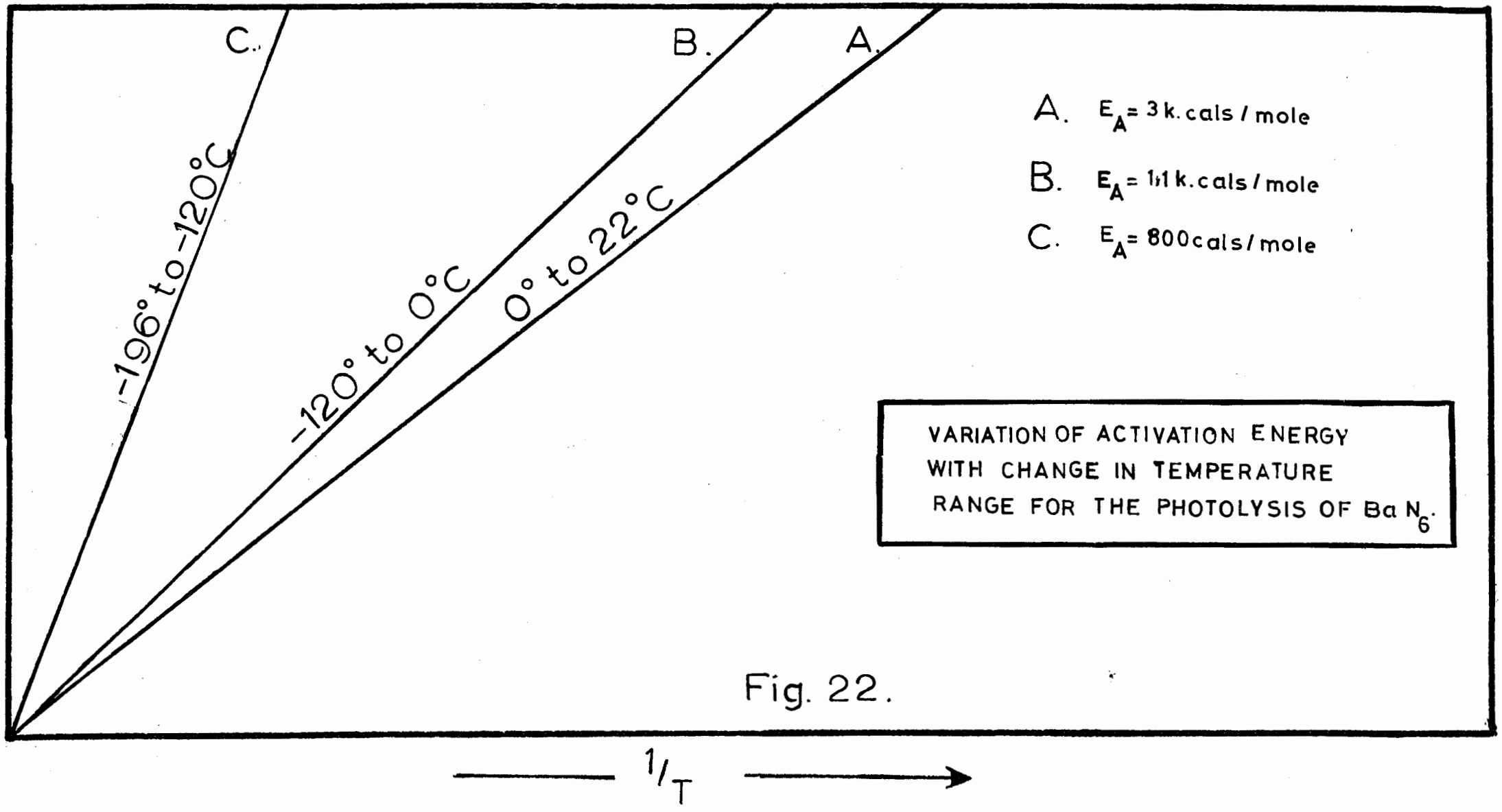
C.
B.
A.
-196° to -120°C
-120° to 0°C
0° to 22°C
A. E_A = 3 k.cals / mole
B. E_A = 1.1 k.cals / mole
C. E_A = 800 cals / mole
VARIATION OF ACTIVATION ENERGY WITH CHANGE IN TEMPERATURE RANGE FOR THE PHOTOLYSIS OF $Ba N_6$.
log rate
1/T

Fig. 22.

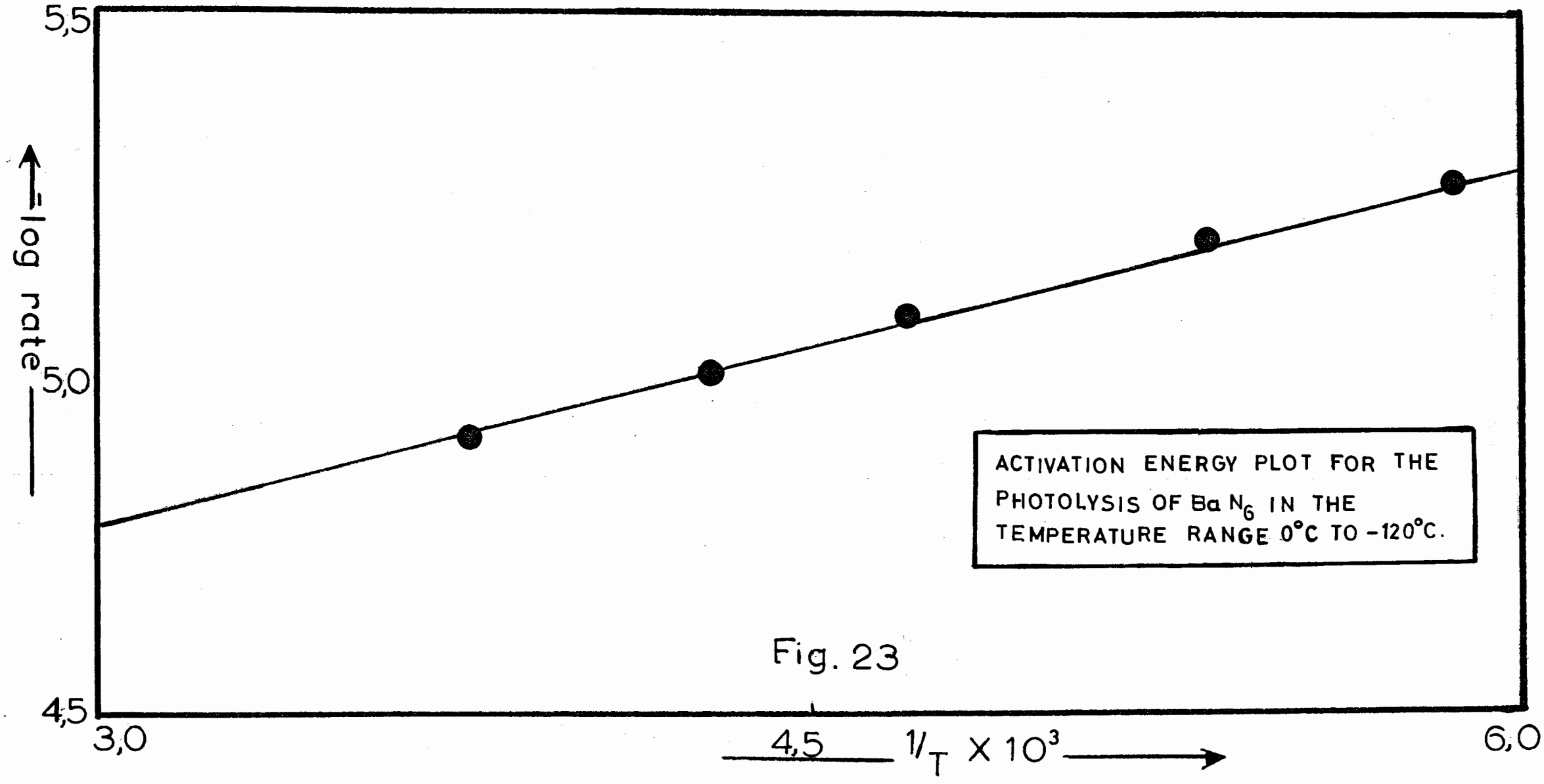
5,5
5,0
4,5
log rate
3,0
4,5
6,0
1/T X 10³
ACTIVATION ENERGY PLOT FOR THE PHOTOLYSIS OF Ba N6 IN THE TEMPERATURE RANGE 0°C TO -120°C.

Fig. 23

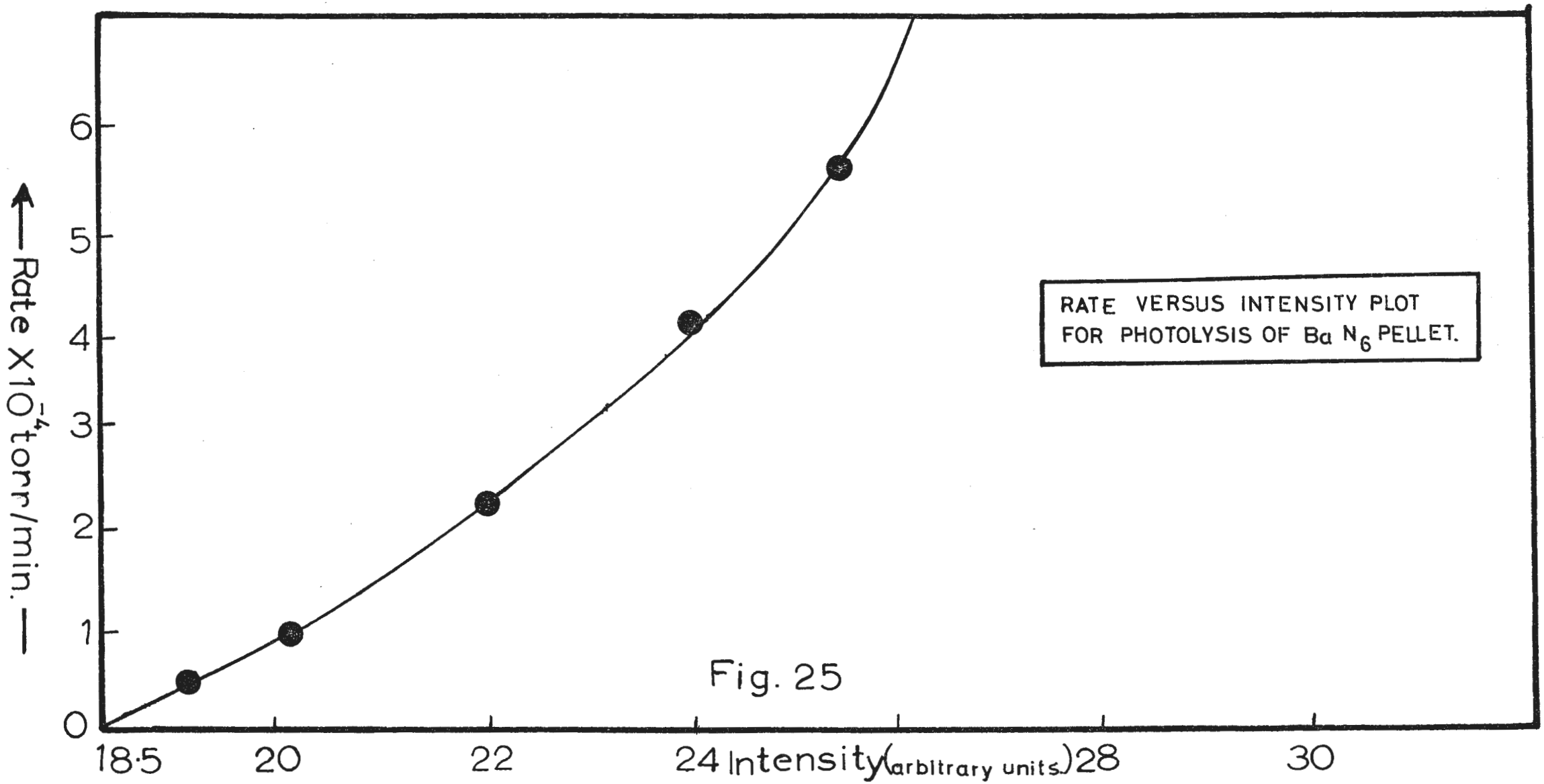
RATE VERSUS INTENSITY PLOT
FOR PHOTOLYSIS OF Ba N_6 PELLET.
Rate X 10^{-4} torr/min.
0
1
2
3
4
5
6
18·5
20
22
24
Intensity (arbitrary units)
28
30

Fig. 25

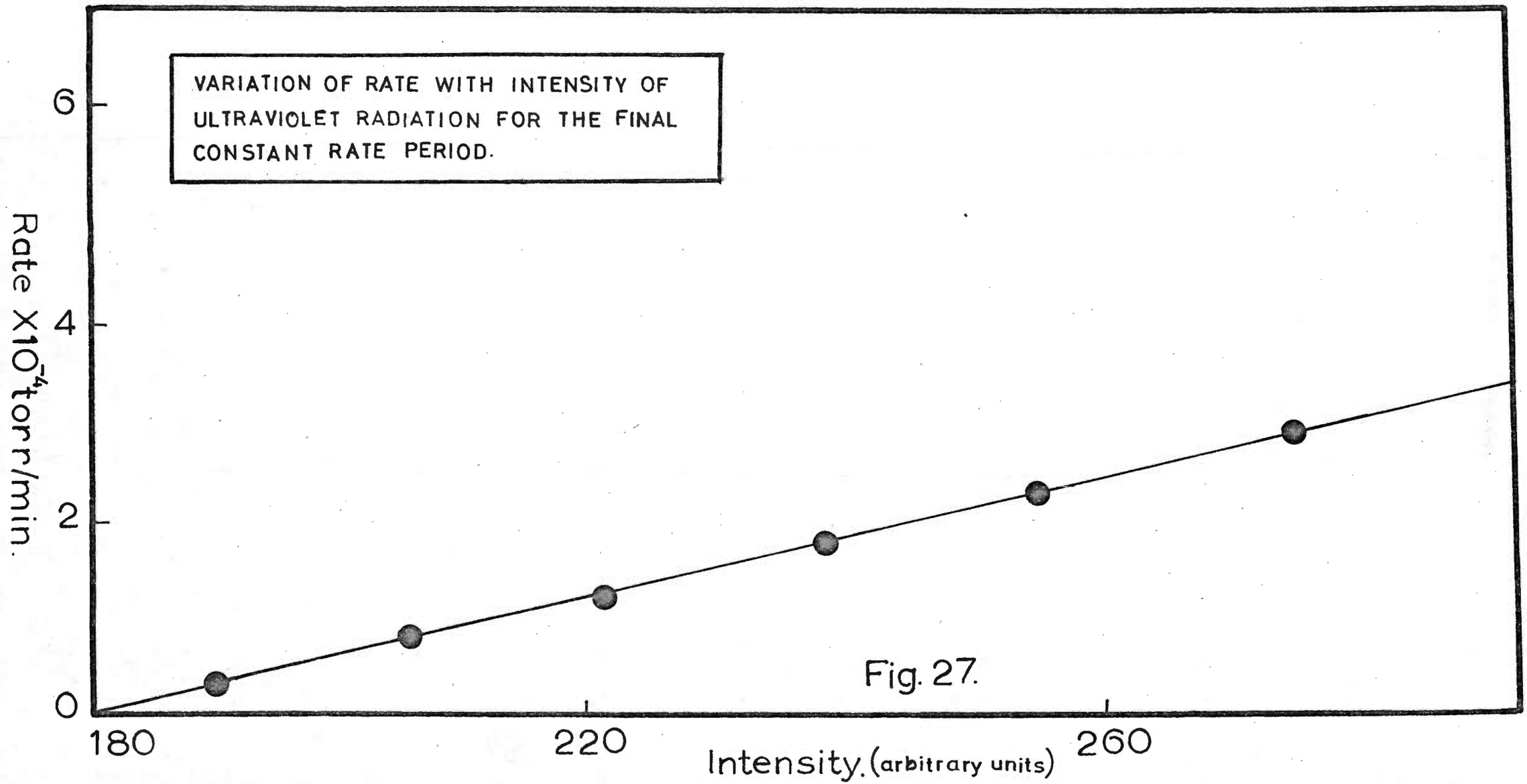
VARIATION OF RATE WITH INTENSITY OF ULTRAVIOLET RADIATION FOR THE FINAL CONSTANT RATE PERIOD.
Rate X10⁻⁴ torr/min.
0
2
4
6
180
220
260
Intensity. (arbitrary units)

Fig. 27.

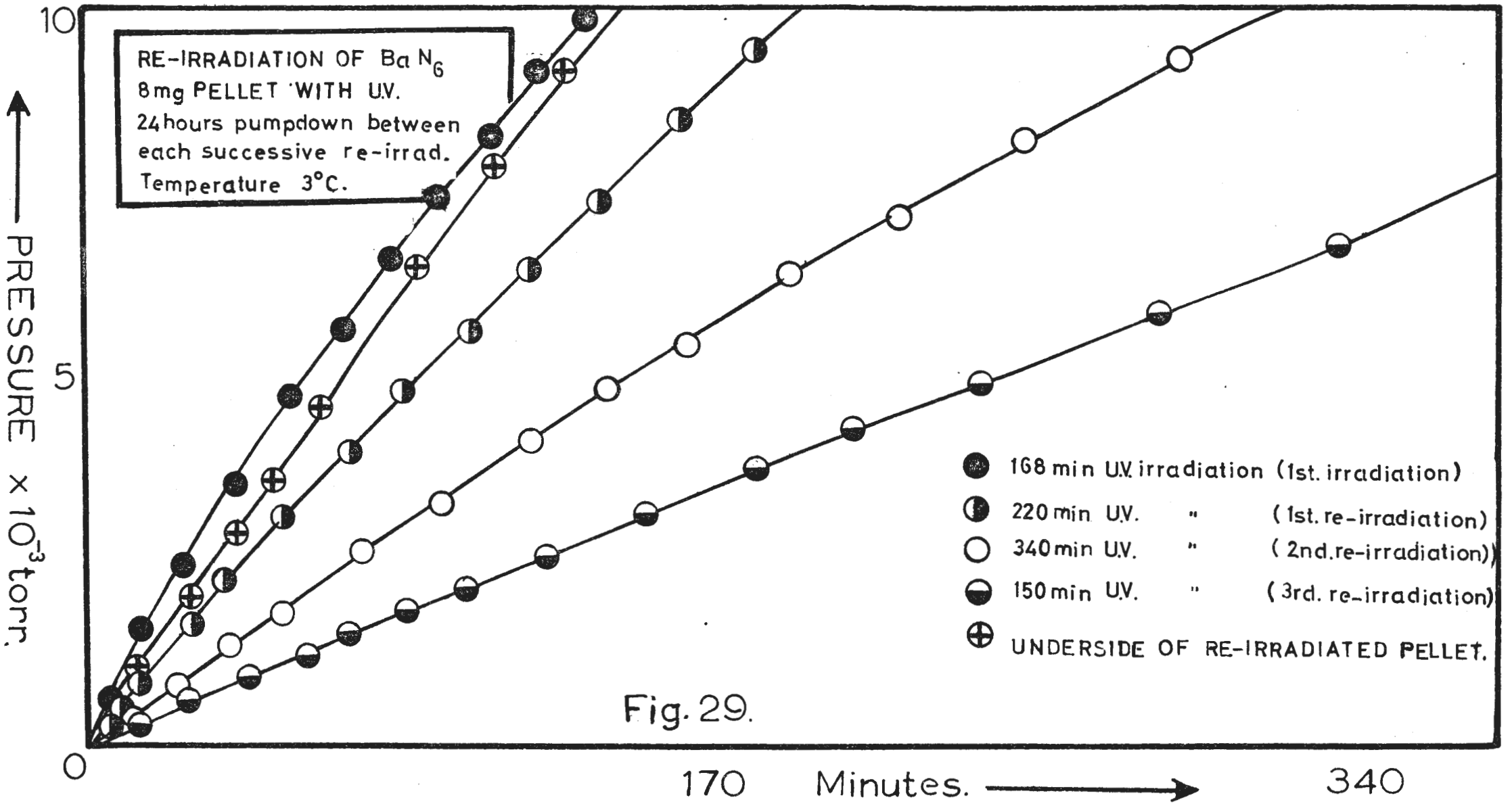
RE-IRRADIATION OF $Ba N_6$
8mg PELLET WITH U.V.
24 hours pumpdown between
each successive re-irrad.
Temperature 3°C.
168 min U.V. irradiation (1st. irradiation)
220 min U.V. " (1st. re-irradiation)
340 min U.V. " (2nd. re-irradiation)
150 min U.V. " (3rd. re-irradiation)
UNDERSIDE OF RE-IRRADIATED PELLET.
PRESSURE × 10^{-3} torr.
10
5
0
170
Minutes.
340

Fig. 29.

within minutes the pellet becomes completely black.

Tests conducted on this pellet in the dry box indicated large amounts of Ba_3N_2 or BaN_3 present. The introduction of water into the decomposition cell caused a violent reaction with the blackened pellet, with copious liberation of ammonia gas, confirmed by the Nessler test for ammonia. After the reaction was complete, only barium hydroxide could be detected in the product of photolysis. Any barium metal present would also react with water to form barium hydroxide and hydrogen gas. Although some barium metal may have been present, it was not possible to detect any hydrogen gas because of the small amount of decomposed azide involved.

Maintaining a temperature of 120°C for periods of 50 minutes or more, drastically reduced the rate of photolysis at 1°C. These observations are shown graphically in fig. 30. Fig. 31 shows the pressure-time plot for the normal thermal decomposition of barium azide pellets at 120°C. The arrows indicate the stage of thermal reaction reached in the thermal pre-treatment experiments.

5.4.5. Pre-irradiation of barium azide pellets with X-rays and γ-rays.

For the purpose of investigating a possible link between the photolysis and the radiolysis of barium azide pellets, the sample in the photolysis cell was subjected to pre-irradiation both by X-rays and γ-rays.

The photolytic rate of barium azide pellets pre-irradiated with X-rays (40 K.V. and 20 ma) diminished slowly with dose of irradiation, but the shape of the pressure-time plot was unchanged. This is shown in fig. 32.

Pre-irradiation with 15,000 and 1M roentgens from a Co^{60} source also tended to suppress the rate of subsequent photolysis of barium azide pellets, as indicated in fig. 33.

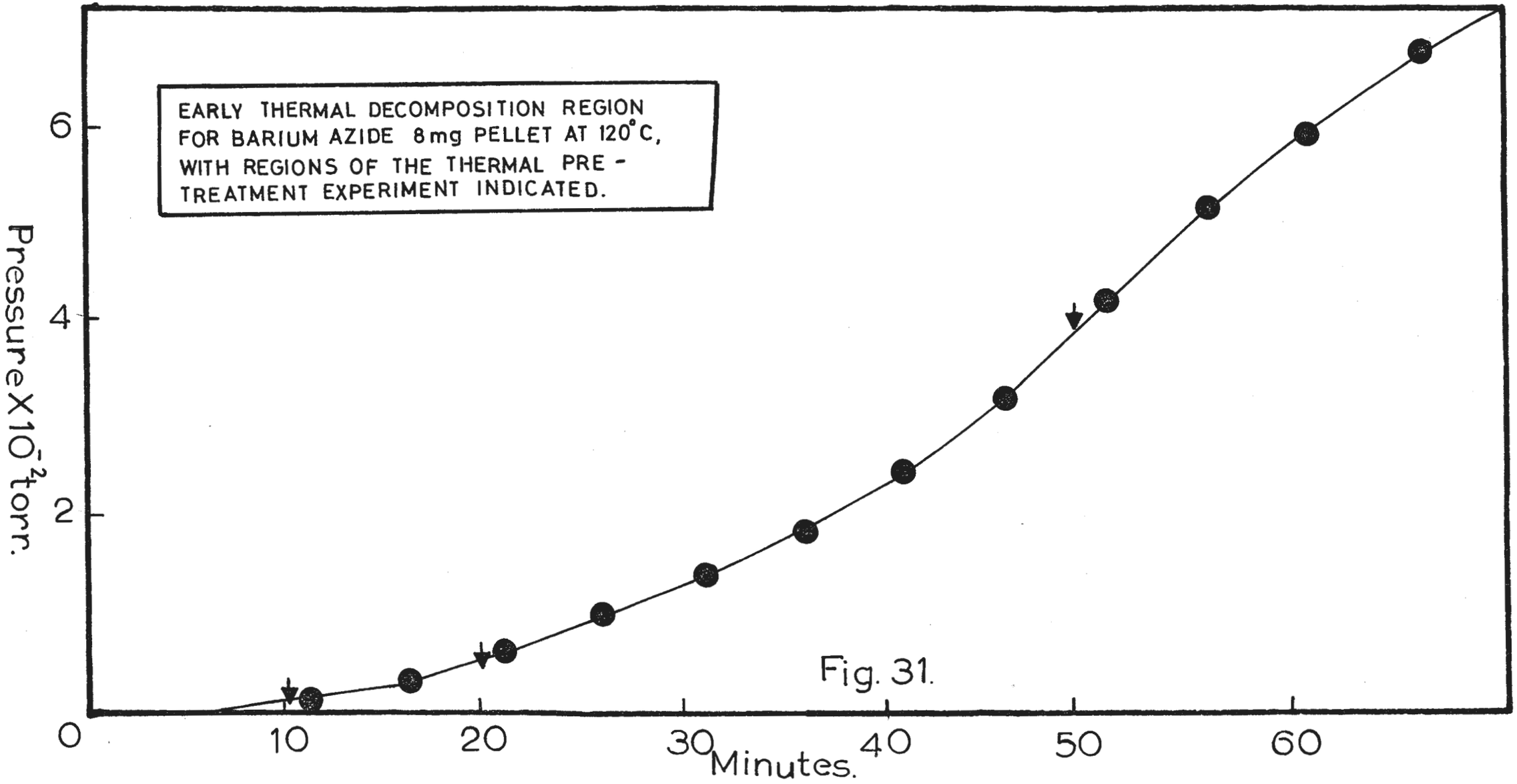
EARLY THERMAL DECOMPOSITION REGION
FOR BARIUM AZIDE 8mg PELLET AT 120°C,
WITH REGIONS OF THE THERMAL PRE -
TREATMENT EXPERIMENT INDICATED.
Pressure X 10⁻² torr.
0
2
4
6
10
20
30
40
50
60
Minutes.

Fig. 31.

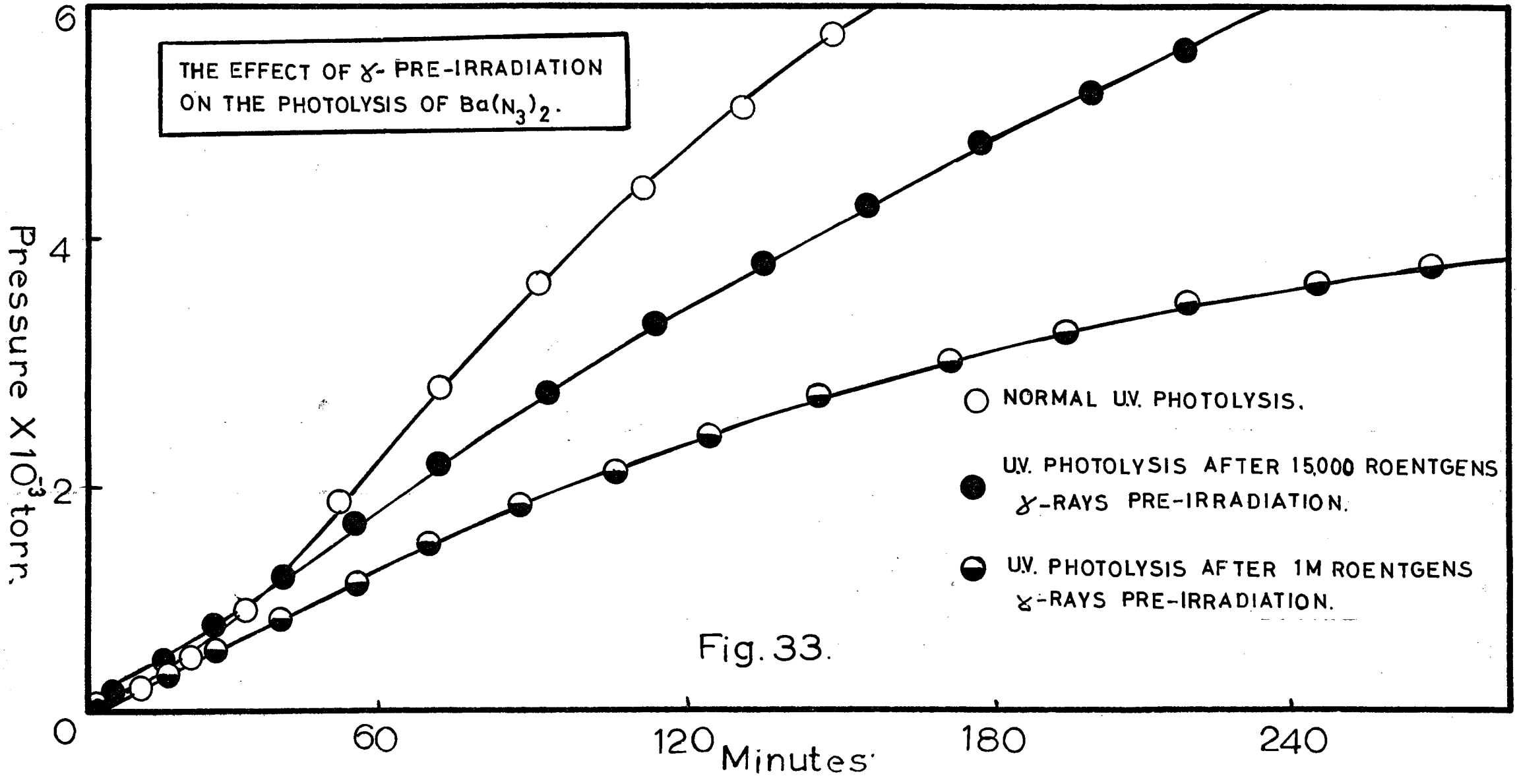
THE EFFECT OF γ- PRE-IRRADIATION ON THE PHOTOLYSIS OF $Ba(N_3)_2$.
Pressure X 10^{-3} torr.
0
2
4
6
60
120
180
240
Minutes
NORMAL U.V. PHOTOLYSIS.
U.V. PHOTOLYSIS AFTER 15,000 ROENTGENS γ-RAYS PRE-IRRADIATION.
U.V. PHOTOLYSIS AFTER 1M ROENTGENS γ-RAYS PRE-IRRADIATION.

Fig. 33.

5.4.6. Photoconductivity tests during the U.V. photolysis of barium azide pellets.

Using the Vibron electrometer, photocurrents were measured on U.V. irradiated KCl and BaN_6 pellets. The KCl was used as a control because it yields a fair photocurrent with U.V. radiation. The circuitry used is shown in fig. 4. The guard ring of painted silver slurry was essential to prevent or minimise stray surface currents on the pellet surface.

A photocurrent in the region of 0.8×10^{-12} amp was constant for irradiated barium azide pellets in spite of increases in the intensity of irradiation.

KCl pellets, however, showed a rapid rise in photocurrent with increasing intensity of irradiation. These results are illustrated in fig. 34.

5.4.7. Photomicrographs of various stages in the photolysis of barium azide pellets.

Photomicrographs were taken during various stages of the photolysis to ascertain whether visible nuclei were formed at any stage during the reaction and also how they behaved as the photolysis proceeded.

A Leitz microscope and vacuum type hotstage was used to follow the various stages of the reaction indicated in fig. 35. The hotstage with its quartz windows was used as the photolysis cell. Low temperatures were maintained by circulating liquid nitrogen vapour through the hot stage cooling system, in response to a contact thermometer activating a vapour pumping device.

The study of the photolytic reaction by taking photomicrographs during various stages of the reaction, yielded the following observations:-

At t = 0 The photomicrograph showed the pellet to be uniformly white in colour, with distinct crystallite faces visible on the pellet surface.

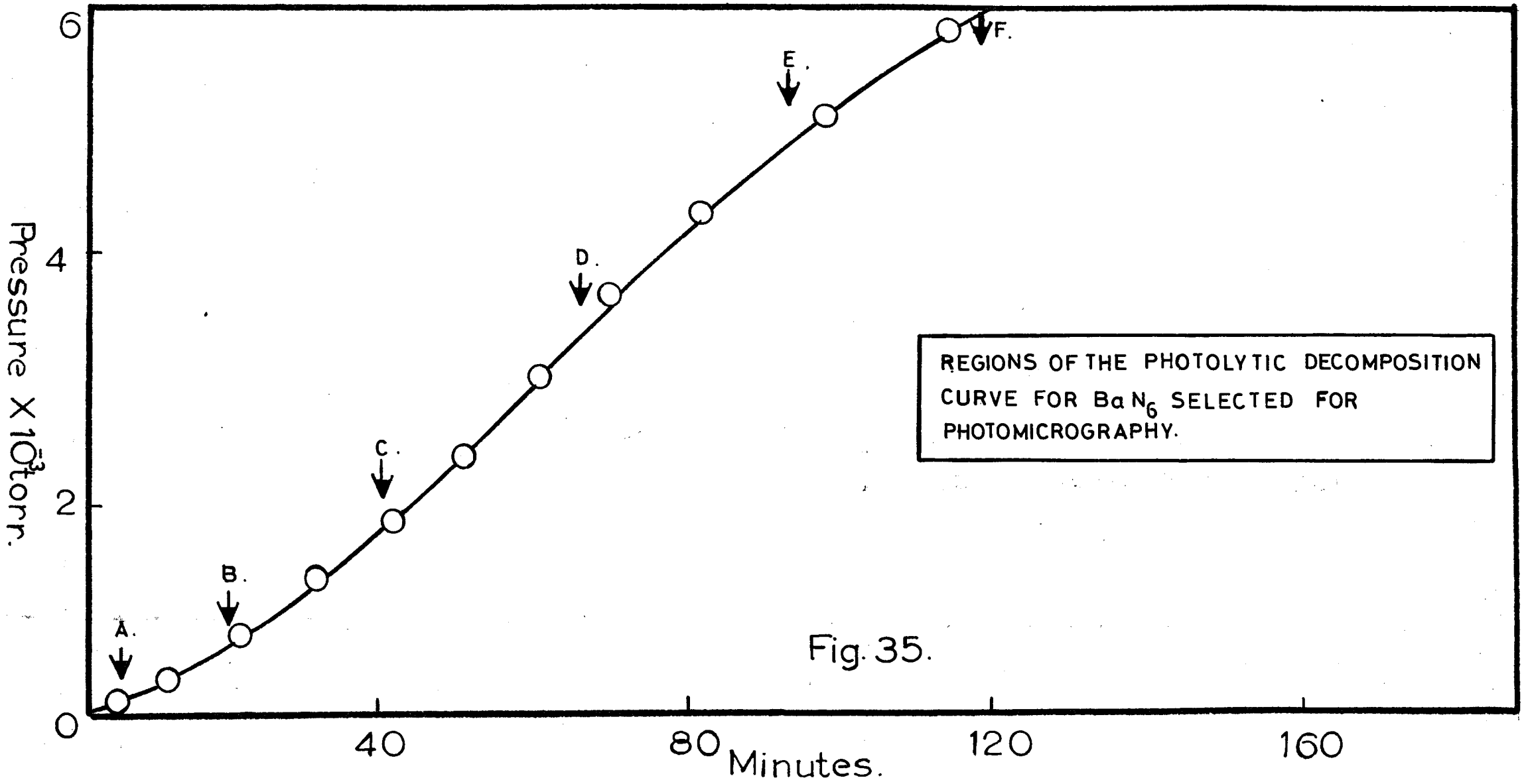
6
4
2
0
Pressure X 10^{-3} torr.
A.
B.
C.
D.
E.
F.
40
80
120
160
Minutes.
REGIONS OF THE PHOTOLYTIC DECOMPOSITION CURVE FOR BaN_6 SELECTED FOR PHOTOMICROGRAPHY.

Fig. 35.

Stage A. A few of the crystallite faces had turned a greyish white colour.

Stage B. The white background between the crystallites appeared darker, while several more darkened crystallite faces were present. The original darkened faces now appeared mottled, owing to very dark localised areas on the crystallite faces.

Stage C. Very many crystallite faces were mottled with very black irregular areas. These black areas covered most of the exposed faces, due to considerable overlapping.

Stage D. The mottled faces of the crystallites were barely distinguishable from the very dark background of the photolysed pellet, and the overall appearance of the pellet was more or less uniformly black.

Stage E. This showed a similar situation to D.

See PLATE II.

PHOTOMICROGRAPHS.

PLATE II.

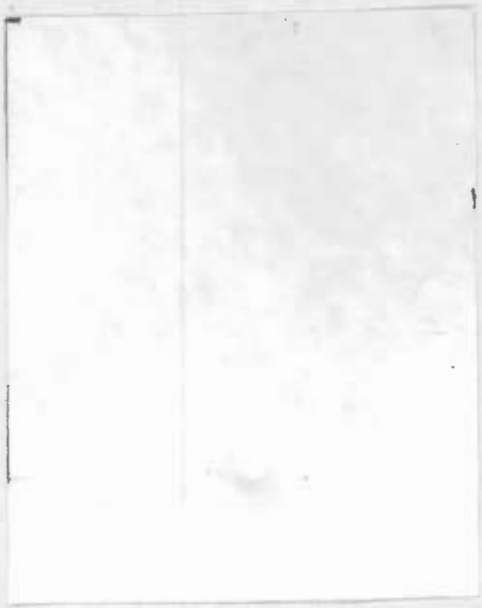

t = 0.

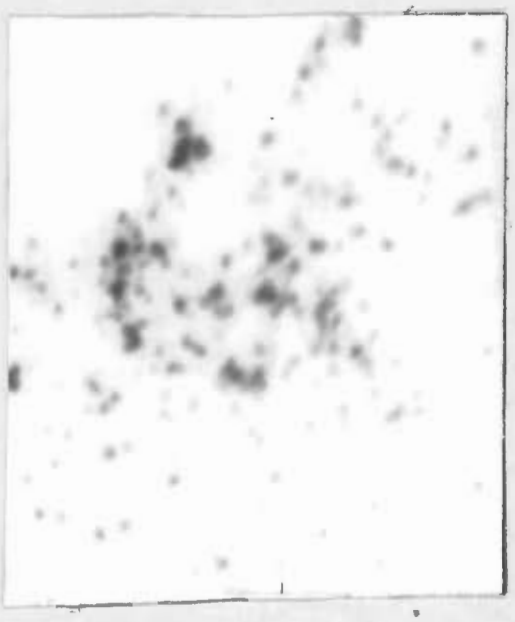

A.

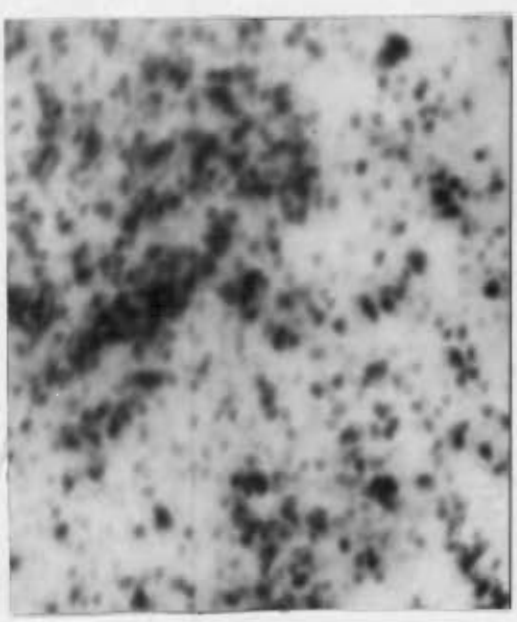

B.

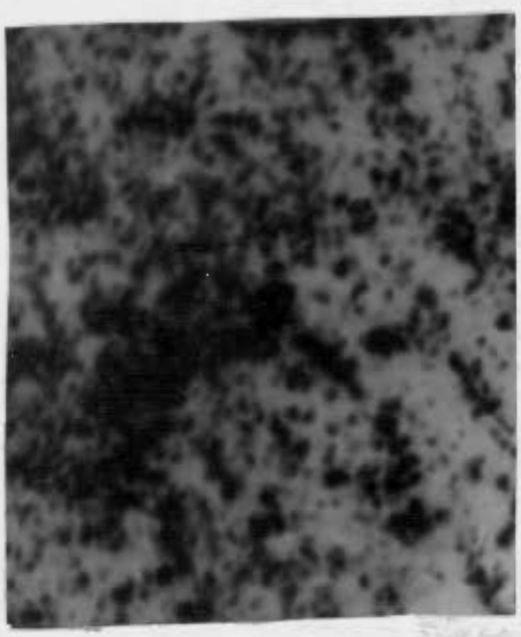

C.

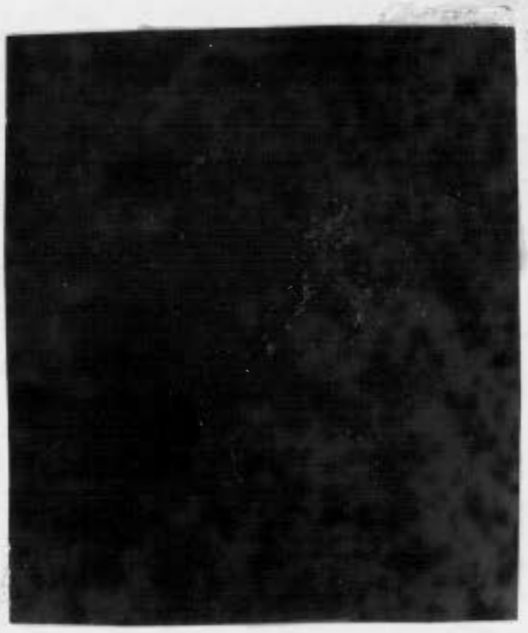

D. & E.

DISCUSSION OF THE RESULTS FOR SECTIONS 5.2. to 5.4.7.

The ultra-violet photolysis of 5 mm diameter 8 mg. pellets of barium azide dehydrated monohydrate at 1°C is characterised by a sigmoid pressure-time plot, with a distinct acceleratory and deceleratory phase.

After a slight initial decreasing rate (usually about 2 minutes) the rate increases over periods ranging from 20 - 30 minutes. Thereafter a very long decay period occurs which persists even after 20 hrs. irradiation. The use of a water filter between the cell window and the U.V. arc makes no significant change to the shape of the pressure-time plots.

By standardising the pelleting and grinding procedure, pellets of a fixed weight give good reproducibility for the photolytic reaction.

The introduction of water vapour or mercury vapour into the decomposition cell at various periods during the photolysis drastically affects the subsequent photolysis.

In the case of introduced water vapour the effect is quite likely due to the formation of a barium hydroxide layer over the surfaces of the pellet, for barium azide, barium metal and barium nitride readily hydrolyse to the hydroxide in the presence of water vapour.

The effect of introducing mercury vapour, although more drastic, is less easily explained. Assuming that insufficient vapour is present to cover the pellet surface with a monolayer of Hg atoms, the marked fall off in photolytic reaction must be linked with the trapping of centres necessary for the photolytic reaction, or the possible formation of Hg - Ba amalgam on the pellet surface.

Grinding of the crystalline barium azide has the effect of increasing the photolytic rate and presumably the increase in the shape of the pressure-time plot is owing to the increasing mechanical damage, resulting in an increase of certain lattice defects necessary for reaction.

This increase cannot be attributed to an increase in surface area, since pelleting the ground material keeps the exposed surface area more or less constant. Verneker and Avrami [65] have shown a direct relationship between particle size and sensitivity. Curve ⊕ (fig. 15) clearly shows the added effect of increase in surface area, since the ground but unpelleted material was used for this decomposition.

Similarly the increased rates due to increased pelleting pressure must again result from increased faulting in the azide lattice owing to mechanical damage during pelleting. From the set of curves in fig. 14 it can be seen that this effect of mechanical damage is not linearly related to pelleting pressure since the most marked effect occurred in the initial increase of 500 lbs/sq. inch.

The investigation of the intensity and rate relationship for the early region AB (see fig. 12) and the final constant rate period DE, suggests that at least two mechanisms appear to operate at various times during the photolysis. The initial dependence of rate on the square of the intensity of irradiation implies a bimolecular reaction involving two excited azide ions, excitons or radicals, because photoconductivity experiments performed during the photolysis showed the absence of any photocurrent. This rules out the production of electrons in the conduction band.

Thus the following possibilities might exist when barium azide is irradiated with ultraviolet light:-

1. Production of excitons and/or excited azide ions.
2. Liberation of pairs of trapped electrons and positive holes.

The excitons would represent excited states of the crystal in which electrons are bound in the electrostatic field associated with positive holes. These excitons should therefore be mobile and able to decay, transferring their energy to lattice vibrations, or they may interact with phonons resulting in dissociation into a free electron and a positive hole. This would however be ruled out by the absence of

any photoconductivity during photolysis. Another possibility would be for the excitons to interact with atoms or ions in the substructure of the azide crystal, leading to photochemical changes.

e.g.

$$N_3^- \overset{h\upsilon}{\rightleftharpoons} N_3^- *$$

$$N_3^- * + N_3^- * \rightleftharpoons N_3^{2-} ** + N_3^2$$

$$2N_3 \longrightarrow 3N_2$$

where * = exciton or excited ion.

If trapping of the above excitons or excited azide ions occurs, neighbouring trapped excitons or excited azide ions may interact to give electrons and positive holes, or trapped entities may interact with untrapped excited states.

$$T + N_3^- * \rightleftharpoons (N_3\ T)^- *$$

$$(N_3\ T)^- * + N_3^- * \longrightarrow 2N_3 + T + 2e$$

$$2N_3 \longrightarrow 3N_2$$

where T = trapping entity,

or neighbouring trapped entities may combine to yield reaction products:-

$$N_3^- * + T \longrightarrow (N_3\ T)^- *$$

$$2(N_3\ T)^- * \rightleftharpoons (N_3T_2N_3)^{2-} * \longrightarrow 2N_3 + 2T + 2e + 2\boxminus$$

$$2N_3 \longrightarrow 3N_2 + 2\boxminus$$

where $\boxminus$ is an anion vacancy and T = a trapping entity.

Barium ions could then react with the two F-centres yielding barium atoms.

$$Ba^{2+} + 2e\boxminus \longrightarrow Ba + 2\boxminus \quad \text{where } e\boxminus = \text{F-centre.}$$

These atoms can aggregate by diffusion through the lattice to form barium metal.

The deep colouration produced under U.V. irradiation supports F-centre formation (electrons are associated with anion vacancies).

$$e + \square \rightleftharpoons e\,\boxminus$$

If F-centres are stable at the decomposition temperatures, electrons will be trapped by anion vacancies and aggregations of F-centres will lead to the formation of barium metal nuclei. If the F-centres are not stable at decomposition temperatures, electrons could be trapped by a barium ion close to a decomposition centre and still lead to the formation of barium atoms.

The early acceleratory period of the photolysis can be explained by assuming the traps T to be anion vacancies already present in the crystalline lattice.

After the reaction

$$(N_3\boxminus\ {}_2N_3)^{2-**} \longrightarrow 2N_3 + 2\boxminus + 2e\boxminus$$

and

$$Ba^{2+} + 2e\boxminus \longrightarrow Ba + 2\boxminus$$

we have an overall reaction as follows :-

$$(N_3\boxminus\ {}_2N_3)^{2-**} \longrightarrow 3N_2 + Ba + 4\boxminus$$

Since the life time of an exciton or an excited azide ion is in the region of 10^{-8} sec., trapping could form the rate determining step. If this is the case, then the production of 4 anion vacancies for the consumption of 2 vacancies will lead to an increase in the number of trapping sites and hence an acceleration of the photolytic reaction. Deb [50] has shown by investigating the absorption spectra and photoelectric properties, that for barium azide, excited azide ions rather than excitons are involved.

The decay of the photolytic rate cannot be due to the consumption of defects or traps as has been suggested by Jacobs, Tompkins, Pai, Verneker [32] and others [30,31], because irradiation of the underside of the pellet yields a normal photolytic curve containing both an acceleratory and deceleratory phase. This occurs regardless of whether the irradiation of the underside is commenced immediately after

the decay period sets in or 24 hrs. afterwards. The decay period must then result from the formation of photolysis products which prevent the ultra violet radiation from reaching deeper layers of azide material. This is supported by the results of re-irradiation shown in fig. 22 and by the fact that X-irradiation of barium azide (see radiolysis section), where higher energies are involved, produces a linear pressure-time plot owing to the fact that the layer of radiolysis product cannot effectively screen the underlying layers from the X-radiation.

This formation of photolysis product will also affect the dependence of the photolytic rate on the square of the intensity, leading to a first power relationship for the final constant rate period.

The fact that the photolytic rate does not easily proceed to zero after prolonged irradiation, could be due to the following three factors:-

i) the slow desorption of nitrogen gas from the pellet surface.

ii) the photolysis of the initial reaction products, leading to secondary photolysis products.

iii) the continued outgassing of the cell system and sample subjected to U.V. irradiation.

The possibilities of ii) are discussed in the section dealing with the thermal pre-treatment and the photomicrography.

It has been demonstrated in the section on "Experimental and Apparatus" under the heading of cell design considerations, that under U.V. irradiation, further outgassing of the cell system occurs. Fig. 6 indicates the extent of this induced outgassing rate.

The above reactions cannot be the only ones involved in the photolysis of barium azide, because recent Electron Spin Resonance (E.S.R.studies)[6,10,11,12,14]. have detected intermediates such as $N2^-$, N_4^-, N_3^{2-} and N atoms.

The following reaction may take place during the later phase of the photolytic reaction, where the rate dependence on the intensity is not strictly according to the second power law.

$$N_3^- \underset{}{\overset{h\nu}{\rightleftharpoons}} N_3^{-*}$$

$$N_3^{-*} + N_3^- \longrightarrow N_3^{2-} + N_3$$

$$N_3 \longrightarrow 3/2\ N_2$$

where * = an exciton or excited state,

i.e. we have the formation of a "nitride type" - $Ba^{2+}N_3^{2-}$.

Since no other acceleratory region (except the initial one of approximately 30 minutes, depending on conditions) was found for the photolysis of barium azide in this work, barium nitride as Ba_3N_2 must be excluded, if the observations of Verneker [35] concerning the acceleratory rate of photolysis of Ba_3N_2 are taken into account.

The increase in the rate of photolysis that occurs after the U.V. radiation is interrupted (fig. 28) could be partly attributed to the expulsion of trapped N_2 from the lattice, since irradiation of nitrogen adsorbed onto silica powder causes effective desorption of the nitrogen, and partly due to the possible accumulation of centres necessary for reaction, during the dark period.

The tendency of pre-irradiation from ionizing radiations like X-rays and γ-rays to depress the photolytic reaction of barium azide (fig. 32 and 33) seems to imply either a screening effect by the radiolytic products, thereby screening the azide somewhat from the U.V. radiation, or a depletion of reaction centres or traps necessary for reaction, during the pre-irradiation period.

The variation of the activation energy with various temperature ranges suggest that certain mechanisms of photlysis might predominate at certain temperatures. At the higher temperature ranges, thermal decomposition may occur to some extent, accounting for the higher activation energies of 3k.cals./mole.

The very low activation energy of 800 cal./mole, in the lowest temperature range implies a predominance of free radical type reactions such as:-

$$N_3^- \rightleftharpoons N_3^{-*} \quad (h\nu)$$

$$2N_3^{-*} \boxminus \longrightarrow 2N_3 + 2e\boxminus$$

$$N_3 + N_3^- \longrightarrow N_4^- + N_2$$

$$N_3 \longrightarrow N + N_2$$

$$N + N_3^- \longrightarrow N_2^- + N_2$$

The above intermediates have all been detected in recent E.S.R. studies [6,10,11,12,14].

Pre-treatment of barium azide pellets with temperatures of 120°C (fig. 25) for sufficient length of time to initiate thermal decomposition, produces a very fast photolysis reaction, probably based on the photolysis of the N_3^{2-} ion.

$$N_3^- \rightleftharpoons N_3^- \quad (h\nu)$$

$$N_3^{-*} + N_3^- \longrightarrow N_3^{2-} + N_3$$

$$N_3^{2-} \rightleftharpoons N_3^{2-*} \quad (h\nu)$$

$$N_3^{2-*} + 2\boxminus \longrightarrow N_3 + 2e\boxminus$$

$$2N_3 \longrightarrow 3N_2 + 2\boxminus$$

$$Ba^{2+} + 2e\boxminus \longrightarrow Ba + 2\boxminus$$

where $\boxminus$ = anion vacancy and $e\boxminus$ = F-centre.

Elevating the temperature to 120°C for longer periods decomposed some of the salt to nitrogen and barium metal. This would then lower the photolytic reaction by virtue of salt depletion and a screening effect by a product layer.

The sensitivity of the prepared barium azide dehydrated monohydrate was found to vary with length of storage time (fig. 28). This fact was also observed by Verneker and Avrami [65] in a study of the explosive behaviour of barium azide.

SUMMARY OF SECTION 5.1 TO 5.4.7., STRESSING THE DIFFERENCES IN THE FINDINGS OF THIS WORK AND THOSE OF PREVIOUS WORKERS FOR THE PHOTOLYSIS OF BARIUM AZIDE.

1. The shape of the pressure-time plots for the photolysis of barium azide, whether as crystals, powder or pellets, was found to be sigmoid in character, with an early acceleratory period lasting on the average 10 - 40 minutes, depending on the reaction temperature. Thereafter a slow deceleratory period persisted, even after 20 hrs irradiation, the final rate period reaching a more or less constant value as the decay in rate becomes less and less.

Findings of other workers.

The early work by Thomas and Tompkins [28,29] stressed a constant rate of photolysis at constant temperature and lamp intensity.

A re-assessment of the photolysis by Jacobs and Tompkins [30] showed the rate to vary with time in a complex manner. They described the rate as decreasing initially for a considerable period of time before an acceleratory rate region occurred. Thereafter a period of constant rate of gas evolution followed.

A recent re-investigation by Pai Verneker [35] using particular wavelength ranges, showed the acceleratory region described by Jacobs and Tompkins to be absent when monochromatic 253.7 nm light was used, while irradiation with ultraviolet light of 184.9 plus 253.7 and 200 - 300 nm gave rise to the pressure-time plot as previously reported by the latter.

2. The use of a water filter between the cell window and the U.V. arc made no significant difference to the shape of the pressure-time plot for the photolysis of barium azide.

trapping centres for electrons.

The decay of reaction rate is attributed to the screening of the U.V. radiation by product formation on the surface of the azide, and not by depletion of centres necessary for reaction. This is substantiated by the re-irradiation of the underside of the irradiated pellet, whereupon a normal pressure-time plot was observed.

Findings of other workers.

Jacobs and Tompkins [30] and Verneker [35] attributed their deceleratory region to the consumption of defects necessary for reaction, while Verneker [35] explained his acceleratory region by supposing it to be caused by the photolysis of Ba_3N_2 formed earlier on in the photodecomposition. He based this on the fact that Ba_3N_2 purchased from K.and K. laboratories yielded an acceleratory pressure-time plot on U.V. photolysis.

Jacobs and Tompkins [30] postulated photo-emission from barium atoms formed in the first part of the reaction, to explain their acceleratory region.

6. The primary photolytic mechanism postulated for barium azide in this work, is based on trapped excitons or azide ions, leading to a bimolecular recombination of the above trapped entities, or trapped entities may interact with untrapped excited states, leading to photochemical changes.

The initial acceleratory rate found in this work could be attributed to anion vacancy production which occurs in the photolytic reaction as follows :-

For the overall reaction we have

$$2N_3^- \underset{}{\overset{h\nu}{\rightleftharpoons}} (N_3 \boxminus N_3)^{2-**} \longrightarrow 3N_2 + Ba + 4\boxminus$$

where $\boxminus$ = anion vacancy and * = exciton or excited state.

of Picien wax and cements for attaching the cell windows, and their use of crystals and powders for the photolysis is most unsatisfactory in the light of certain investigations performed in this work, in particular the problem of obtaining reproducible results from the photodecomposition of barium azide powders and crystals.

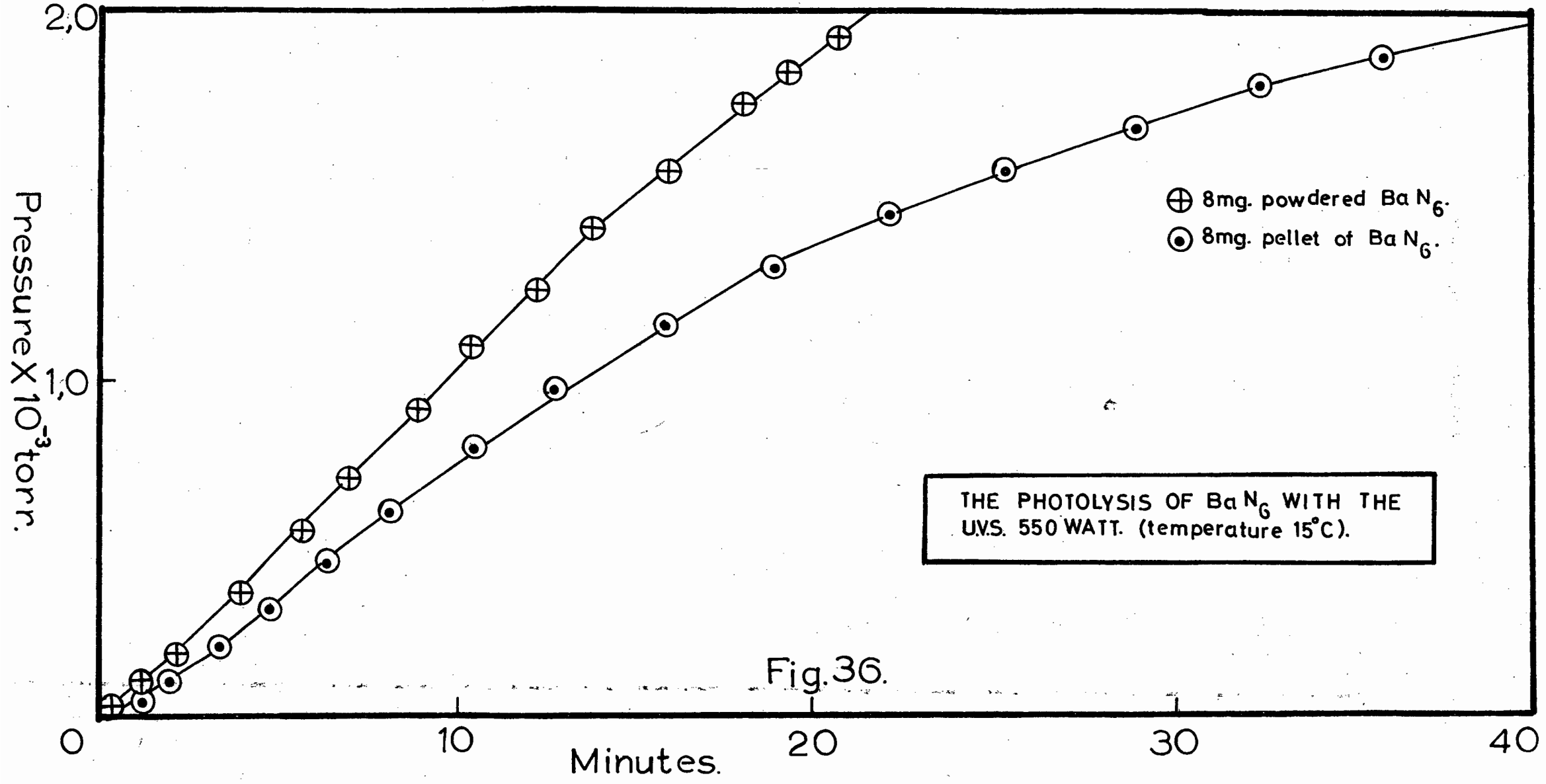
2,0
1,0
Pressure X 10^{-3} torr.
0
10
20
30
40
Minutes.
⊕ 8mg. powdered $Ba N_6$.
⊙ 8mg. pellet of $Ba N_6$.
THE PHOTOLYSIS OF $Ba N_6$ WITH THE U.V.S. 550 WATT. (temperature 15°C).

Fig.36.

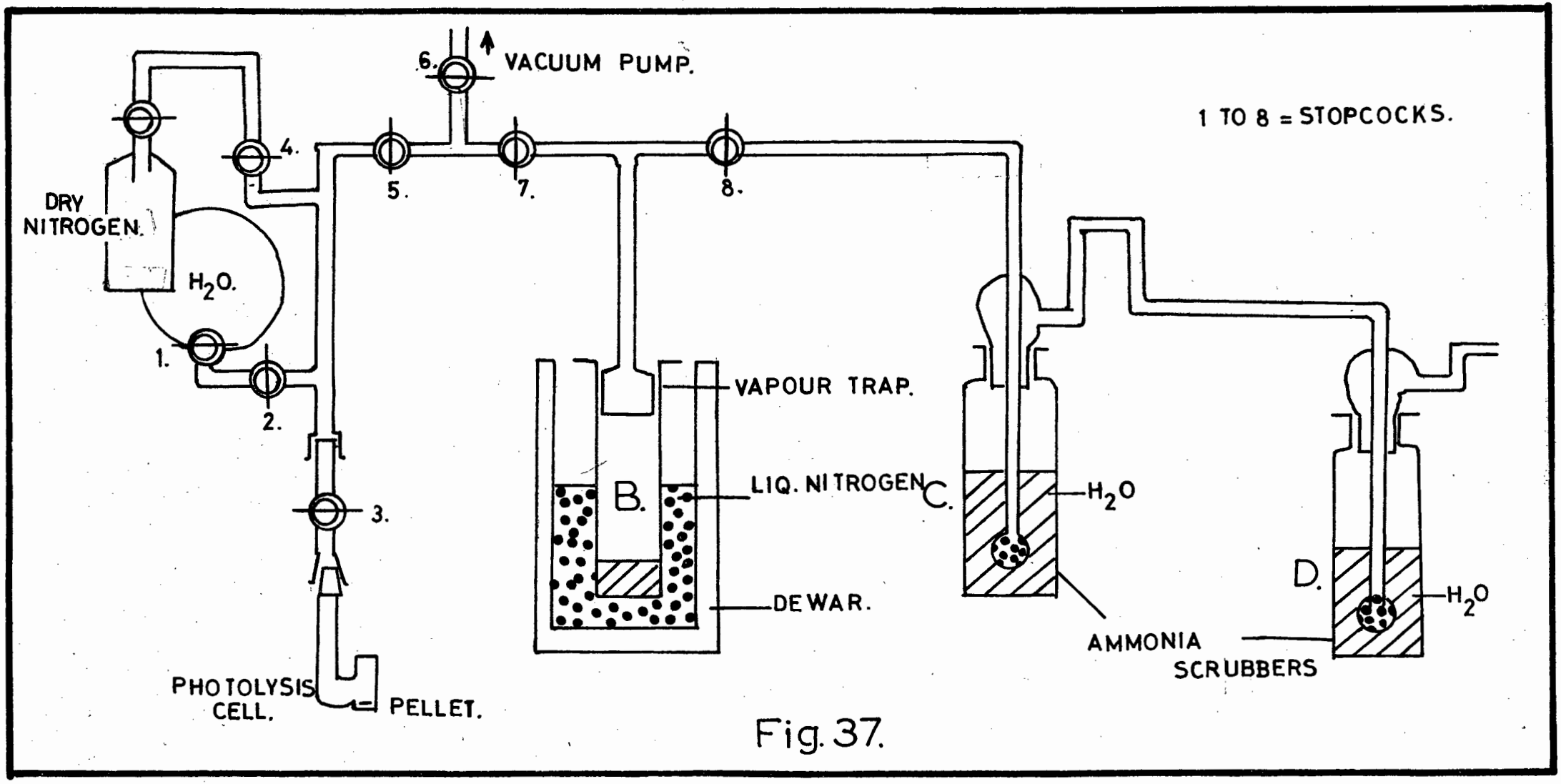
6.
VACUUM PUMP.
1 TO 8 = STOPCOCKS.
4.
5.
7.
8.
DRY
NITROGEN.
H_2O.
1.
2.
3.
VAPOUR TRAP.
B.
LIQ. NITROGEN
C.
H_2O
DEWAR.
D.
H_2O
AMMONIA
SCRUBBERS
PHOTOLYSIS
CELL.
PELLET.

Fig. 37.

NH_3 gas was then converted to NH_4OH by allowing it to vaporise and bubble through a known volume of water in the ammonia scrubbers C. and D. The amount of NH_4OH could then be obtained by titration.

Using the equation

$$BaN_3 + 4\ H_2O \longrightarrow Ba(OH)_2 + 2\ NH_3 + N + O_2$$

the weight of NH_3 and hence the weight of BaN_3 in the reaction product was obtained.

For 5 pellets photolysed at room temperature for 70 minutes, the percentage of BaN_3 in the reaction product was found to be as follows:-

Pellet no.	% BaN_3	Average %
1	79	
2	74	
3	65	73
4	80	
5	68	

For another five 200 mg pellets photolysed at the same temperature, but for 300 minutes, the values for BaN_3 present were as below.

Pellet no.	% BaN_3	Average %
1	38	
2	49	
3	33	40
4	43	
5	35	

These results lend support to the assumption that the photolysis of primary reaction products also occurs at the later stages of the photo-decomposition, leading to changes in the intensity dependence and the reaction rate.

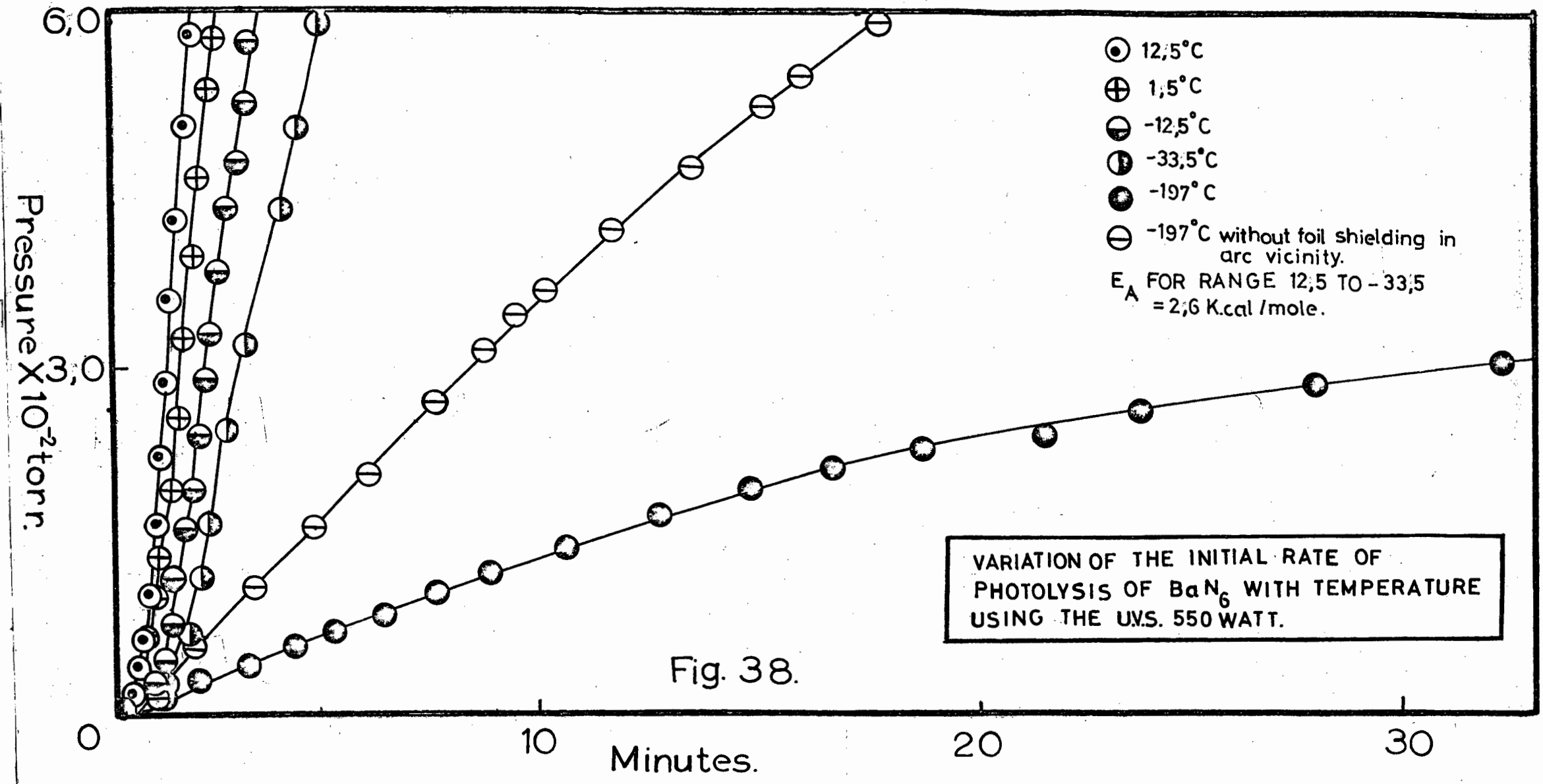
6,0
3,0
0
Pressure X 10^{-2} torr.
10
20
30
Minutes.
12,5°C
1,5°C
-12,5°C
-33,5°C
-197° C
-197°C without foil shielding in arc vicinity.
E_A FOR RANGE 12,5 TO -33,5 = 2,6 K.cal /mole.
VARIATION OF THE INITIAL RATE OF PHOTOLYSIS OF BaN_6 WITH TEMPERATURE USING THE U.V.S. 550 WATT.

Fig. 38.

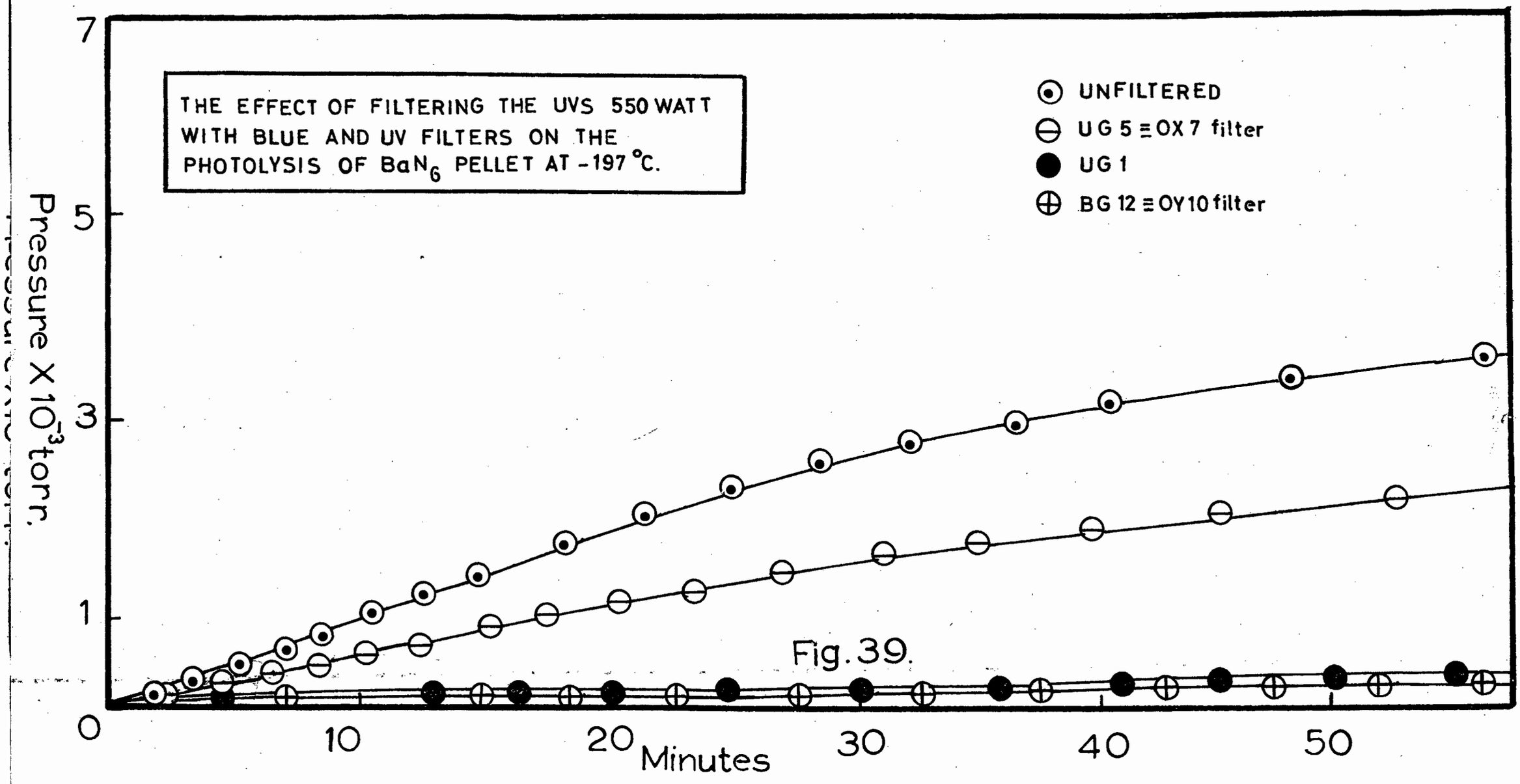
THE EFFECT OF FILTERING THE UVS 550 WATT WITH BLUE AND UV FILTERS ON THE PHOTOLYSIS OF BaN_6 PELLET AT -197 °C.
UNFILTERED
UG 5 ≡ OX 7 filter
UG 1
BG 12 ≡ OY10 filter
Pressure X 10^{-3} torr.
0
1
3
5
7
10
20
30
40
50
Minutes

Fig. 39.

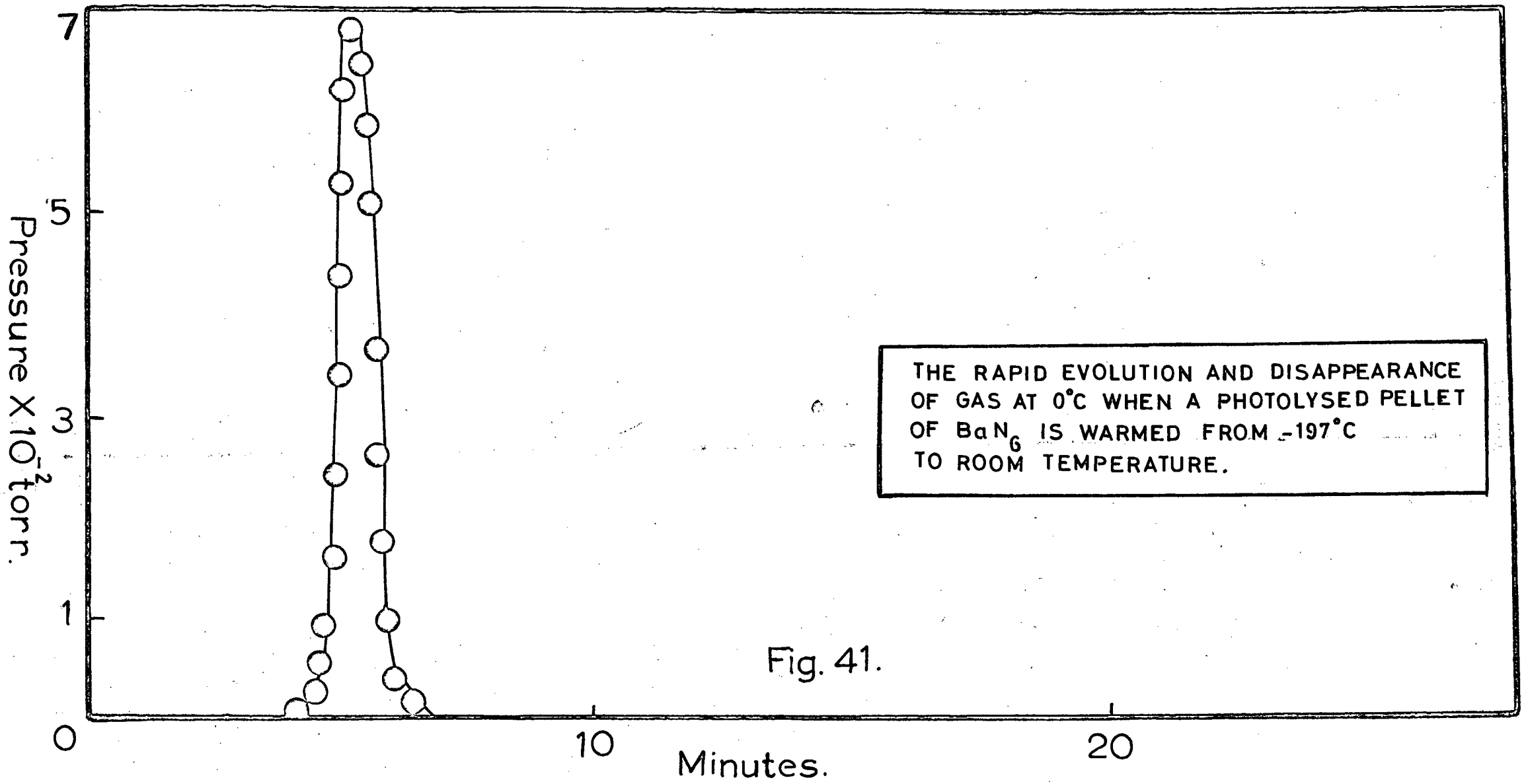
7
5
3
1
0
Pressure X 10^{-2} torr.
10
20
Minutes.
THE RAPID EVOLUTION AND DISAPPEARANCE OF GAS AT 0°C WHEN A PHOTOLYSED PELLET OF BaN_6 IS WARMED FROM -197°C TO ROOM TEMPERATURE.

Fig. 41.

likely to account for the bilateral symmetry of the pressure-time plot, in that 4 molecules enter the decomposition system, become transformed into 4 other entities of gas and become condensed in the cold trap. (N atoms could combine with O_2 to form NO_2).

Reaction ....(1) involves the introduction of 6 molecules of water for the production of only 2 molecules of ammonia.

The only positive way to determine whether in fact water was entering the cell system at the ice melting stage, was to exclude the formation of ice on the cell walls, when the liquid nitrogen dewar was lowered after photolysis.

This was achieved by immediately replacing the dewar containing liquid nitrogen, with a beaker containing propanol, before ice formation could take place. Apart from a very slight initial rise owing to a temperature effect on the system, no burst of gas evolution took place and significantly, the blackened pellet did not change colour even after being allowed to stand at room temperature for some hours.

Thus, by eliminating the formation of water on the outside of the cell, the mysterious gas evolution was completely suppressed. This conclusively proves that water derived from the melting ice, on the outside of the quartz photolysis cell, somehow is able to migrate through the quartz, as a result of the temperature changes involved, or by the U.V. and infrared radiation it is exposed to during photolysis or a combination of both factors. This effect does not occur when a beaker of water or a wet cloth is placed around the photolysis cell, after photolysis performed at higher temperatures.

Yet more evidence against the evolution of trapped nitrogen as theorised by other workers [32] in this field, is the vast amount of gas involved in this burst of gas. Fig. 41 shows that the pressure increases quite rapidly from 1×10^{-4} torr to 6×10^{-2} torr within a matter of seconds, which means that more gas is involved here than occurred during the average photolysis of a barium azide pellet.

his reported acceleratory rate must be due to the photolysis of Ba_3N_2

formed in the earlier photolytic reaction.

However, E.S.R.[6, 10, 11, 12, 14] studies have not as yet detected the presence of the N_3^{3-} ion.

Since in this work no late acceleratory region was found, and because there is evidence for the N_3^{2-} ion in E.S.R. studies, together with the observed fact of ammonia evolution when the photolysis products are mixed with water, BaN_3 instead of Ba_3N_2 is postulated here as a photolysis product.

From the results of filtering the high intensity mercury arc (Table 3 and figs. 39 and 40) it would appear that the most effective region of the ultra-violet spectrum for the photolysis of barium azide, is the narrow region between 200 and 220 nm. This seems reasonable on the grounds of higher energies of the photons at these short wavelengths. Provided that these photons can be utilised in accordance with the Quantum rule, greater rates should result when using this region of the ultra-violet spectrum for photodecomposition.

5.6. The photolysis of Barium Azide pellets using the low intensity lamp.

For this section, the U.V.S. employed was the portable Hanovia low intensity lamp, whose principal output was at 253,7 nm. The lamp was placed at a height of 1 cm from the cell window. An arc warm up time of 12 minutes was used.

IN THIS SECTION BARIUM AZIDE PELLETS WILL MEAN 8 mg OF DEHYDRATED BARIUM AZIDE MONOHYDRATE, GROUND FOR 4 MINUTES AND PELLETED AT 2000 lbs/sq.inch IN A 5 mm EVACUABLE DIE.

5.6.1. The low intensity photolysis of Barium Azide pellets.

In order to investigate the effects of the 253,7 nm region of the spectrum on the photolysis of barium azide, it was decided to use the low intensity lamp for this, especially since most of the earlier work on the photolysis has been done with such a lamp.

The sigmoid character of the pressure-time plot for the photolysis of barium azide pellets with the low intensity lamp is not as pronounced as with the higher intensity arcs. However, the basic features are still the same, with an initial acceleratory region, followed by a slow decay period, which persists for long periods of irradiation. This is illustrated in fig. 42, which also shows the variation of the photolytic rate with temperature.

5.6.2. The activation energy for the low intensity photolysis of Barium Azide pellets.

Owing to the unapplicability of the Prout - Tompkins[107] or the Avrami - Erofeyev[108] equation, and because the pressure-time plots were fairly linear, the split run method was employed.

For the temperature range 21 to -10°C, the average activation energy was found to be 2,5 k.cal./mole, using the split run technique,

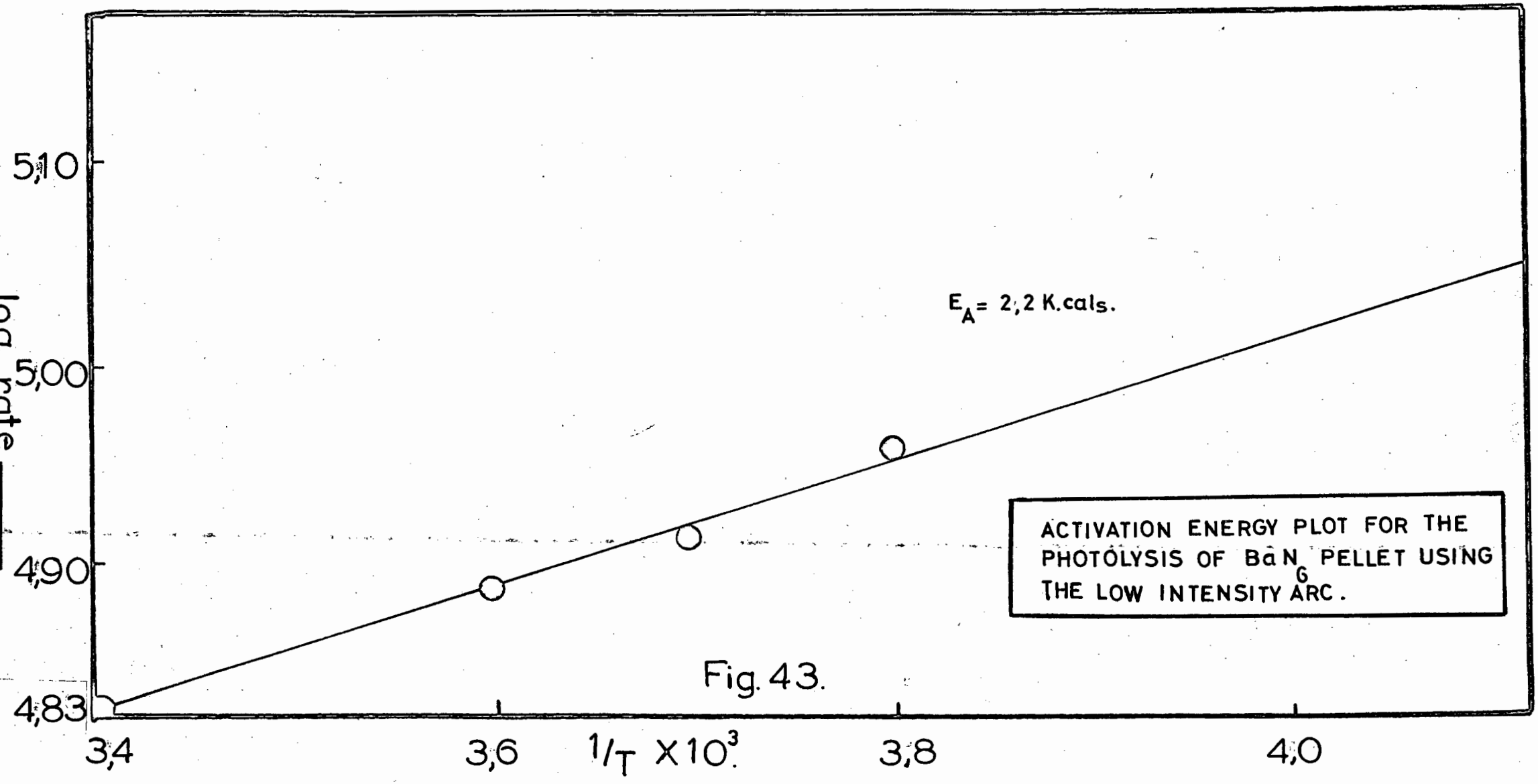
5,10
5,00
4,90
4,83
-log rate
3,4
3,6
3,8
4,0
1/T X10³
E_A = 2,2 K.cals.
ACTIVATION ENERGY PLOT FOR THE PHOTOLYSIS OF BaN6 PELLET USING THE LOW INTENSITY ARC.

Fig. 43.

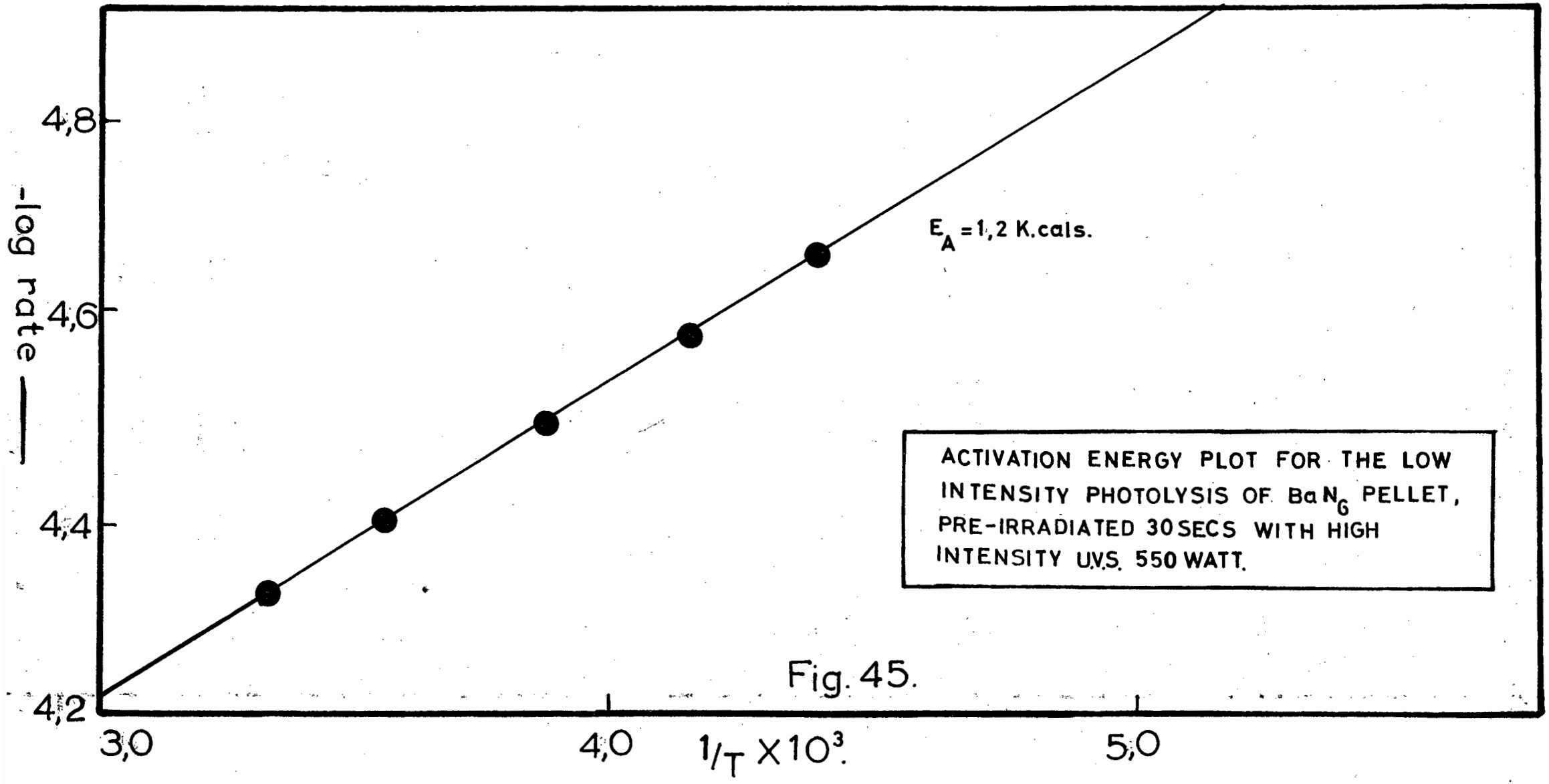
4,8
4,6
4,4
4,2
-log rate —
3,0
4,0
5,0
1/T X10³.
E_A = 1,2 K.cals.
ACTIVATION ENERGY PLOT FOR THE LOW INTENSITY PHOTOLYSIS OF Ba N6 PELLET, PRE-IRRADIATED 30 SECS WITH HIGH INTENSITY U.V.S. 550 WATT.

Fig. 45.

DISCUSSION OF RESULTS OF SECTION 5.6.1. TO 5.6.4.

As with the high intensity photolysis, the shapesof the pressure-time plots were again different from those obtained by Thomas and Tompkins[28, 29], Jacobs and Tompkins[30] and Pai Verneker[35].

The average value of 2,5 k.cals./mole for the activation energy of the low intensity photolysis of barium azide pellets for the temperature range -10 to 21°C is in keeping with the value of 3 k.cals./mole obtained for the photolysis using the medium intensity U.V.S. S100. This value of 2,5 k.cals./mole is half that obtained by Jacobs and Tompkins[30] for the photolysis of barium azide using the low intensity lamp, with a wavelength of 253,7 nm as the principal output.

From the experiments on high intensity pre-irradiation, it would appear that either the lower wavelength region (200 - 220 nm) is more effective in creating reaction centres, or that the much higher intensity of the more or less continuous spectrum of the high intensity mercury arc is responsible. However, from the experiments on the filtering of the high intensity arc (section 5.5) it seems more likely that the creation of reaction centres occurs more readily with the shorter wavelengths of U.V. radiation. This assumption is also supported by the fact that a lowering of activation energy occurs with pre-irradiation from the high intensity arc.

5.7. The Ultra-Violet photolysis of Lithium Azide pellets.

In this section, the U.V.S. S100 was employed with an arc warm up time of 12 minutes and an arc height of 9 cm. from the cell window. Lithium azide was prepared by neutralising a concentrated solution of lithium hydroxide with 3% hydrazoic acid. The water was removed by the vacuum oven at 40°C. Throughout the dehydration period, the solution was kept acid by addition of hydrazoic acid.

LITHIUM AZIDE PELLETS WILL MEAN LITHIUM AZIDE GROUND FOR 4 MINUTES, 8 mg OF WHICH HAS BEEN PELLETED AT 2000 lbs./ sq.inch, IN A 5 mm EVACUABLE DIE.

All handling of material had to be performed in the drybox under subdued lighting, owing to its deliquescent nature and light sensitivity.

5.7.1. A comparison of the pressure-time plots for the Ultra-Violet photolysis of Barium and Lithium Azide pellets.

Prout and Liddiard[58] have studied the thermal decomposition of lithium azide, in particular the effect of pre-irradiation by X-rays, γ-rays (Co^{60}) and ultraviolet light. These workers have demonstrated that lithium azide is extremely sensitive to the above radiations. This prompted an investigation into the ultraviolet photolysis of this salt, especially since this has not been previously reported. A comparison between lithium and barium azide would also be useful, since this would give some indication as to whether the pressure-time plots reported for barium azide could also be extended to the alkali metal azides.

Fig. 46 shows a comparison of the pressure-time plots obtained for the photolysis of lithium and barium azide pellets at 0°C. It can be seen that lithium azide is vastly more sensitive to ultraviolet radiation, the sigmoid nature of the curve being very evident, resembling closely the pressure-time plots for the unirradiated thermal decomposition obtained by Prout and Liddiard[58].

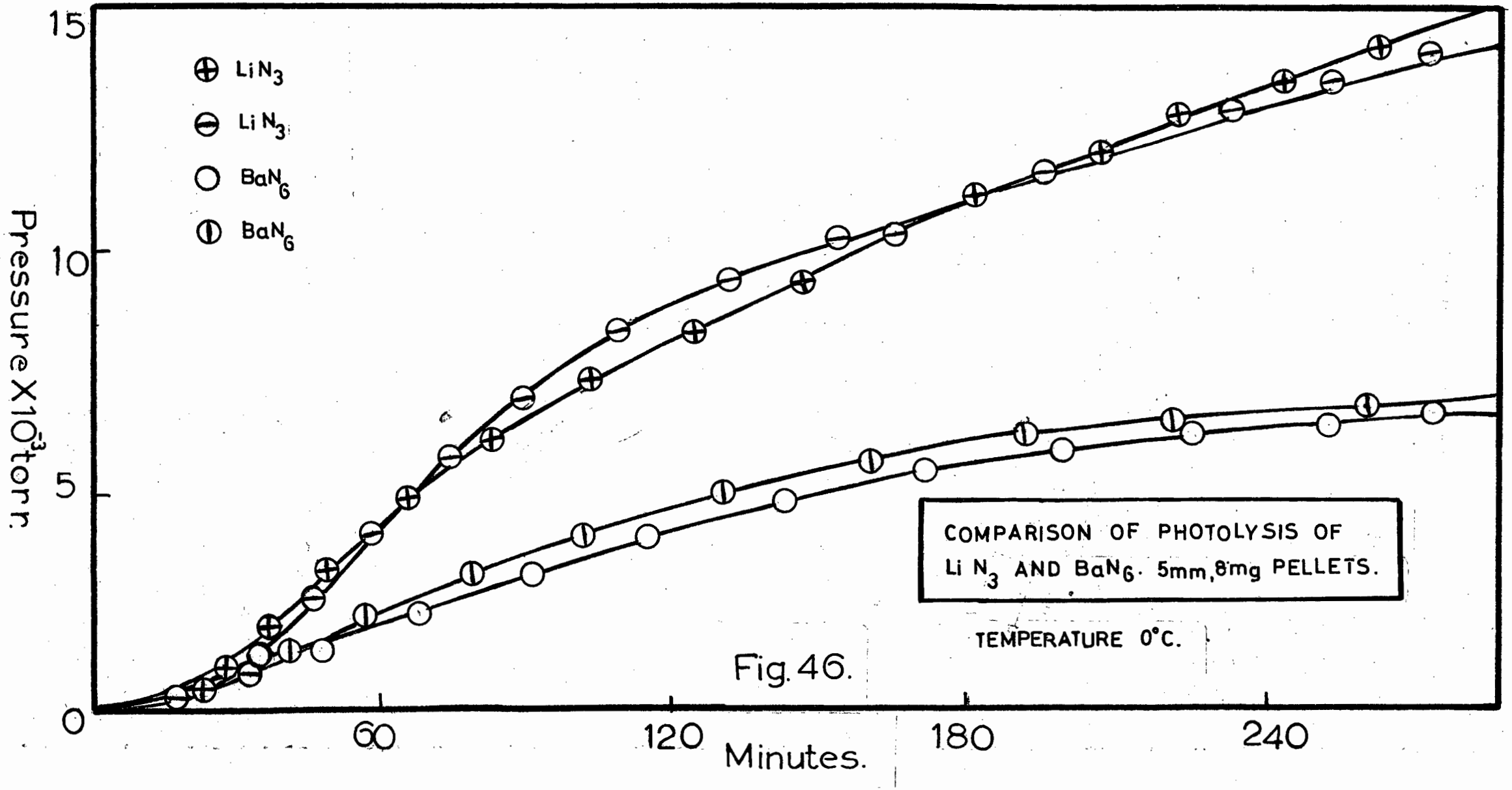
15
10
5
0
Pressure X 10^{-3} torr.
LiN_3
LiN_3
BaN_6
BaN_6
60
120
180
240
Minutes.
COMPARISON OF PHOTOLYSIS OF
LiN_3 AND BaN_6. 5mm, 8mg PELLETS.
TEMPERATURE 0°C.

Fig. 46.

The initial acceleratory phase is more pronounced than for barium azide and the onset of the decay period is clearly evident. This deceleratory phase soon flattened out and led to a constant rate of photolysis for the final rate period, after prolonged photolysis.

The appearance of the pellet after photolysis was a dark brown.

5.7.2. Reproducibility of results for the Ultra-Violet photolysis of Lithium Azide pellets.

The pressure-time plots for the photolysis were highly reproducible under standardised conditions and fig. 47 illustrates graphically the extent of reproducibility obtained for five decompositions at $0^{\circ}C$.

5.7.3. Activation Energies for the photolysis of Lithium Azide pellets.

As with barium azide, activation energies were determined for a high and a low temperature range. The shapes of the pressure-time plots were however more sigmoid in nature, and hence the split run technique was replaced by the method of individual decompositions, using appropriate equations to describe the acceleratory and deceleratory stages.

Fig. 47a illustrates a typical pressure-time plot for the ultraviolet photolysis of a lithium azide pellet at $0^{\circ}C$. The acceleratory period ABC can be described perfectly by the Avrami-Erofeyev[107,108] equation, with $n = 3$, if the final pressure p_f is taken as the pressure recorded after 300 minutes of photolysis. This time was arbitrarily selected because of the failure of the rate to proceed to zero even after prolonged photolysis. At 300 minutes however, the rate begins to reach a more or less constant value and this was then taken as a convenient point to select the final pressure p_f.

Using the above equation in the form below,

$$\left[- \log \left(1 - p/p_f \right) \right]^{1/3} = k_1 t + c$$

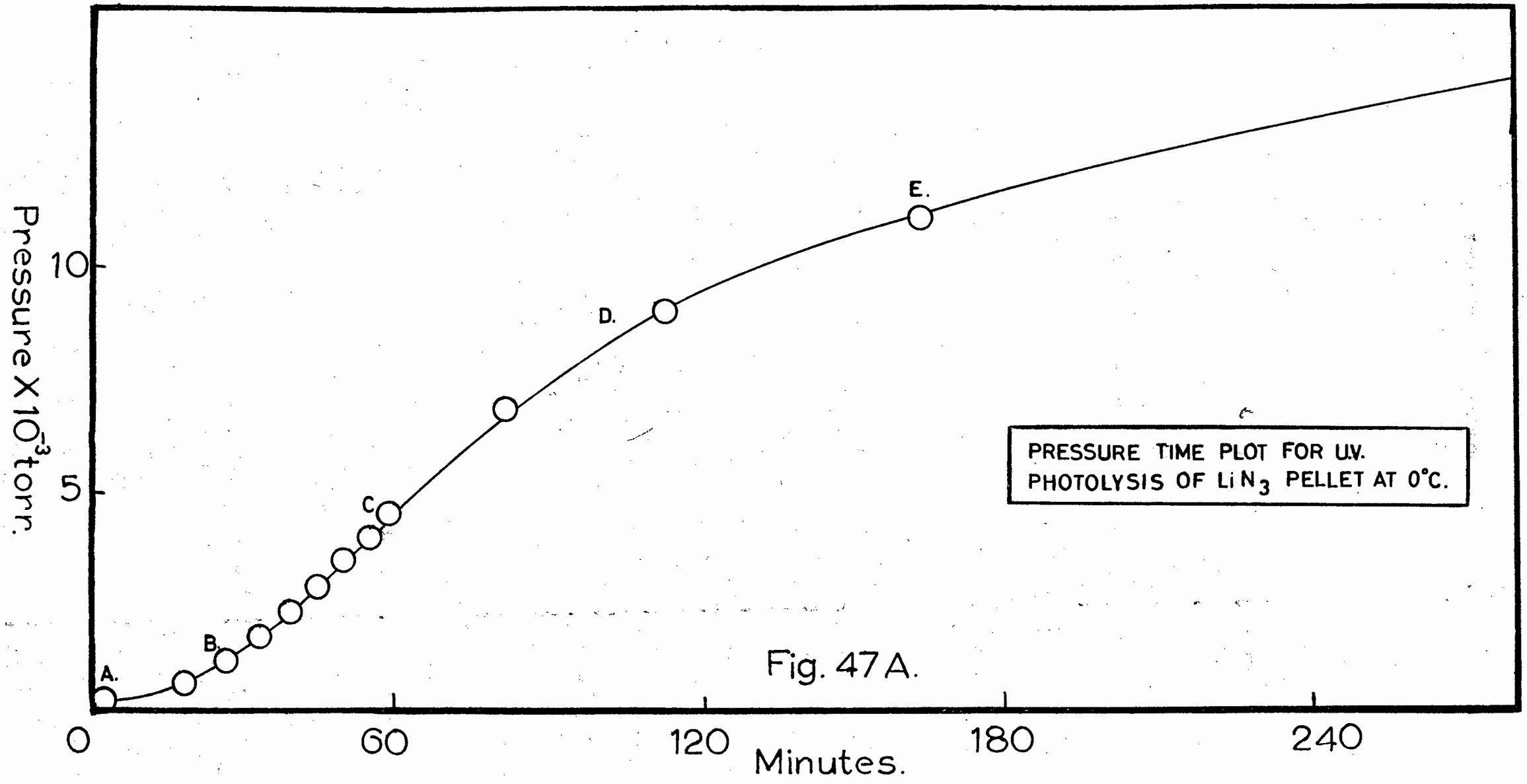
Pressure X 10^{-3} torr.
10
5
0
60
120
180
240
Minutes.
A.
B.
C.
D.
E.
PRESSURE TIME PLOT FOR U.V.
PHOTOLYSIS OF LiN_3 PELLET AT 0°C.

Fig. 47A.

where p = pressure

p_f = final pressure

k_1 = rate constant for acceleration

t = time in minutes

a plot of $\left[- \log (1 - p/p_f)\right]^{1/3}$ versus t for the acceleratory period, yielded a perfectly linear plot as indicated in fig. 47b. The relevant values plotted are listed below.

$\left[- \log (1 - p/p_f)\right]^{1/3}$	t
0,258	17
0,324	27
0,374	33
0,413	38
0,447	45
0,479	49

The decay reaction of the photolysis could not be described by the contracting sphere formula

$$1 - (1 - p/p_f)^{1/3} = k_2 t$$

because the photodecomposition is limited to the surface layer of the pellet only. A careful mathematical analysis of the deceleratory phase showed that it could be defined as follows:-

$$1/ - \log (p/p_f) = k_2 t$$

Fig. 47c shows a plot of $1/ - \log (p/p_f)$ versus t to be perfectly linear. The plotted values are listed below.

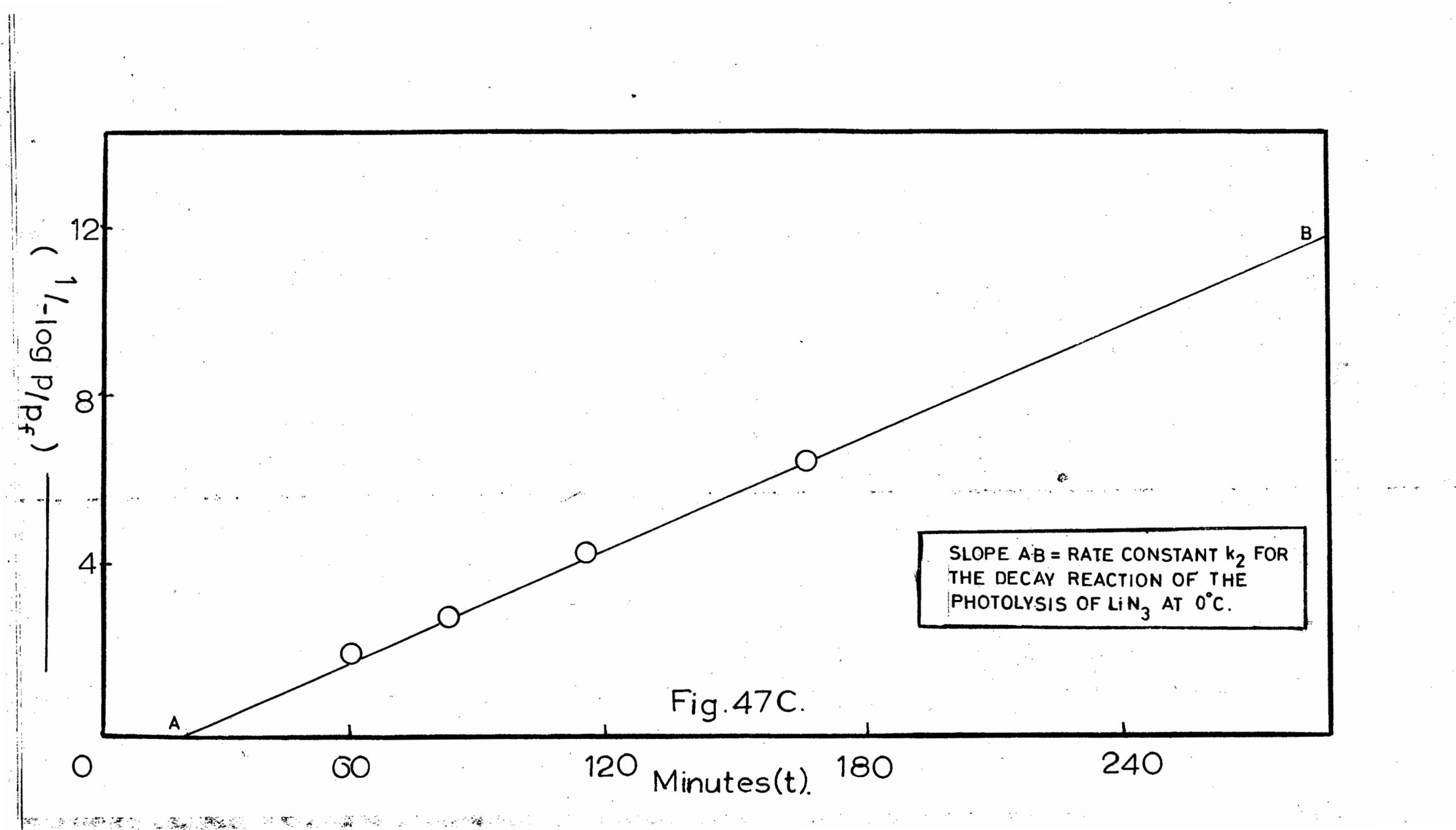
12
8
4
0
60
120
180
240
Minutes(t).
A
B
SLOPE AB = RATE CONSTANT k_2 FOR THE DECAY REACTION OF THE PHOTOLYSIS OF LiN_3 AT 0°C.

Fig.47C.

Table 5.

°C	$1/T \times 10^3$ (A)	$-\log k_1$ (B)	$-\log k_2$ (C)	slope A vs B $\times 10^3$	slope A vs C $\times 10^3$	E_{A_1}	E_{A_2} cals./mole
18,0	3,439	4,4900	4,8275				
1,0	3,651	4,5401	4,8853	0,218	0,229	995	1047
-10,0	3,810	4,5703	4,9168				
-18,0	3,921	4,6050	4,9371				

Figs. 48 and 49 show the relevant activation energy plots for Tables 4 and 5 respectively.

The activation energy appears to increase in the higher temperature range.

5.7.4. The variation of photolytic rate with intensity of ultraviolet radiation, for Lithium Azide pellets.

To ascertain whether a bimolecular decomposition of the azide ion was also involved in the early photodecomposition of lithium azide pellets, the effect of varying the intensity on the photolytic rate was studied.

The plot of rate versus intensity shown in fig. 50 indicates a second order dependence on intensity of irradiation. This is confirmed by the plot of rate versus $(\text{intensity})^2$ depicted in fig. 51, as the above plot is linear.

5.7.5. The effect of pre-irradiation with X-rays on the photolysis of Lithium Azide pellets.

Prout and Liddiard[58] have shown that X-rays will sensitise lithium azide, with great enhancement of the subsequent thermal decomposition. It was of interest to note whether X-rays would in fact sensitise lithium azide pellets to ultraviolet photolysis.

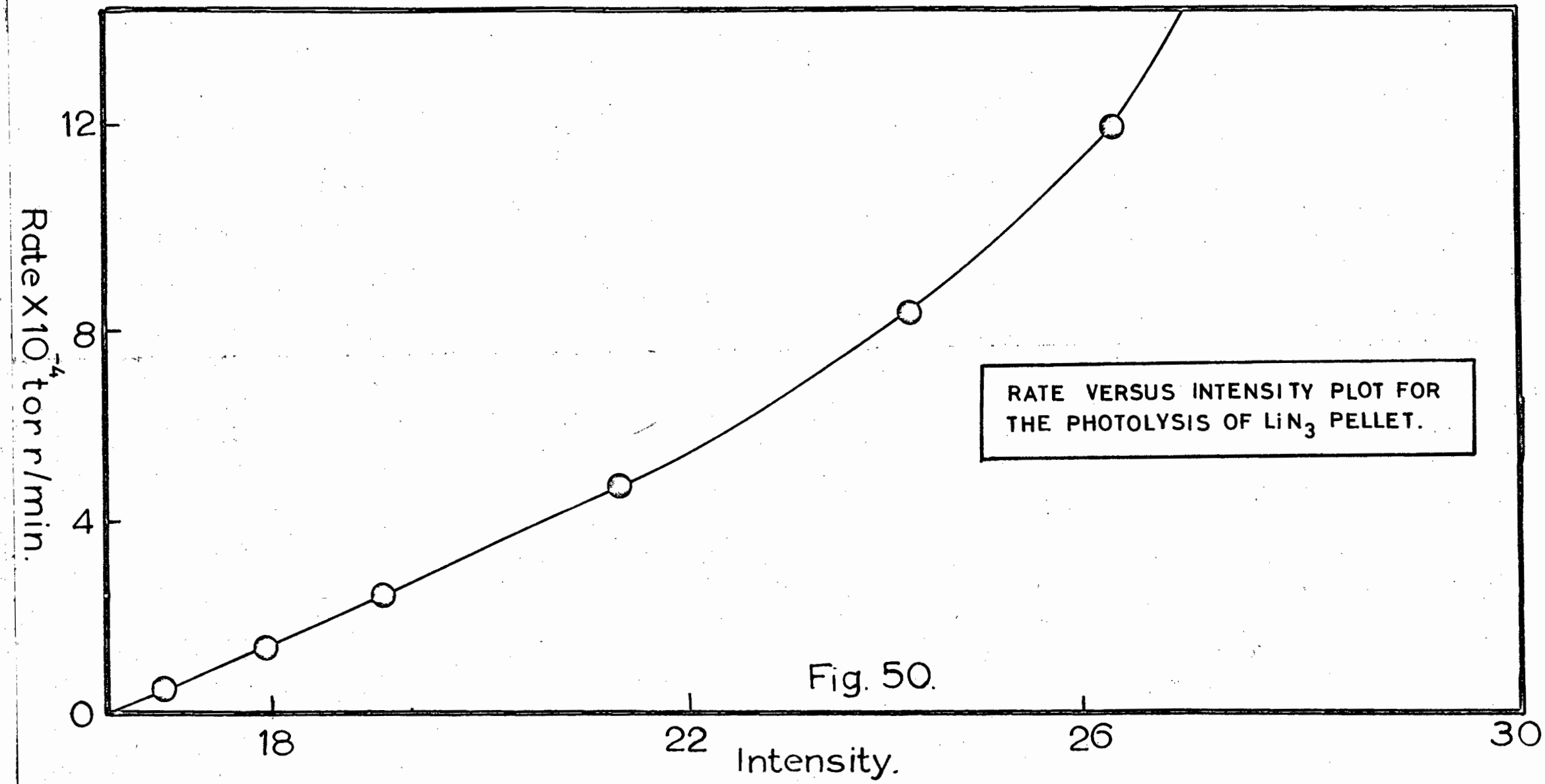
RATE VERSUS INTENSITY PLOT FOR THE PHOTOLYSIS OF LiN_3 PELLET.
Rate X 10^{-4} torr/min.
0
4
8
12
18
22
26
30
Intensity.

Fig. 50.

Fig. 52 shows the effect on the photolysis of lithium azide pellets when pre-irradiated for 7 hrs. with X-rays Mo 40 KV 20 ma.

It is seen that the acceleratory phase is depressed considerably in spite of an initially faster rate, and the decay period is not as marked as in the unirradiated salt.

5.7.6. The effect of γ-ray pre-irradiation on the photolysis of Lithium Azide pellets.

Since γ-ray pre-irradiation also affects the subsequent thermal decomposition, and since this radiation is exceedingly penetrating, it was decided to investigate the effects of 1 M roentgens γ-ray (Co^{60}) pre-irradiation on the photolysis. A more drastic change in the pressure-time plot was expected in the light of the findings of X-ray pre-irradiation.

The result of the above γ-ray irradiation is illustrated in fig. 53. The decomposition temperature was $0^{\circ}C$.

The shapes of the pressure-time plots show marked changes from the unirradiated plots, in that the initial rate of decomposition is drastically suppressed and the period for the onset of the acceleratory phase has been doubled. After this phase, the photodecomposition proceeded as for the unirradiated salt.

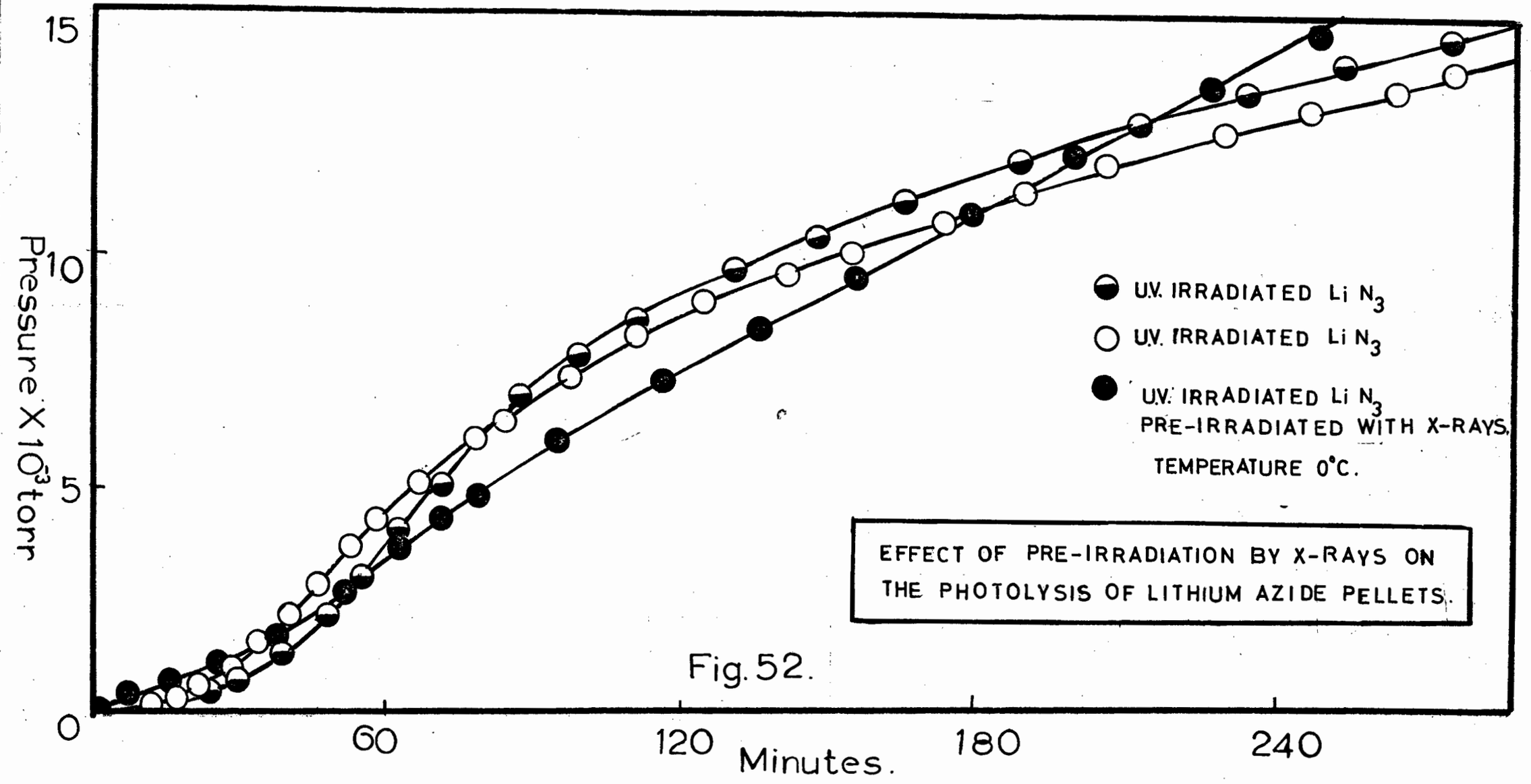
15
10
5
0
Pressure X 10³ torr
60
120
180
240
Minutes.
U.V. IRRADIATED Li N3
U.V. IRRADIATED Li N3
U.V. IRRADIATED Li N3
PRE-IRRADIATED WITH X-RAYS.
TEMPERATURE 0°C.
EFFECT OF PRE-IRRADIATION BY X-RAYS ON
THE PHOTOLYSIS OF LITHIUM AZIDE PELLETS.

Fig. 52.

5.8. Radiolysis of some inorganic azides.

5.8.1. A preliminary study of the radiolysis, by X-rays, of Barium, Strontium, Sodium and Lithium Azides.

IN THIS SECTION PYREX SAMPLE CELLS WITH THIN ALUMINIUM FOIL OR THIN PYREX WINDOWS WERE USED. THE X-RAY GENERATOR WAS A PHILIPS TYPE PW 1009 CAPABLE OF DELIVERING 1 000 WATTS (50 kV 20 mA). NO FILTER WAS USED WITH THE Cu AND Mo TUBES EMPLOYED.

The pressure-time plots for the above azides, irradiated with X-rays from a Cu or Mo target operated at 40 kV, 20 mA, were found to be linear, even after twenty hours continuous irradiation. Fig. 55 illustrates the pressure-time plots for barium, strontium, sodium and lithium azides, at a radiolysis temperature of $0^{\circ}C$. The above observations apply to powders, crystals and pellets.

Of the above azides, barium azide proved to be the most reactive, as can be seen from fig. 55. Sodium and lithium followed next, while strontium azide gave very low rates of radiolysis. Sodium and lithium azides were almost completely transparent to the X-rays used, while barium azide was more opaque. This might account for its higher reactivity.

5.8.2. The radiolysis of Sodium Azide by X-rays.

For the purpose of formulating reaction mechanisms for the radiolysis of azides, activation energies and the dependence of the radiolytic rates on the intensity of X-irradiation was investigated for the azides mentioned in section 5.8.1.

Owing to the small evolution of gas with sodium azide pellets, fine crystals of B.D.H. sodium azide were employed in the decompositions, and the results quoted below are for crystals and Mo target operated at 50 kV, 20 mA.

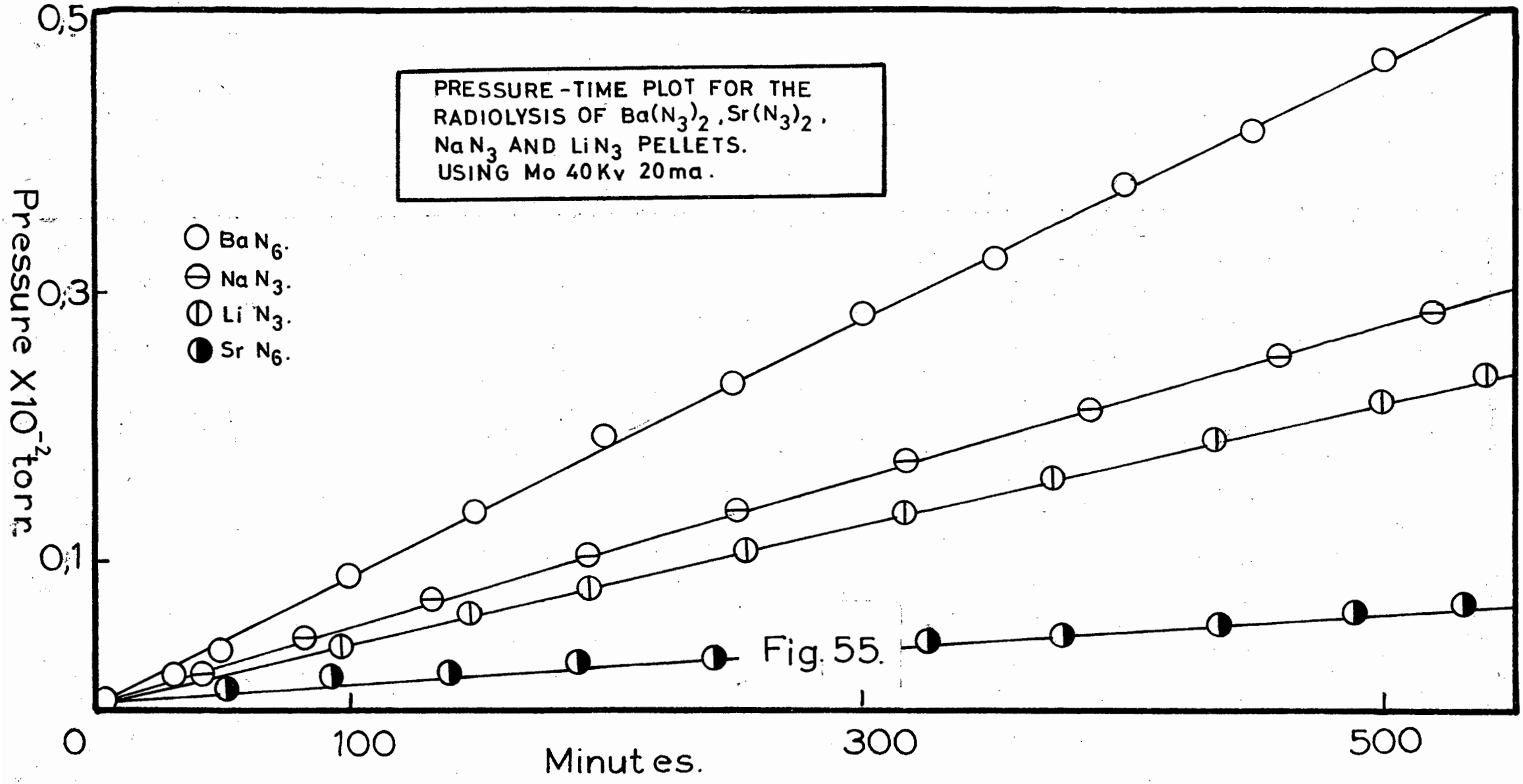
PRESSURE-TIME PLOT FOR THE RADIOLYSIS OF $Ba(N_3)_2$, $Sr(N_3)_2$, NaN_3 AND LiN_3 PELLETS. USING Mo 40Kv 20ma.
BaN_6.
NaN_3.
LiN_3.
SrN_6.
Pressure $X10^{-2}$ torr.
0,5
0,3
0,1
0
100
300
500
Minutes.

Fig. 55.

Fig. 56 shows the activation energy plots for four decompositions using the split run technique. Table 6 lists the relevant values used in the calculation of the activation energies. This table shows that the average activation energy is of the order of 4 k.cals./mole, irrespective of the temperature range used.

TABLE 6.

°C	1/T x 10^3	-log rate	slope of log rate vs 1/T	E_A in k.cals./mole
14,5	3,478	5,0996		
11,0	3,521	5,1415		
6,5	3,577	5,1805		
0,5	3,656	5,2034	0,782 x 10^3	3,6
-7,5	3,767	5,2924		
-11,0	3,817	5,3468		
-16,5	3,898	5,3788		
14,0	3,484	5,0999		
8,0	3,559	5,1615		
-7,5	3,767	5,3000	0,949 x 10^3	4,3
-17,0	3,906	5,3734		
-26,5	4,057	5,4952		
-16,0	3,891	5,1315		
-24,0	4,016	5,2062	0,872 x 10^3	4,1
-30,0	4,115	5,2579		
-35,0	4,202	5,3152		
-2,0	3,690	5,2020		
-11,5	3,824	5,2950	0,734 x 10^3	3,3
-20,0	3,953	5,4271		
-25,0	4,032	5,4535		
Average Activation Energy =				3,8

The dependence of the radiolytic rate on the intensity of irradiation was determined. This was found to be quite linear as is depicted in fig. 57.

After X-radiolysis, in all the temperature ranges investigated, the salt was coloured a deep yellow.

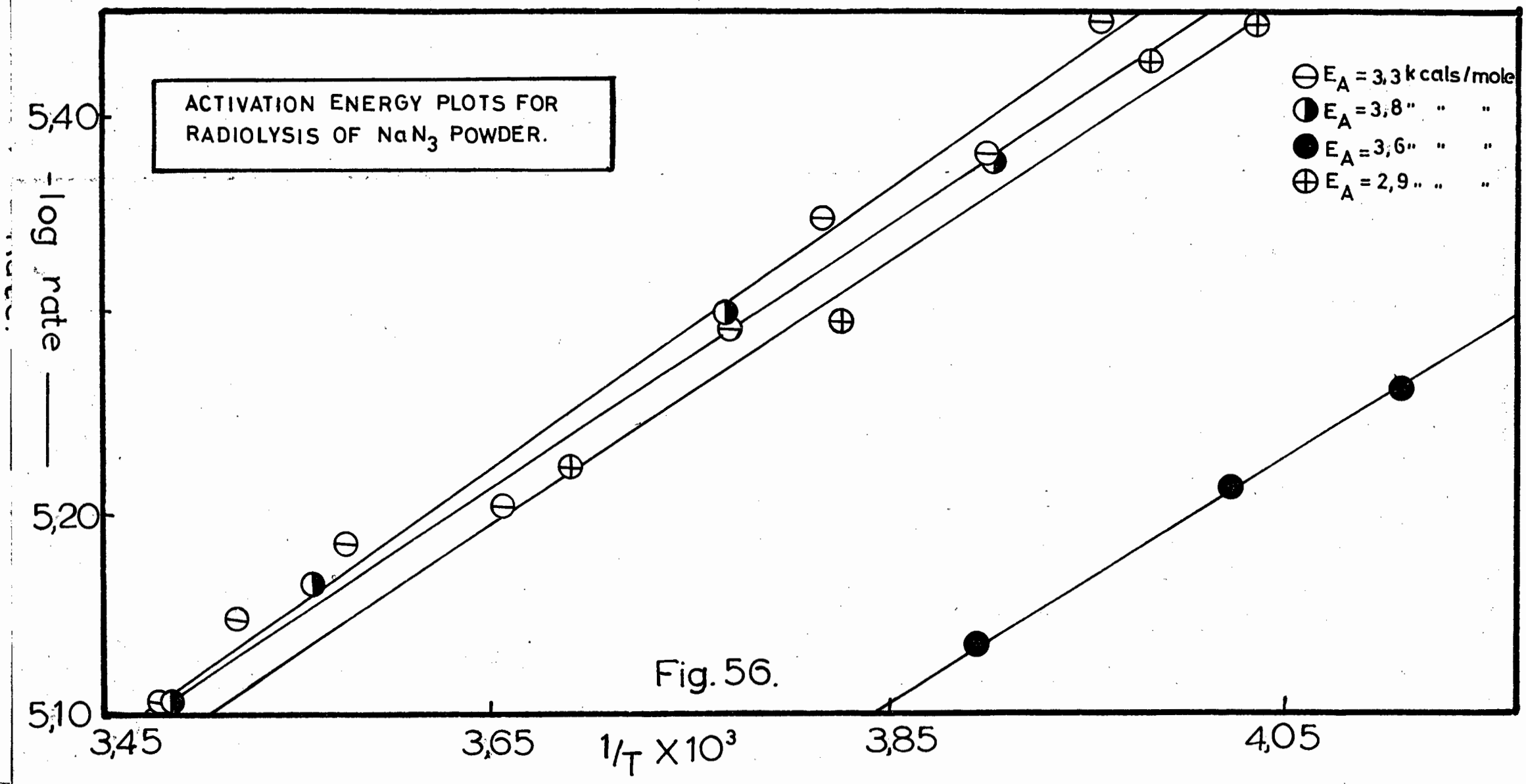
ACTIVATION ENERGY PLOTS FOR
RADIOLYSIS OF NaN_3 POWDER.
E_A = 3,3 k cals/mole
E_A = 3,8 " " "
E_A = 3,6 " " "
E_A = 2,9 " " "
5,40
5,20
5,10
-log rate
3,45
3,65
3,85
4,05
$1/T \times 10^3$

Fig. 56.

5.8.3. The radiolysis of Lithium Azide pellets.

IN SECTIONS 5.8.3. TO 5.8.5. LITHIUM AZIDE PELLETS WILL MEAN 200 mg OF LITHIUM AZIDE CRYSTALS, GROUND FOR 4 MINUTES AND PELLETED AT 4 000 lbs./sq.inch IN A 14 mm EVACUABLE DIE.

5.8.4. Reproducibility of results for the radiolysis of Lithium Azide pellets.

A series of decompositions was carried out under standardised conditions at $0^{o}C$, in order to ascertain whether the radiolytic rates were reproducible.

The high degree of reproducibility of the pressure-time plots obtained is depicted graphically in fig. 60.

5.8.5. Activation energies for the radiolysis of Lithium Azide pellets.

As in the case of sodium azide, the dependence of the radiolytic rate on the intensity of irradiation was perfectly linear. This is indicated in fig. 58.

The determination of activation energies using the split run method, for the radiolysis of lithium azide for various temperature ranges yielded much lower values to those obtained for the radiolysis of sodium azide. Table 7 lists the relevant data for the calculation of these values, while fig. 59 shows the plotted values of - log rate versus 1/T. An average value of 892 cals./mole was obtained for the temperature ranges investigated.

Extensive colour centre formation occurred, which was fairly stable at room temperature. The colour of the pellet after radiolysis ranged from a light blue to deep purple at low temperatures.

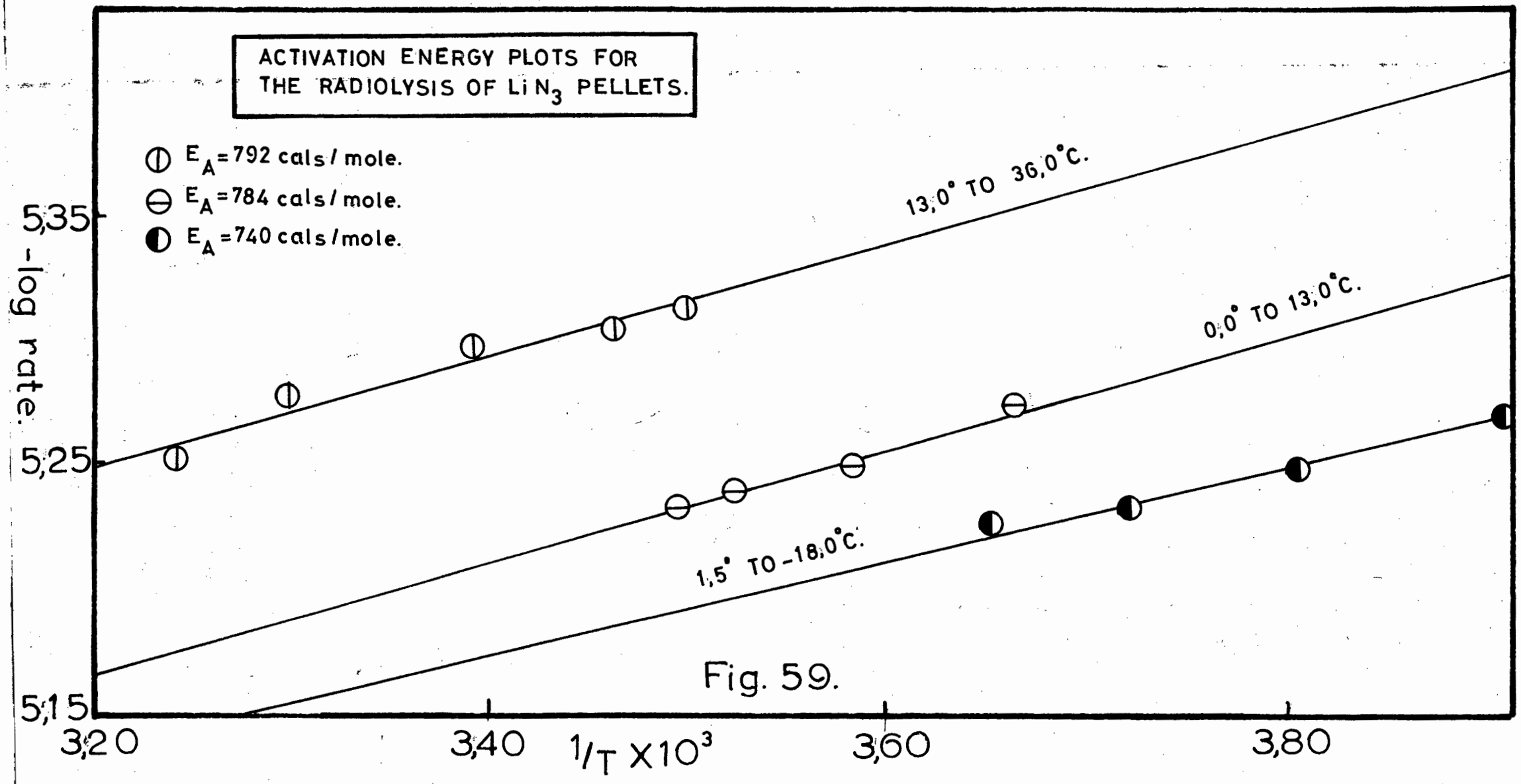
ACTIVATION ENERGY PLOTS FOR THE RADIOLYSIS OF LiN_3 PELLETS.
E_A = 792 cals / mole.
E_A = 784 cals / mole.
E_A = 740 cals / mole.
13,0° TO 36,0°C.
0,0° TO 13,0°C.
1,5° TO -18,0°C.
5,35
5,25
5,15
- log rate.
3,20
3,40
3,60
3,80
$1/T \times 10^3$

Fig. 59.

TABLE 7.

°C	$1/T \times 10^3$	- log rate (p/t)	slope log rate versus 1/T	E_A in cals./mole
-18,0	3,922	5,2810		
-10,5	3,810	5,2579	$0,187 \times 10^3$	852
-4,0	3,717	5,2432		
1,5	3,649	5,2300		
0,0	3,660	5,2743		
6,5	3,577	5,2520	$0,198 \times 10^3$	903
11,0	3,521	5,2400		
13,0	3,497	5,2341		
13,0	3,497	5,3098		
16,0	3,460	5,3054		
22,0	3,390	5,3000	$0,200 \times 10^3$	911
31,0	3,289	5,2757		
36,0	3,236	5,2518		
Average value for E_A				892

5.8.6. The effect of pre-irradiation by ultra-violet light on the radiolysis of Lithium Azide pellets.

The effect of pre-irradiation of lithium azide pellets by X-rays on the subsequent U.V. photolysis has been investigated in section 5.7.5 and it was found that in spite of a slightly higher initial rate of photolysis, a depressed acceleratory phase resulted, together with a slower deceleratory period. It was therefore of interest to see whether there would be any effect on the rate and shape of the pressure-time plots for the radiolysis of lithium azide pellets, pre-irradiated with ultraviolet light.

Fig. 61 shows the effect of various periods of ultraviolet pre-irradiation on the radiolytic rate at 0°C. The lowering of the radiolytic rate appears to be directly proportional to the length of the ultraviolet pre-irradiation period.

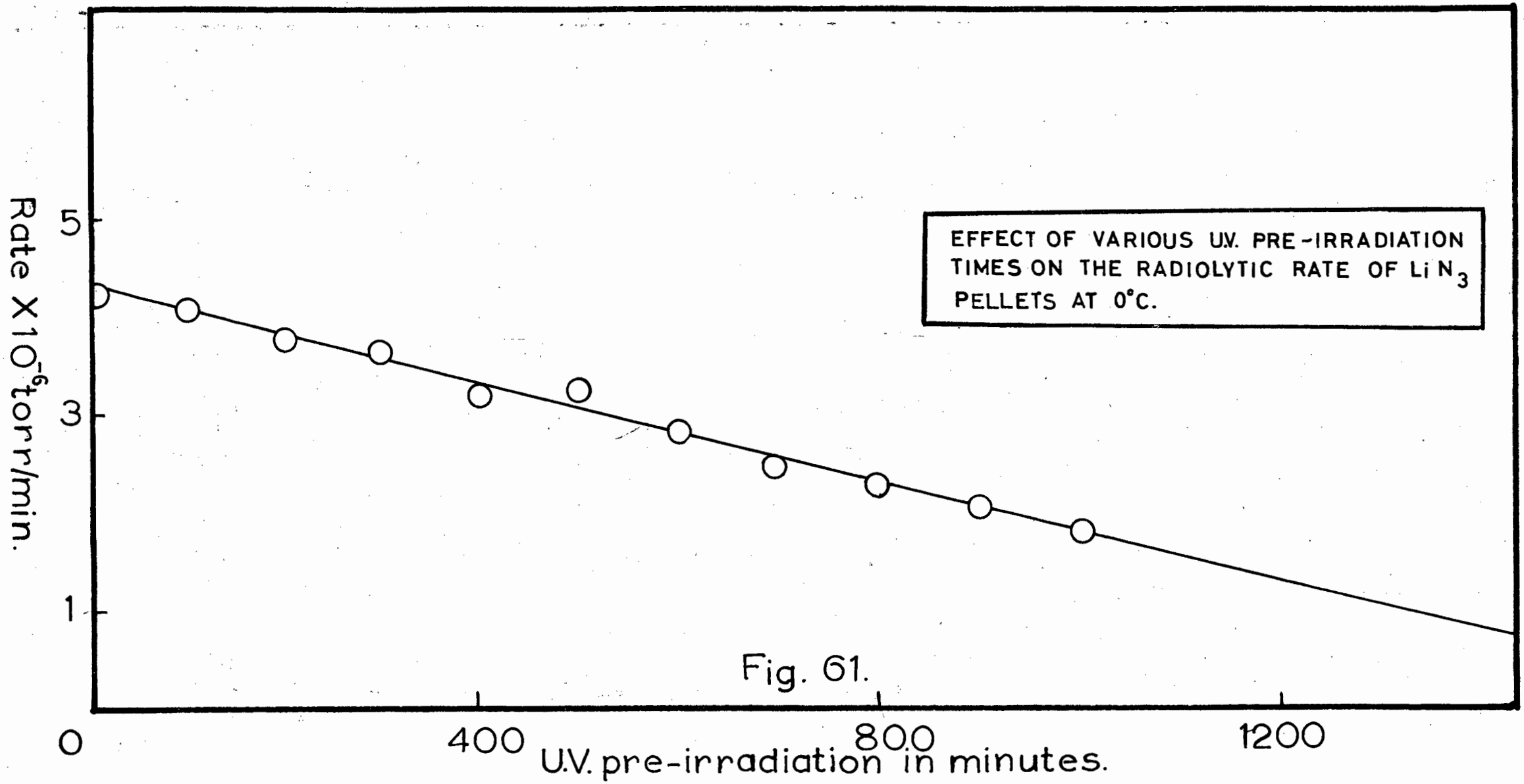
EFFECT OF VARIOUS U.V. PRE-IRRADIATION TIMES ON THE RADIOLYTIC RATE OF LiN_3 PELLETS AT 0°C.
Rate X 10^{-6} torr/min.
5
3
1
0
400
800
1200
U.V. pre-irradiation in minutes.

Fig. 61.

5.8.7. The effect of grinding time on the subsequent radiolysis of Lithium Azide pellets.

In the section on the photolysis of barium azide, it was found that grinding of the azide material for various lengths of time sensitised the material to ultraviolet photolysis, and so the effect of such mechanical damage on the radiolytic rate of lithium azide was investigated.

Crystals of lithium azide were gound for periods of 1, 2, 4 and 8 minutes and pelleted at 4 000 lbs./sq.inch.

A definite sensitisation effect occurred on grinding the azide and this is illustrated in fig. 62. A plot of radiolytic rate versus grinding time is shown in fig. 63. The temperature of radiolysis in the above determinations was $0^{\circ}C$.

5.8.8. The radiolysis of anhydrous single crystals of Barium Azide by X-rays.

Well formed single crystals of anhydrous barium azide were subjected to radiolysis at $0^{\circ}C$. It was felt that since they had been exposed to the least mechanical damage and were not exposed to the crystal lattice strains that the monohydrate undergoes on dehydration, different radiolysis rates may be expected to occur.

The results of the radiolysis of anhydrous crystals was found to differ very markedly from that of the dehydrated monohydrate. This is clearly evident from fig. 64, which shows a very drastic reduction in decomposition rate for the former. The pressure-time plots for anhydrous crystals were, however, still perfectly linear.

The rates of radiolysis could be vastly increased if the crystals were mechanically damaged, i.e. grinding the material to a powder. Fig. 64 also shows the effect of grinding the anhydrous material for 5 minutes in the Grindex mill.

Another way in which the radiolytic rate for the anhydrous crystals

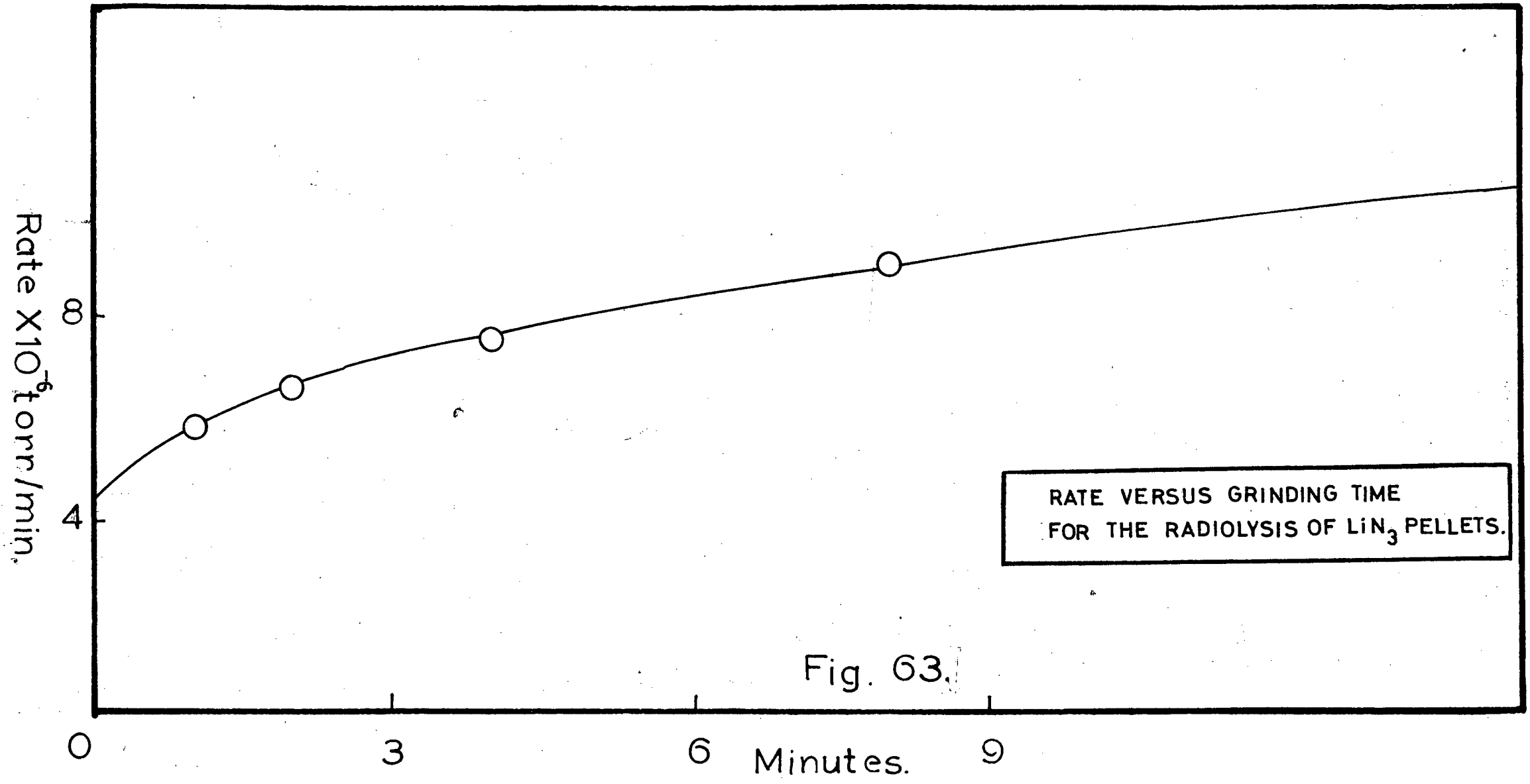
Rate X10⁻⁶ torr/min.
8
4
0
3
6
9
Minutes.
RATE VERSUS GRINDING TIME
FOR THE RADIOLYSIS OF LiN3 PELLETS.

Fig. 63.

of barium azide could be enhanced, was to introduce water vapour into the decomposition cell and then re-evacuate the system for 12 hours, followed by radiolysis. This is again depicted in fig. 64. The crystals were a very dark green colour after radiolysis.

5.8.9. Reproducibility of results for the radiolysis of anhydrous single crystals of Barium Azide by X-rays.

The pressure-time plots for the decompositions were reproducible to a very high degree, as indicated in fig. 65. The decomposition temperature was $0^{\circ}C$.

5.9.0. Activation energies for the radiolysis of anhydrous single crystals of Barium Azide by X-rays.

Table 8 lists the relevant values used in the determination of activation energies (using the split run technique) as well as the slope of the Arrhenius plot and the activation energies.

TABLE 8.

(* = anhydrous crystals of barium azide)

Sample pre-treatment	°C	1/T x 10^3 (A)	-log rate (B)	slope A vs B x 10^{-3}	E_A k.cals./mole
None	19,0	3,430	5,6600		
	24,0	3,371	5,5374		
	28,0	3,320	5,4060	2,498	11,4
	31,0	3,290	5,3003		
	22,2	3,390	5,6961		
	26,0	3,343	5,6004	2,207	10,8
	29,6	3,310	5,5152		
* pelleted at 4 000 lbs./ sq.inch	18,8	3,440	5,6650		
	24,0	3,371	5,5381		
	27,5	3,332	5,4071	2,500	11,4
	32,0	3,279	5,3000		
	15,8	3,465	5,5000		
	21,2	3,395	5,3839		
	27,8	3,321	5,1952	2,237	10,2
	34,2	3,238	5,0531		

The low rates obtained for the radiolysis of the above crystals (see 5.8.9) appears to be linked with relatively high activation energies, an average value of 11,1 k.cals./mole being obtained. Pelleting the crystals at 4 000 lbs./sq.inch had very little effect on the rate of the activation energy. These values are also shown in Table 8. Fig. 66 shows the activation energy plots for the values tabulated in Table 8.

Since grinding increased the rate of radiolysis markedly (5.8.9) the activation energies for ground anhydrous crystals of barium azide were determined as well. The relevant values for 5 and 15 minutes grinding time appear in Table 9. It can be seen that the activation energies were drastically lowered by grinding the material, the lowest

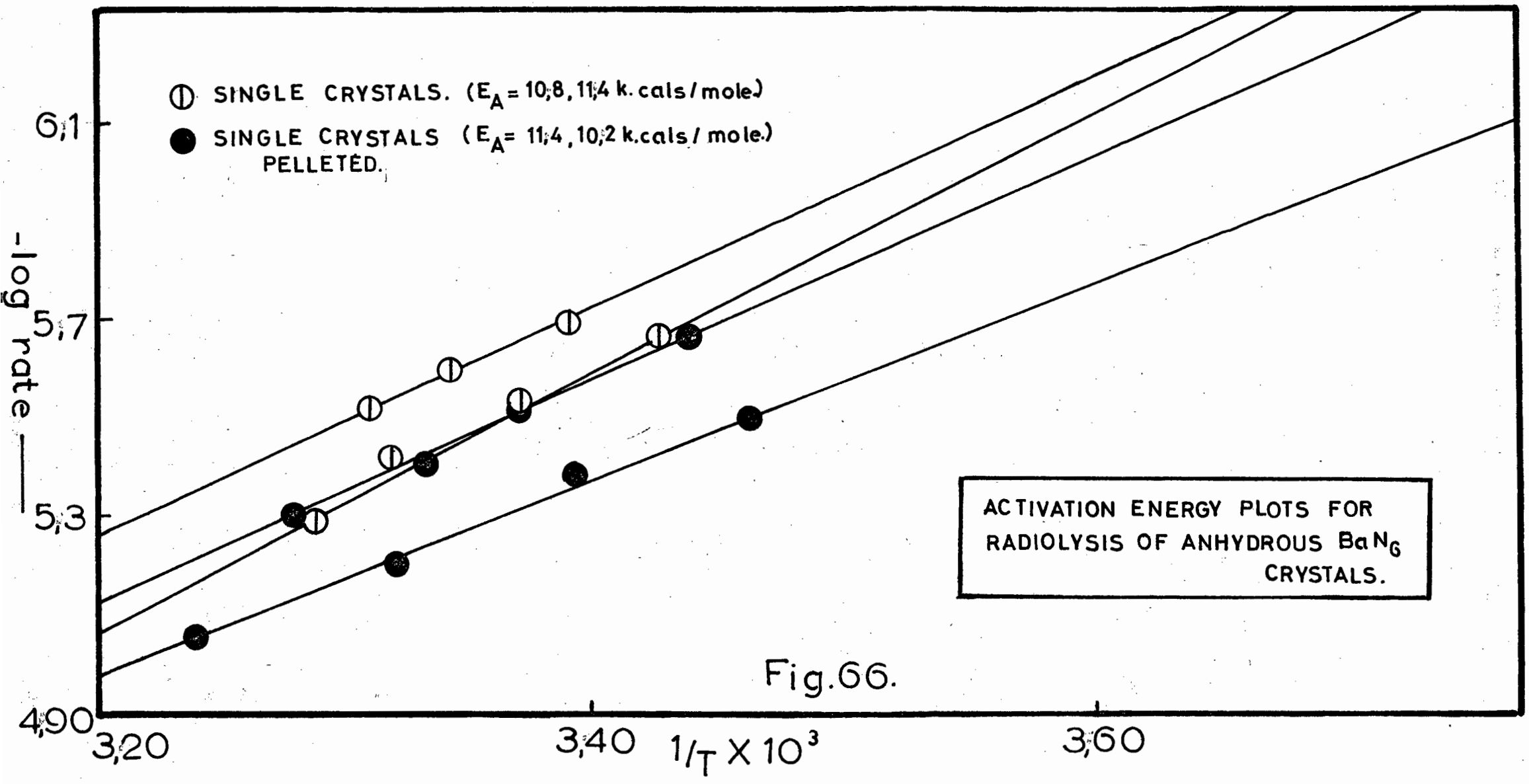
SINGLE CRYSTALS. (E_A = 10;8, 11;4 k. cals / mole.)
SINGLE CRYSTALS (E_A = 11;4, 10;2 k.cals / mole.)
PELLETED.
6;1
5;7
5;3
4;90
-log rate
3;20
3;40
1/T X 10³
3;60
ACTIVATION ENERGY PLOTS FOR RADIOLYSIS OF ANHYDROUS BaN_6 CRYSTALS.

Fig.66.

values being obtained for the longest grinding times. Fig. 67 illustrates the activation energy plots for ground anhydrous crystals of barium azide.

Table 10 shows the effect of grinding the material for 15 minutes followed by pelleting at 4,000 lbs./sq.inch. The pellting seems to raise the activation energy to those values obtained for anhydrous crystals ground for 5 minutes. Fig. 68 shows the relevant activation energy plots.

Since pelleting after grinding raises the activation energy slightly, it was felt that the sequence, grinding followed by pelleting and then regrinding the pelleted material, should lower the activation energy again. This does in fact occur as shown in Table 11. The plotted values of -log rate versus 1/T are to be found in fig. 68.

5.9.1. The effect of ultraviolet pre-irradiation on the radiolysis by X-rays of anhydrous single crystals of Barium Azide.

In an attempt to create reaction centres in anhydrous single crystals for X-radiolysis, they were subjected to 8 hours pre-irradiation by the 550 Watt ultraviolet arc.

The resultant linear pressure-time plots were, however, not enhanced in any way, as indicated in fig. 69, and the activation energies were still of the order of 10 k.cals./mole (see Table 12).

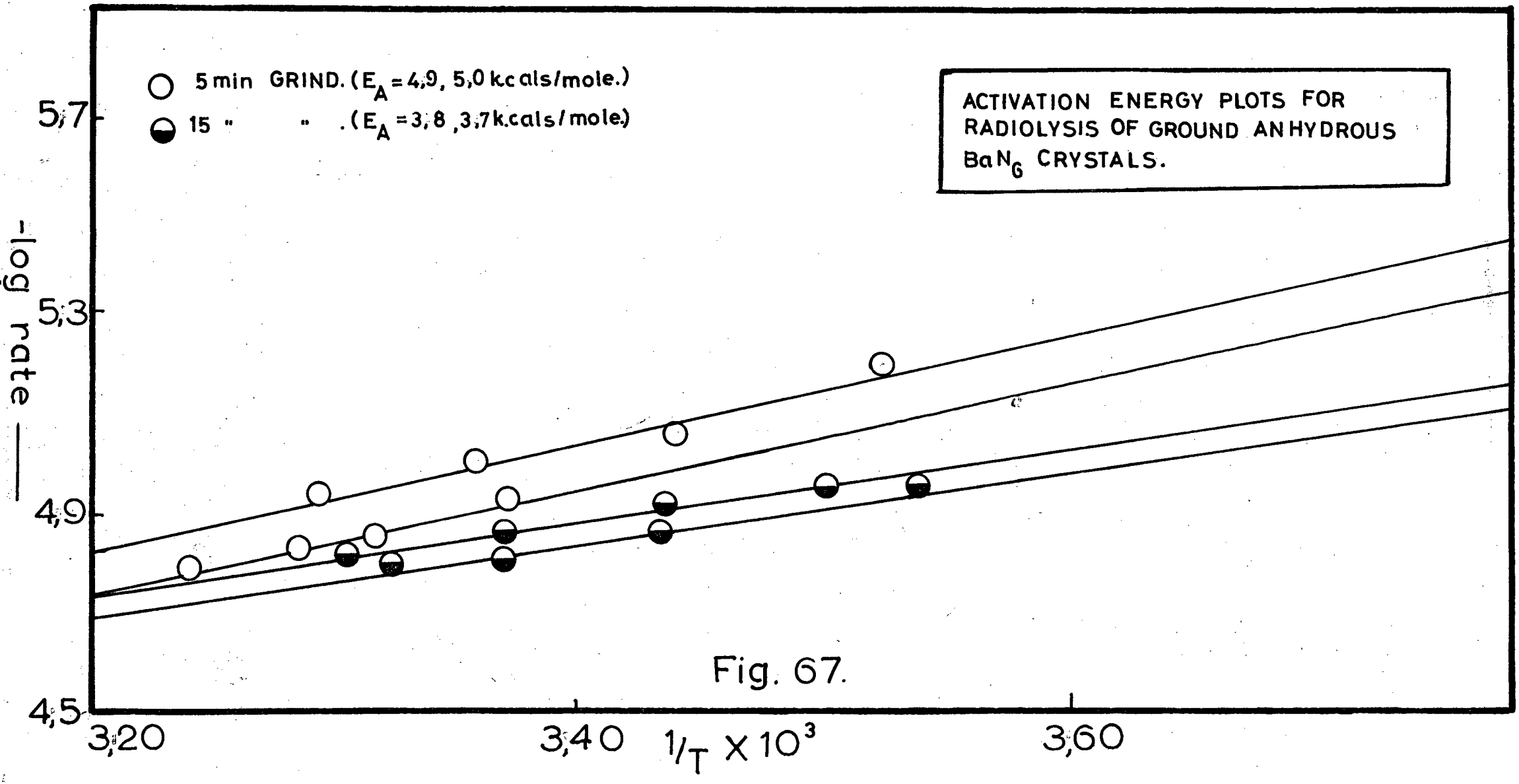
5 min GRIND. (E_A = 4,9, 5,0 k.cals/mole.)
15 " " . (E_A = 3,8 , 3,7 k.cals/mole.)
ACTIVATION ENERGY PLOTS FOR RADIOLYSIS OF GROUND ANHYDROUS BaN_6 CRYSTALS.
-log rate
5,7
5,3
4,9
4,5
3,20
3,40
3,60
$1/T \times 10^3$

Fig. 67.

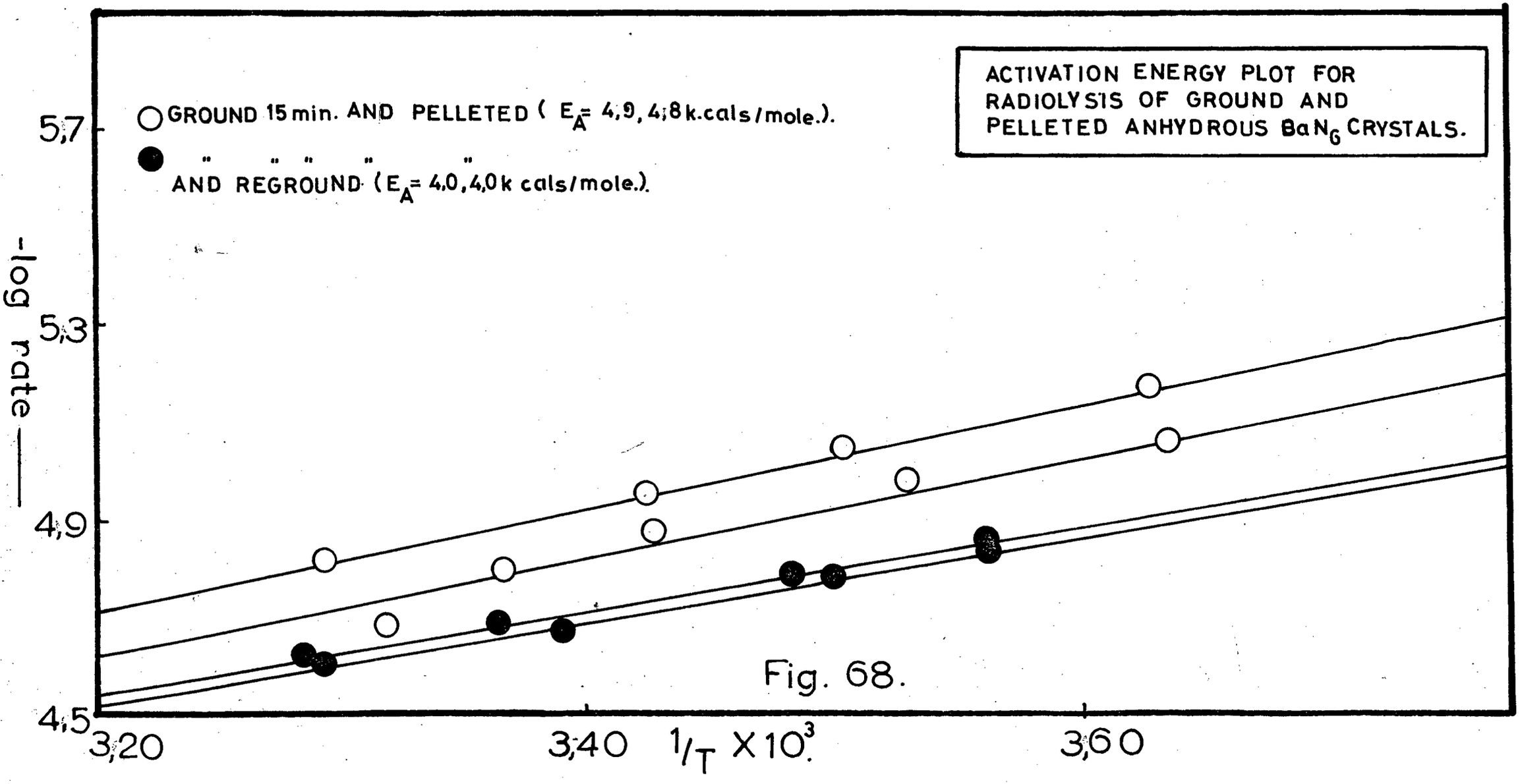
ACTIVATION ENERGY PLOT FOR RADIOLYSIS OF GROUND AND PELLETED ANHYDROUS BaN_6 CRYSTALS.
○ GROUND 15 min. AND PELLETED (E_A= 4,9, 4,8 k.cals/mole.).
● " " " " " AND REGROUND (E_A= 4,0, 4,0 k cals/mole.).
-log rate
5,7
5,3
4,9
4,5
3,20
3,40
3,60
$1/T \times 10^3$

Fig. 68.

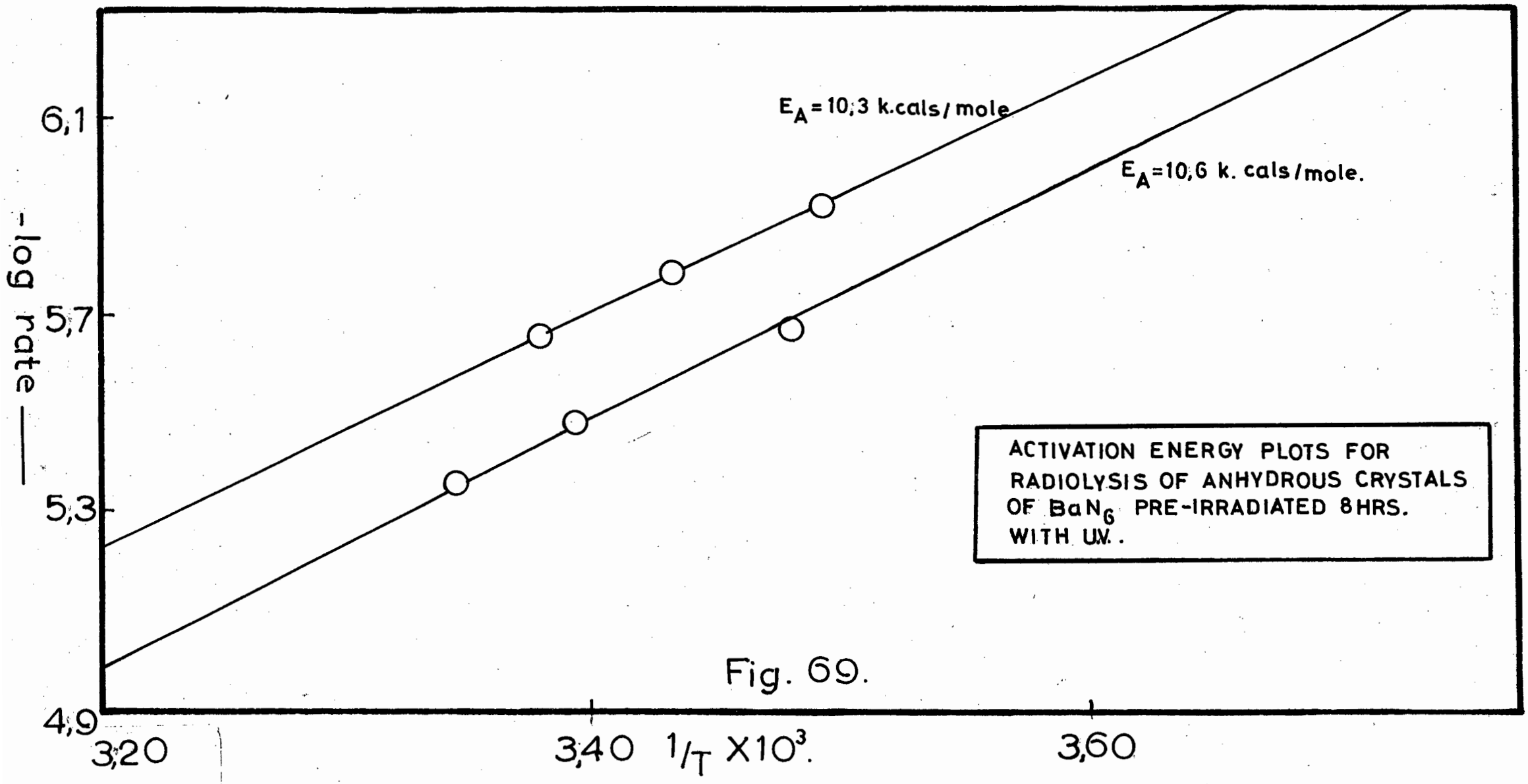
6,1
5,7
5,3
4,9
-log rate
3,20
3,40
1/T X10³.
3,60
E_A = 10;3 k.cals/mole
E_A = 10;6 k. cals/mole.
ACTIVATION ENERGY PLOTS FOR RADIOLYSIS OF ANHYDROUS CRYSTALS OF BaN6 PRE-IRRADIATED 8HRS. WITH U.V.

Fig. 69.

TABLE 9.

(* = anhydrous crystals of barium azide).

Sample pre-treatment	°C	1/T x 10^3 (A)	-log rate (B)	slope A vs B	E_A k.cals./mole
* ground 5 min.	10,8	3,520	5,2098		
	19,7	3,438	5,0802		
	25,0	3,358	5,0101	1,066	4,9
	30,4	3,297	4,9401		
	11,3	3,519	5,0852		
	16,6	3,457	5,0150		
	23,7	3,370	4,9400		
	28,6	3,317	4,8462	1,087	5,0
	31,6	3,284	4,8281		
	35,4	3,240	4,7853		
* ground 15 min.	4,9	3,600	5,0359		
	12,9	3,500	4,9599		
	18,6	3,434	4,9252	0,836	3,8
	24,0	3,370	4,8685		
	29,4	3,306	4,8132		
	1,7	3,642	5,0334		
	10,0	3,535	4,9722		
	18,3	3,434	4,8752	0,805	3,7
	23,2	3,374	4,8150		
	28,1	3,327	4,7921		

TABLE 10

(* = anhydrous crystals of barium azide)

Sample pre-treatment	°C	1/T x 10^3 (A)	-log rate (B)	slope A vs B	E_A k.cals./ mole.
* ground 15 min and pelleted 4,000 lbs./sq. inch	2,3	3,634	5,0433		
	10,5	3,530	4,9550		
	19,2	3,425	4,8554	1,069	4,9
	24,3	3,365	4,7811		
	30,4	3,319	4,6708		
	3,1	3,624	5,1344		
	12,6	3,503	5,0284		
	19,2	3,425	4,9322	1,057	4,8
	24,3	3,365	4,8360		
	30,4	3,293	4,0051		

TABLE 11.

(* = anhydrous crystals of barium azide)

Sample pre-treatment	°C	1/T x 10^3 (A)	- log rate (B)	slope A vs B	E_A k.cals./ mole.
* ground 15 min pelleted 4,000 lbs./sq.inch and reground 15 min	8,1	3,560	4,8270		
	14,0	3,482	4,7798	0,871	4,0
	22,7	3,363	4,6750		
	31,4	3,284	4,6072		
	8,5	3,559	4,8169		
	13,0	3,499	4,7699	0,873	4,0
	22,2	3,390	4,6647		
	31,0	3,290	4,5970		

TABLE 12.

Sample pre-treatment	°C	1/T x 10^3 (A)	- log rate (B)	slope A vs B	E_A k.cals./mole
anhydrous crystals pre-irradiated with U.V.S. 8 hours	13,4	3,491	5,8883		
	18,4	3,432	5,7500	2,260	10,3
	23,0	3,379	5,6301		
	14,5	3,480	5,6479		
	21,7	3,392	5,4600	2,316	10,6
	26,1	3,344	5,3330		

5.9.2. The X-radiolysis of dehydrated Barium Azide monohydrate pellets.

The radiolytic rate for crystals of dehydrated barium azide monohydrate, being very much greater than that of anhydrous crystals (see fig. 64) made this material more suitable for a detailed investigation of the X-radiolysis of barium azide.

Since pellets of the azide are much more convenient to handle, and because the surface area can be kept constant, it was decided to use pellets for the investigations.

Optimum grinding times and pelleting pressures were first determined in the followeing sections so that a satisfactory combination of these two variables could be selected.

5.9.3. The effect of grinding on the X-radiolysis of Barium Azide pellets.

IN ALL THE FOLLOWING SECTIONS, UNLESS OTHERWISE STATED, BARIUM AZIDE PELLETS WILL MEAN 14 mm DIAMETER PELLETS OF THE DEHYDRATED MONOHYDRATE.

The 200 mg pellets for this section were prepared from:

1. unground barium azide.
2. barium azide ground 1 minute.

3. barium azide ground 2 minutes

4. " " " 4 "

5. " " " 8 "

A pelleting pressure of 4 000 lbs./sq.inch was employed with the 14 mm diameter evacuable die.

Fig. 70 illustrates a very definite grinding effect at a decomposition temperature of -2,0°C. Radiolysis on the above pellets was also carried out at -7,1, 2,8 and 13,4°C.

Table 13 lists the radiolytic rates and the activation energies for the different grinding times at the various decomposition temperatures. Fig. 71 depicts the plots of rate (p/t) versus grinding time for each of the four different decomposition temperatures.

Although the rates were slightly higher for 8 minutes of grinding the azide, this very finely powdered material was not easily pelleted and a grinding time of 4 minutes was selected for further work.

5.9.4. The effect of pelleting pressure on the X-radiolysis of Barium Azide pellets.

Using the optimum grinding time determined above for the dehydrated monohydrate, 200 mg pellets were pressed at 2 000, 4 000 and 6 000 lbs./sq.inch.

X-radiolysis was carried out on each of the above pellets at -7,1, -2,0, 2,8 and 13,4°C. These temperatures were selected because they were the ones employed in the section on grinding, and thus a direct comparison of rates can be made.

In order to check the reproducibility of the rates of decomposition, all determinations were carried out in quadruplicate.

Table 14 lists the rates and activation energies for the various pelleting pressures used at the different decomposition temperatures. The quadruplicate determinations tabulated in Table 14 clearly show the very high degree of reproducibility of the radiolytic rates at each temperature.

TABLE.13.

(all pellets pressed at 4.000 lbs./sq.in.)

Horizontal rows of figures are rates in mm./min.X10^{-5}

Temperature °C	Grinding time				
	Unground	1 minute	2 minutes	4 minutes	8 minutes
- 7,1	0,49	0,90	0,97	1,06	1,40
- 2,0	0,62	1,07	1,10	1,23	1,52
2,8	0,74	1,17	1,23	1,31	1,72
13,4	0,81	1,28	1,53	1,50	1,94
Activation energy K.cal./mole.	3,0	2,5	4,0	3,1	2,4

TABLE.14.

Work below performed in quadruplicate to check reproducibility.

Rates are in mm./min. X10^{-5}.

Temperature °C	Pressing pressure 2.000 lbs./sq.in.				
	Run 1	Run 2	Run 3	Run 4	Average Rate
- 7,1	0,63	0,52	0,56	-	0,57
- 2,0	0,59	0,71	0,61	0,65	0,64
2,8	0,67	0,80	0,70	0,71	0,72
13,4	0,84	0,97	0,82	0,91	0,88
Activation energy K.cal./mole.	3,4	3,3	3,5	3,5	

Temperature °C	Pressing pressure 4.000 lbs./sq.in.				
	Run 1	Run 2	Run 3	Run 4	Average Rate
- 7,1	0,51	0,49	0,51	0,47	0,57
- 2,0	0,58	0,63	0,68	0,63	0,63
2,8	-	0,78	0,72	0,71	0,74
13,4	0,69	0,74	1,03	0,90	0,84
Activation energy K.cal./mole.	2,0	2,9	3,0	4,4	

Temperature °C	Pressing pressure 6.000 lbs./sq.in.				
	Run 1	Run 2	Run 3	Run 4	Average Rate
- 7,1	0,39	-	-	-	0,39
- 2,0	0,45	0,40	0,38	0,38	0,40
2,8	0,54	0,46	0,44	0,45	0,47
13,4	0,61	0,55	0,48	0,55	0,55
Activation energy K.cal./mole.	3,2	3,3	2,2	3,4	

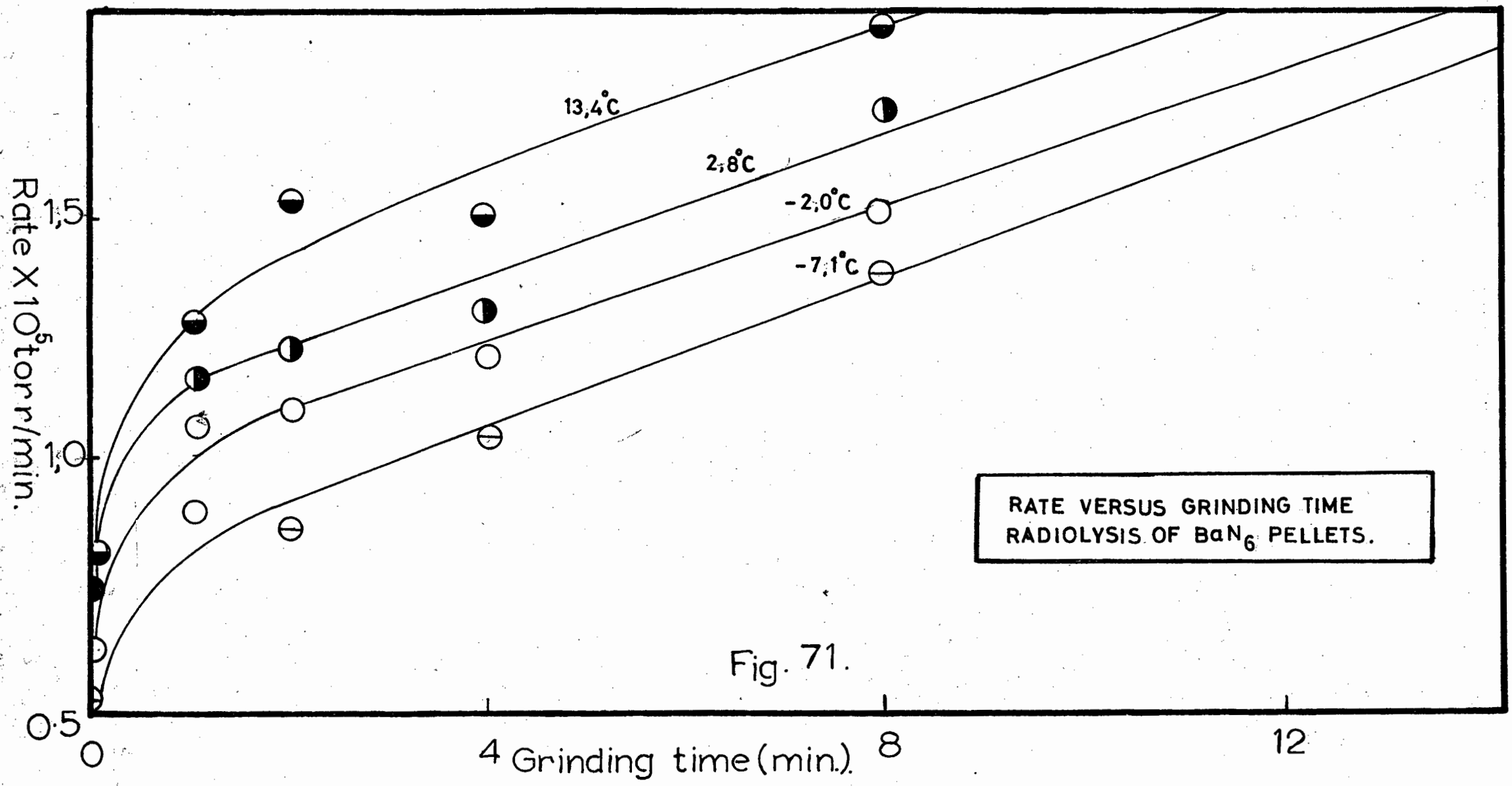
13,4°C
2,8°C
-2,0°C
-7,1°C
Rate X 10⁵ torr/min.
1,5
1,0
0·5
0
4
8
12
Grinding time (min.)
RATE VERSUS GRINDING TIME
RADIOLYSIS OF BaN6 PELLETS.

Fig. 71.

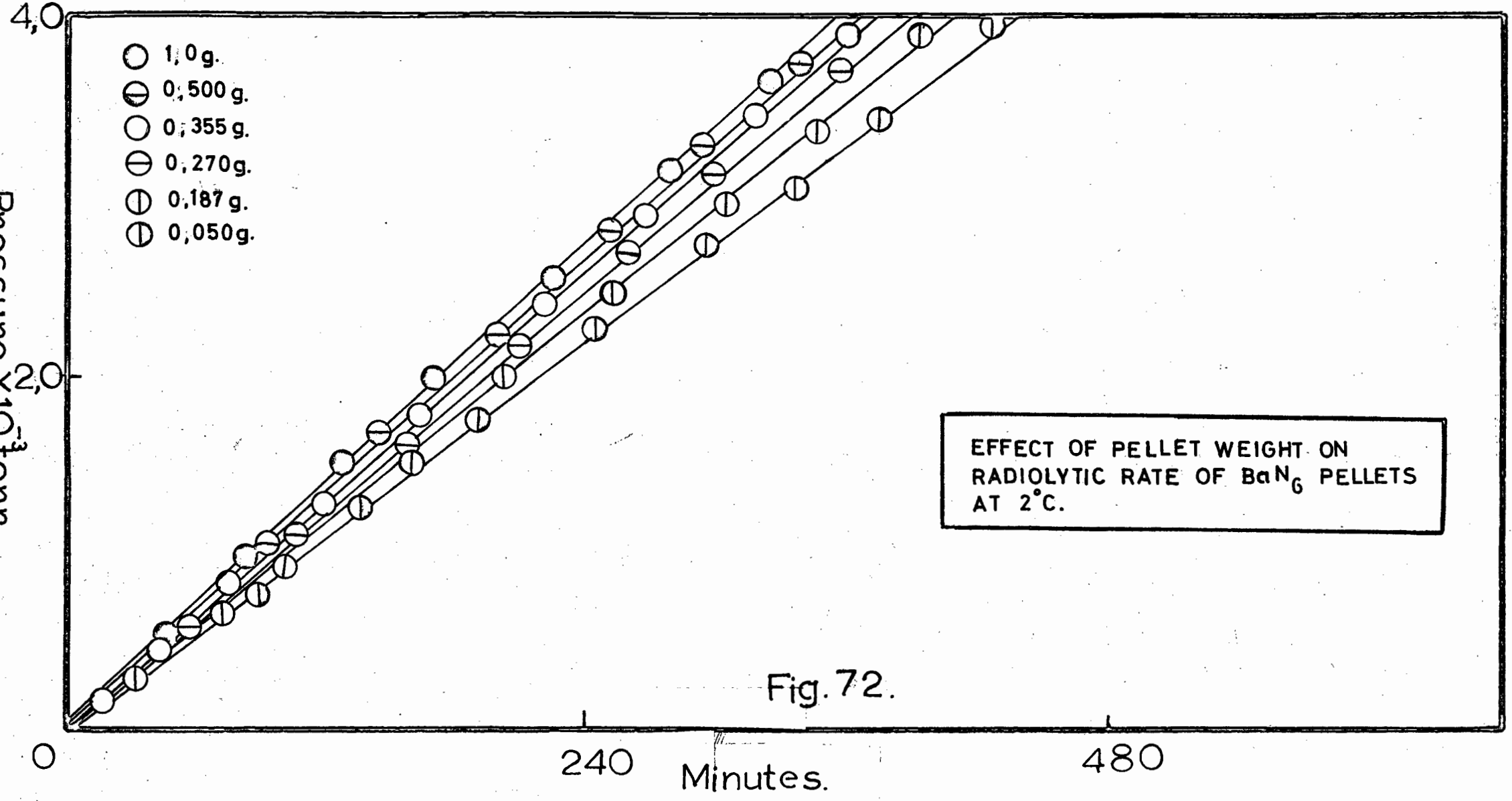
4,0
2,0
0
Pressure X10⁻³ torr.
240
480
Minutes.
1,0 g.
0,500 g.
0,355 g.
0,270 g.
0,187 g.
0,050 g.
EFFECT OF PELLET WEIGHT ON RADIOLYTIC RATE OF BaN_6 PELLETS AT 2°C.

Fig. 72.

5.9.6. The variation of radiolytic rate with the intensity of X-irradiation for Barium Azide pellets.

The intensity dependence of the radiolytic rate for barium azide pellets was investigated at different temperatures in order to determine whether the decomposition was unimolecular or bimolecular with respect to the azide ion.

Fig. 73 shows the plots of radiolytic rate versus intensity of X-irradiation for 2, -20 and -120°C. All the plots were perfectly linear, indicating a unimolecular decomposition of the azide ion in the radiolytic reaction.

5.9.7. The effect of ageing Barium Azide on the subsequent radiolytic rate of Barium Azide pellets.

X-radiolysis was carried out on two samples of stored barium azide and their rates of decomposition were compared to that of freshly prepared dehydrated monohydrate.

Fig. 74 shows the X-radiolysis pressure-time plots for pellets made from 1 year old, 4 months old and freshly prepared barium azide. A definite sensitisation of the material appears to take place with increasing storage time.

5.9.8. Activation energies for the X-radiolysis of dehydrated Barium Azide monohydrate pellets.

A detailed investigation of activation energies over a wide range of temperatures (50 to -101,5°C) indicated that distinct changes in the activation energy occurred for different temperature ranges.

Changes in the slope of the activation energy plot of log rate vs 1/T took place in the region of 0°C and in the region -30 to -40°. This is illustrated in fig. 75. Table 15 lists the relevant values used to calculate the activation energies.

It was found that the activation energy for the range 50 to 0°C

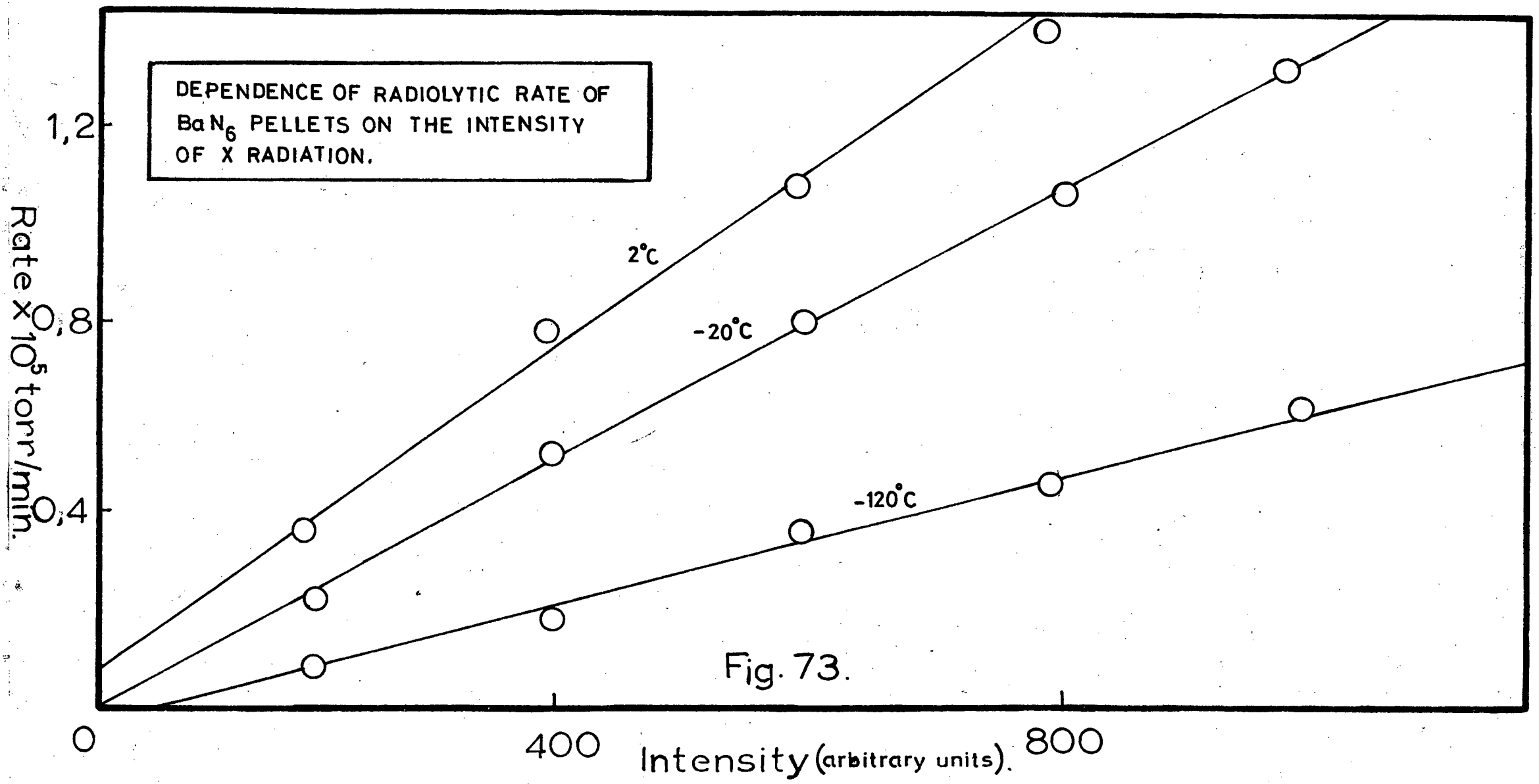
DEPENDENCE OF RADIOLYTIC RATE OF BaN_6 PELLETS ON THE INTENSITY OF X RADIATION.
2°C
-20°C
-120°C
Rate x 10^5 torr/min.
1,2
0,8
0,4
0
400
800
Intensity (arbitrary units).

Fig. 73.

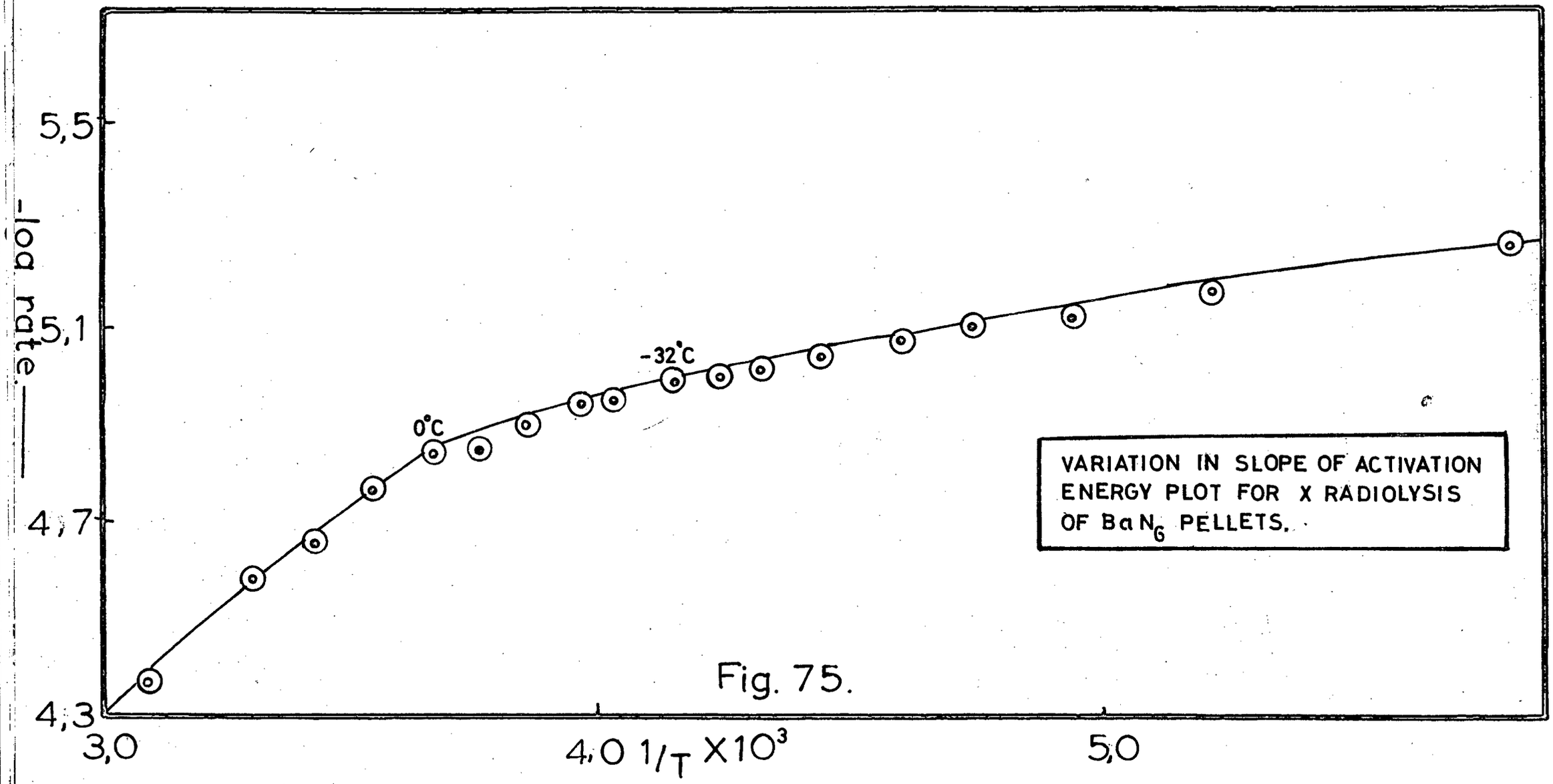
5,5
5,1
4,7
4,3
-log rate
3,0
4.0 1/T X10³
5,0
0°C
-32°C
VARIATION IN SLOPE OF ACTIVATION ENERGY PLOT FOR X RADIOLYSIS OF BaN6 PELLETS.

Fig. 75.

6.0.0. Successive re-irradiation and its effect on the rate and activation energy for the X-radiolysis of Barium Azide pellets.

In order to investigate any sensitisation of the azide material by administering the X-rays in interrupted dosages, successive re-irradiations were carried out at $-10^{\circ}C$ after 10 hours radiolysis, followed by 12 hours re-evacuation of the cell system.

Fig. 77 shows no significant change in the rate of radiolysis, but Table 17 shows a definite increase in the activation energy with each successive re-irradiation. Fig. 78 illustrates the actual activation energy plots.

TABLE 17.

Remarks	$1/T \times 10^3$ (A)	- log rate (B)	slope A vs B.	E_A k.cals./mole
1st re-irradiation	3,415 3,440 3,475 3,499 3,543	5,5000 5,5104 5,5199 5,5244 5,5401	$0,318 \times 10^3$	1,5
2nd re-irradiation	3,407 3,480 3,517 3,559	5,4481 5,4481 5,5200 5,5498	$0,482 \times 10^3$	2,2
3rd re-irradiation	3,360 3,444 3,510 3,552	5,4278 5,5049 5,5600 5,5960	$0,933 \times 10^3$	4,3
4th re-irradiation	3,380 3,424 3,447 3,510	5,4002 5,4479 5,4702 5,5405	$1,029 \times 10^3$	4,7

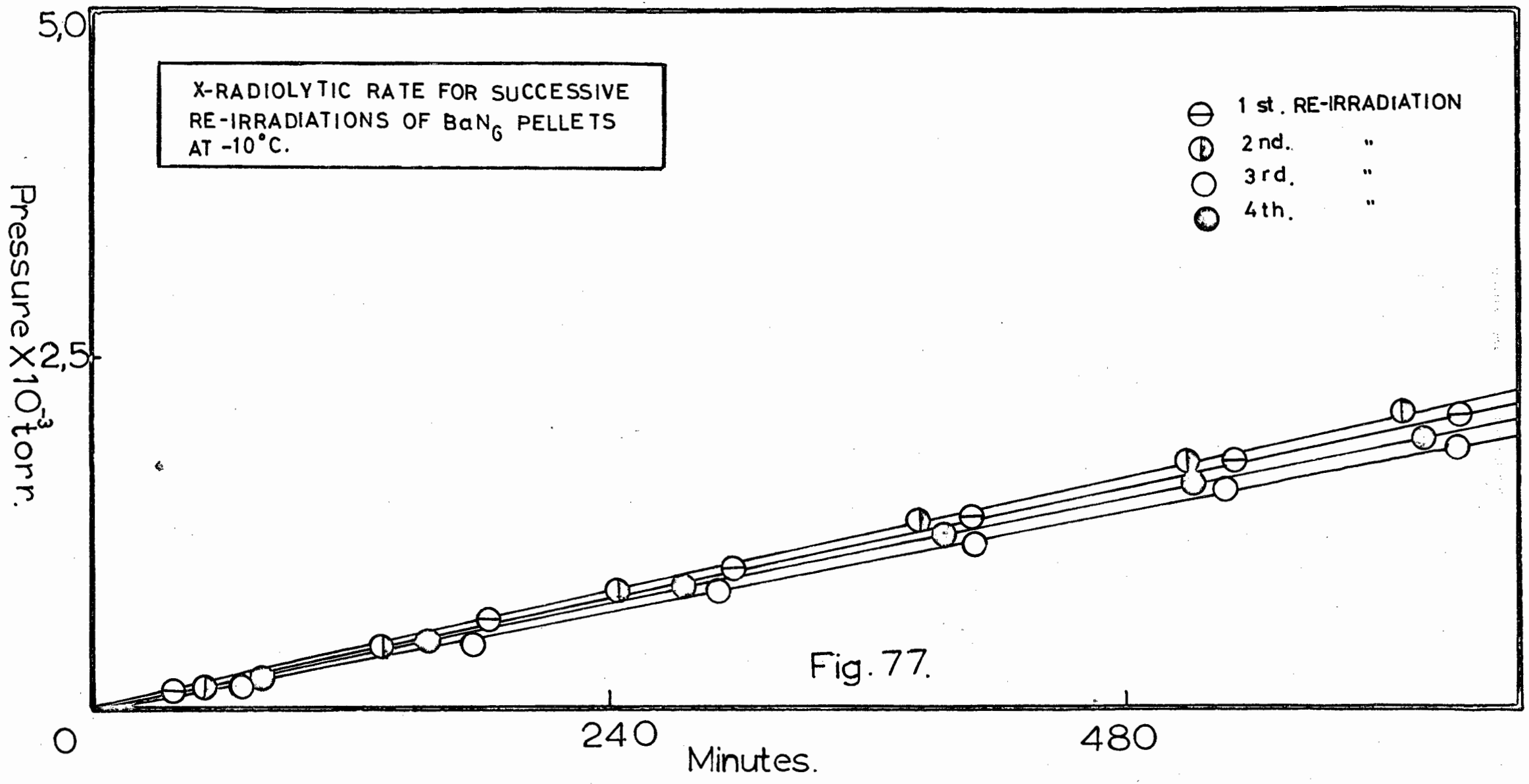
X-RADIOLYTIC RATE FOR SUCCESSIVE RE-IRRADIATIONS OF BaN_6 PELLETS AT -10°C.
1 st. RE-IRRADIATION
2 nd. "
3 rd. "
4th. "
Pressure X 10^{-3} torr.
5,0
2,5
0
240
480
Minutes.

Fig. 77.

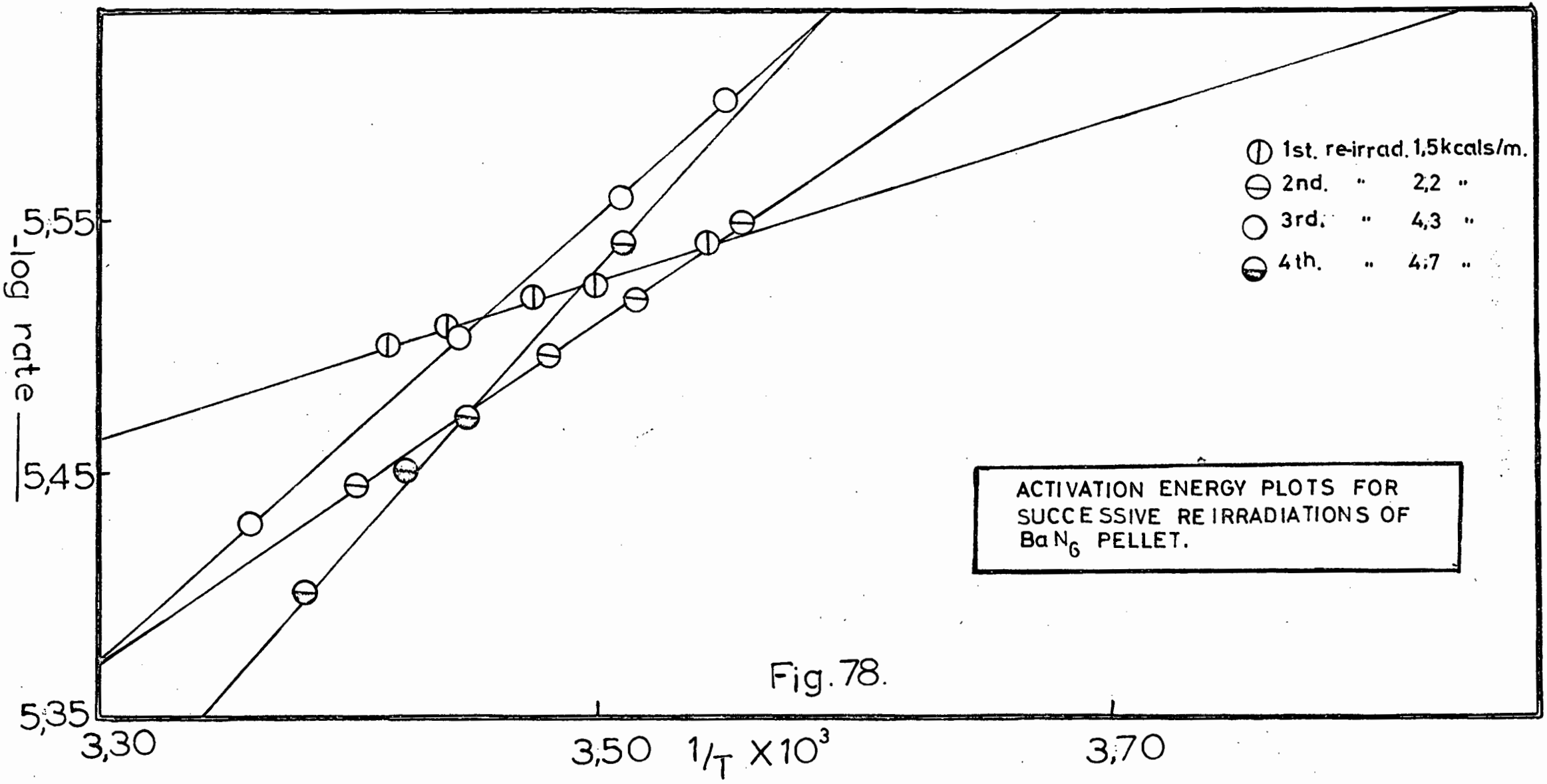
1st. re-irrad. 1,5kcals/m.
2nd. " 2,2 "
3rd. " 4,3 "
4th. " 4,7 "
ACTIVATION ENERGY PLOTS FOR SUCCESSIVE REIRRADIATIONS OF BaN_6 PELLET.
-log rate
5,55
5,45
5,35
3,30
3,50
3,70
$1/T \times 10^3$

Fig. 78.

6.0.1. The effect of ultra-violet pre-irradiation on the subsequent X-radiolysis of Barium Azide pellets.

Pre-irradiating the barium azide pellets with ultraviolet light for 2 to 10 hours had very little effect on the slope of the pressure-time plots (a slightly depressed rate resulted) and the activation energies were of the usual order of magnitude for the temperatures employed.

Table 18 shows a comparison of activation energy data for the X-radiolysis of unirradiated and ultraviolet pre-irradiated pellets of barium azide.

TABLE 18.

Remarks	$1/T \times 10^3$ (A)	- log rate (B)	slope A vs B	E_A k.cals./mole
no pre-irrad.	3,364 3,406 3,438 3,477	5,2002 5,2408 5,2666 5,2998	$0,787 \times 10^3$	3,6
2 hrs. pre-irradiation	3,405 3,481 3,508 3,555	5,2180 5,2799 5,3110 5,3375	$0,814 \times 10^3$	3,7
10 hrs. pre-irradiation	3,382 3,420 3,475 3,528	5,2300 5,2697 5,3099 5,3540	$0,783 \times 10^3$	3,6

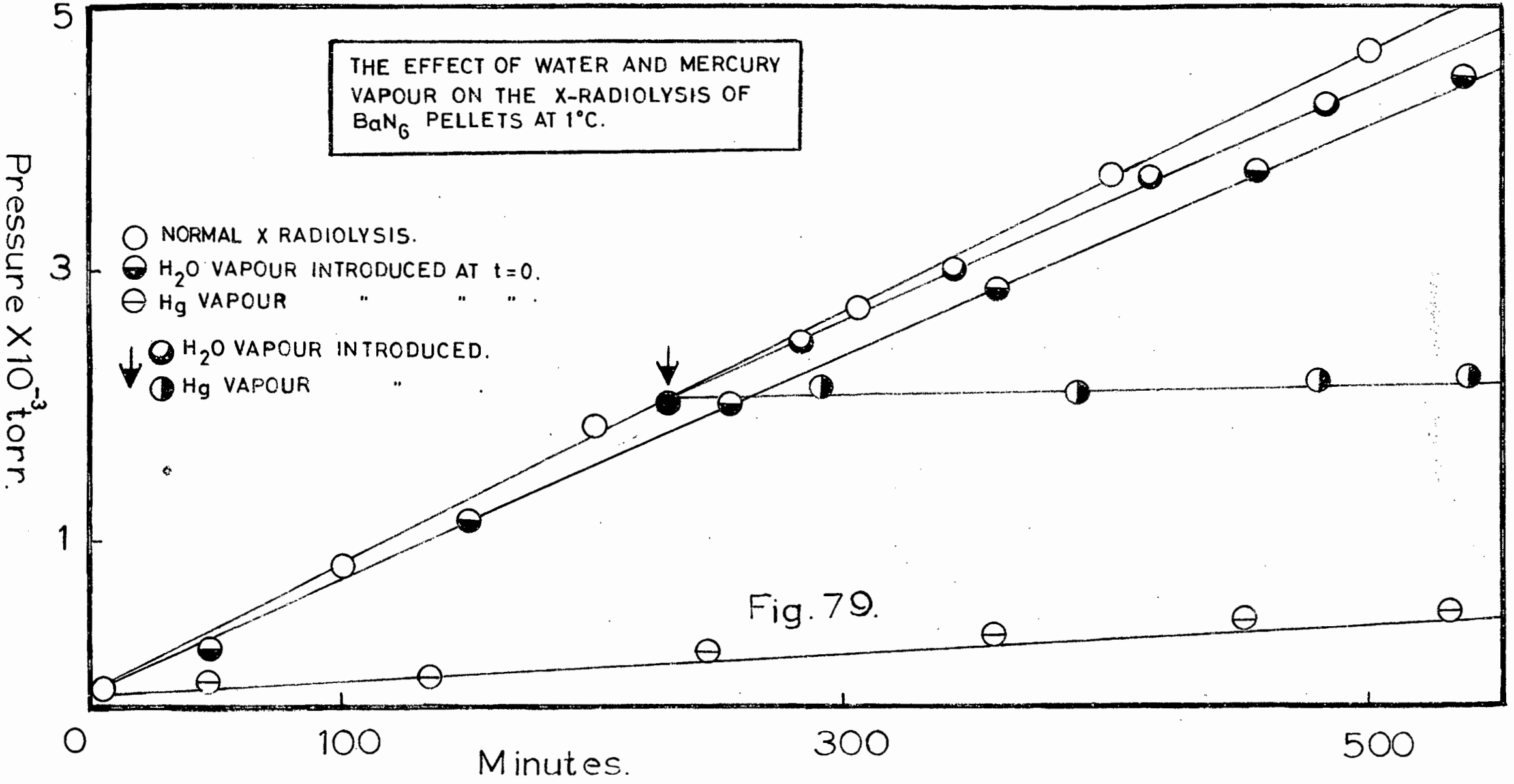
THE EFFECT OF WATER AND MERCURY VAPOUR ON THE X-RADIOLYSIS OF BaN_6 PELLETS AT 1°C.
NORMAL X RADIOLYSIS.
H_2O VAPOUR INTRODUCED AT t=0.
Hg VAPOUR " " " .
H_2O VAPOUR INTRODUCED.
Hg VAPOUR "
Pressure X 10^{-3} torr.
5
3
1
0
100
300
500
Minutes.

Fig. 79.

DISCUSSION OF RESULTS FOR SECTIONS 5.8.1 TO 6.0.2.

It would appear from the study of the X-radiolysis of lithium, sodium, barium and strontium azides, that in general the pressure-time plots for the radiolysis of the alkali metal azides and alkaline earth azides are linear, and that the radiolytic rate is directly proportional to the intensity of X-irradiation. This suggests that the radiolysis is unimolecular with respect to the azide ion.

The relatively high activation energy of 4.k.cals./mole (at all the temperature ranges studied) for the radiolysis of sodium azide when compared to the average of 800 cals./mole for the radiolysis of lithium azide pellets, may be explained by the fact that sodium azide crystals (B.D.H.) were used for the radiolysis. It has been shown in section 5.8.8. that anhydrous crystals of barium azide which were not subjected to mechanical damage such as grinding or pelleting, gave high activation energies (10-11 k.cals./mole). Heal[55] in his observations on the decomposition of solid sodium azide by X-rays, obtained a value of 500 cal./mole for the activation energy of radiolysis. However, he only used two temperatures (51 and 102°C) for his calculations and these temperatures were simply the operating temperatures of the X-ray tube at two different tube currents. The influence of room temperature on the radiolytic temperature was simply ignored. This state of affairs is highly unsatisfactory for the calculation of accurate activation energies, and large errors must be involved in his calculations.

Heal[57] has proposed two mechanisms for the X-radiolysis of sodium azide.

A. A process, the rate of which varies little with temperature (low E_A), responsible for decomposition at low temperatures.

B. A temperature-dependent process, effective mainly above room temperature.

In the study of the X-radiolysis of pellets of dehydrated barium azide monohydrate (section 5.9.2.), a temperature range of 50 to -101°C was employed in the determination of activation energies, and Table 15 shows a definite increase in activation energy with increasing temperature range. This suggests that for the radiolysis of barium azide there also exists a high and a low temperature process.

At low temperatures, the activation energy was of the order of 700 cals./mole which is relatively temperature independent, while above room temperature the value was as high as 4 k.cals./mole. No such variation in activation energy for lithium azide pellets was demonstrated in the temperature range -18 to 36°C. However, Prout and Liddiard[58] and Prout and Moore[106] have studied the thermal decompositions of lithium and barium azides respectively and these workers have shown that lithium azide requires much higher temperatures for thermal decomposition. This might account for the apparent absence of a thermal contribution to the radiolysis rate of lithium azide in the temperature range studied.

Heal's[57] low temperature mechanism for sodium azide (process A) is as follows :

$$N_3^- \rightleftharpoons^{h\nu} N_3 + e$$

$$N_3 + N_3 \rightarrow 3N_2 + e$$

where N_3 = azide radical

e = electron.

Furthermore, he maintained that F-centre formation was negligible and that the above electrons are excited into the conduction band. The above reaction may be unimolecular with respect to the azide radical, but the overall reaction is bimolecular in that one photon produces 3 molecules of nitrogen. The results of the X-radiolysis of sodium, lithium and barium azide in this thesis are in contradiction with Heal's mechanism

because the intensity dependence of the radiolytic rate clearly indicates a unimolecular decomposition of the azide ion. Furthermore, the absence of any photoconductivity during irradiation with X-rays excludes the formation of free electrons in the conduction band. Clearly electron trapping must occur, probably to form colour centres. This is supported by the deep colouration of the above azides after radiolysis.

Colour centre formation such as V-centre formation (positive hole associated with cation vacancy) should occur readily since the energy of the X-ray photon is energetic enough to form Frenkel[109] defects (interstitial ion plus ion vacancy) and since interstitial cations are more readily formed because of their smaller size, large numbers of cation vacancies must be produced. Thus a suggested low temperature radiolytic mechanism for the azides of sodium, lithium and barium could be as follows :-

$$N_3^- \rightleftharpoons^{h\nu} N_3^{-*}$$

$$N_3^{-*} + \boxminus \rightarrow N_3 + e\boxminus$$

$$N_3 + \boxplus \rightarrow N_3\boxplus$$

where N_3^{-*} = exciton

$\boxminus$ = anion vacancy

$\boxplus$ = cation vacancy

N_3 = positive hole

e = F-centre

N_3 = V-centre.

V-bands have been detected in X-irradiated KCl and NaCl at low temperatures. Repetition of the above process would provide adjacent trapped positive holes which could then decompose as follows :-

$$2N_3\boxplus \rightarrow 3N_2 + 2\boxplus$$

The overall reaction would then be

$$2N_3^- \xleftrightarrows{2h\nu} 3N_2 + 2\oplus + 2\ominus$$

Metal atoms could be formed as follows:-

$$M^{n+} + ne\ominus \longrightarrow M + n\ominus$$

Microscopic examination of the azide pellts during X-irradiation, using the Leitz microscope with the evacuable stage, showed no evidence of nuclei, indicating that metal colloid formation does not occur to any extent. Thus metal catalysis of the reaction would be absent. The absence of any acceleratory reaction during the radiolysis seems to confirm this.

The percentage decomposition of the azides under X-irradiation must be small, and the formation of radiolysis products must be diffuse, since no fall off in rate is observed even after very prolonged X-irradiation. This would exclude the growth and overlapping of reaction centres.

The high temperature mechanism proposed by Heal[57] for the radiolysis of sodium azide involves thermal decomposition of excitons trapped at lattice imperfections.

$$N_3^- + T \xleftrightarrows{h\nu} N_3^{-*}T$$

$$N_3^{-*}T \xrightarrow{kT} N_3 + T + e$$

$$N_3 + N_3^- \longrightarrow 3N_2 + e$$

where T = trap.

This is again a bimolecular decomposition of azide ion with the production of electrons in the conduction band. The above mechanism is again contrary to the findings of this work in that it involves a bimolecular reaction of azide ions and the production of free electrons, both of which have been shown to be absent.

From the evidence gathered in this thesis, the following high temperature mechanism is suggested for the radiolysis of sodium and

GENERAL DISCUSSION OF THE RESULTS OF THE PHOTOLYSIS AND RADIOLYSIS OF BARIUM AND LITHIUM AZIDE.

The re-investigation of the photolysis of barium azide undertaken in this work, gave results which were in conflict with those obtained by Pai Verneker[35] in a recent re-investigation of the photolysis of barium azide.

The shape of the pressure-time plots, the activation energies and the effect of filtering the ultraviolet irradiation, investigated in this thesis, differed considerably from the results obtained by previous workers (see page 59).

The differences in the results for the photolysis of barium azide in this work, when compared to the findings of previous workers, may be explained by the following factors:-

1. An exhaustive study was made of vacuum line systems, in order to obtain the most suitable system for carrying out this type of kinetic study.

2. Very sensitive pressure measuring devices were employed, including a new improved design of Pirani gauge (see experimental).

3. Very low pressures (10^{-7} torr) were attainable with careful design of the pumping systems of the vacuum line.

4. An intensive investigation of decomposition cells was undertaken, and the results show that the use of cements, greases, epoxies and waxes in the vicinity of the ultraviolet sources can lead to serious error in determining pressures, and this could account for the failure of other workers to detect the early acceleratory period for the photolysis of barium azide. Any spurious gas evolution from the above causes would easily obliterate this

unimolecular decomposition of an azide ion in the latter. Studies with superimposed radiations of ultraviolet, X-rays and γ -rays indicated that the reaction centres in the photolytic and radiolytic decompositions were not similar, with no enhancement of the reaction rate in either case when pre-irradiated with a different form of radiation.

BIBLIOGRAPHY.

1. Jacobs and Tompkins, Chemistry of the Solid State, Ed. Garner, Chap. 3 (Butterworths 1955).
2. Seitz, Modern Theory of Solids, Chap. 8 (McGraw Hill 1940).
3. Pohl, Proc. Phys. Soc. Lond., 49, 3 (1937).
4. De Boer, Electron and Emission Phenomena, Cambridge (1935).
5. Mollwo, Ann, Phys.Lpz., 29, 394 (1937).
6. King, Carlson, Miller, and McMillan, J.Chem.Phys., 34, 1499, (1961).
7. Cunningham and Tompkins, Proc. Roy. Soc., A 251, 27 (1959).
8. Pringle and Noakes, Acta Crystallogr., 24, 262 (1968).
9. Torkar, Spath, and Mayer, Monatsh. Chem., 98, 2362 (1968).
10. Carlson, King, Miller, J.Chem.Phys., 33, 1266 (1960).
11. Miller, J.Chem.Phys., 33, 889 (1960).
12. King, Miller, Carlson and McMillan, J.Chem.Phys., 35, 1442, (1961).
13. Mott, Proc.Roy.Soc., A, 172, 325 (1939).
14. Shuskus, Young, Gilliam, Levy, J.Chem.Phys., 33, 622 (1960).
15. Mitchell, Chemistry of the Solid State, Ed. Garner, Chap. 13, (Butterworths 1955).
16. Torkar, Krischner and Radl, Monatsh.Chem., 97, 313 (1966).
17. Luckey, J.Phys.Chem., 57, 791 (1953).
18. Tompkins, Ind.Eng.Chem., 44, 1336 (1952).
19. Pai Verneker and Maycock, J.Phys.Chem., 72, 2798 (1968).
20. Tompkins and Young, Discuss. Faraday Soc., 23, 202 (1957).
21. Maycock, Pai Verneker and Witten, J.Phys.Chem., 71, 2107 (1962).
22. Todd and Parry, Nature, 186, 543 (1960).
23. Dawood, Forty and Tubbs, Proc. Roy. Soc., 284, 282 (1965).

24. Krause, Z.Krist., 115, 413 (1961).

25. Kaldor and Somorjai, J.Phys.Chem., 70, 3538 (1966).

26. Lieber, U.S. Dept. Com. Office Tech. Serv., 156, 460 (1962).

27. Herley and Levy, J.Chem.Phys., 46, 627 (1967).

28. Thomas and Tompkins, Proc. Roy. Soc., A, 210, 111 (1951).

29. Thomas and Tompkins, J.Chem. Phys., 20, 662 (1952).

30. Jacobs and Tompkins, Proc. Roy. Soc., A, 215, 254 (1952).

31. Jacobs, Tompkins and Young, Discuss. Faraday Soc., 28, 234 (1959).

32. Jacobs, Tompkins and Pai Verneker, J.Phys.Chem., 66, 1113 (1962).

33. Jacobs, Sheppard and Tompkins, International Symp. of the Reactivity of Solids, R 5-45, 509 (1964).

34. Tompkins and Young, Discuss. Faraday Soc., 52, 202 (1957).

35. Pai Verneker, J.Phys. Chem., 72, 1733 (1968).

36. Leffler and Gibson, J.Amer.Chem.Soc., 90, 4117 (1968).

37. Saveliev, Gavrishenenko and Zakharov, Izv.Vyssh.Ucheb.Zaved. Fiz, 11, 71 (1968).

38. Brezina, Gelerinter, J.Chem.Phys., 49, 3293 (1968).

39. Courtney-Pratt and Rogers, Nature, 175, 632 (1955).

40. Rosenwasser, Dreyfus and Levy, J.Chem.Phys., 24, 184 (1956).

41. Marcontonio and Thekkekandam, J.Amer.Chem.Soc., 93, 1524 (1971).

42. Kelly and Smith, J.Chem. Soc., 55, 1479 (1961).

43. Marinkas and Bartram, J.Phys.Chem., 48, 927 (1968).

44. Bube, J.Phys.Chem., 57, 785 (1953).

45. Jacobs and Tariq Kureishy, J.Chem.Soc., 911, 4723 (1964).

46. Gelerinter and Silsbee, J.Chem.Phys., 45, 1703 (1966).

47. Deb, Trans. Faraday Soc., 65, 3187 (1969).

48. Pai Verneker and Blais, Mat.Res.Bull., 3, 127 (1968).

49. Deb, Trans. Faraday Soc., 59, 1414 (1963).

50. Deb, Trans. Faraday Soc., 59, 1423 (1963).

51. Deb, J.Chem.Phys., 35, 2122 (1961).

52. Smith, Leivo and Smoluchowski, R.Phys.Rev., 94, 1435 (1954)

53. Deb, J.Chem.Phys., 55, 3660 (1971).

54. Verwey, J.Phys.Chem. Solids, 31, 163 (1970).

55. Heal, Canadian J.Chem., 31, 1153 (1953).

56. Mergenian and Marshall, Phys.Rev., 127, 2015 (1962).

57. Heal, Trans. Faraday Soc., 53, 210 (1957).

58. Prout and Liddiard, J.Phys.Chem., 72, 2281 (1968).

59. King, Carlson, Miller, and McMillan, J.Chem.Phys., 34, 1499 (1961).

60. Jensen, Ann.Phys.Lpz., 34, 161 (1939).

61. Seitz, Rev.Mod.Phys., 23, 328 (1951).

62. Pai Verneker, Inorg.Nucl.Chem.Lett., 4, 327 (1968).

63. Torkar and Spath, Mn.Chem., 98, 1696 - 1712 (1967).

64. Walitzi and Krischner, Z.Kristallogr., 129, 153 (1969).

65. Pai Verneker and Avrami, J.Phys.Chem., 72, 778 (1968).

66. Pai Verneker, J.Phys. Chem., 72, 774 (1968).

67. Shinohara, Shida, and Saito, J.Chem.Phys., 37, 2791 (1962).

68. Krause, J.Chem.Phys., 39, 1706 (1963).

69. Carlson, J.Chem.Phys., 39, 1206 (1963).

70. Bryant, J.Chem.Phys., 42, 2270 (1965).

71. Pai Verneker and Blais, J.Phys.Chem., 72, 774 (1968).

72. Brooks, Mater. Res.Bull., 3, 389 (1968).

73. Zakharov, Ryabykh, and Lysykh, Kinet.Katal., 9, 679 (1968).

74. Ryabykh, Lysykh, and Zakharov, Khim.Vys.Energ., 2, 344 (1968).

75. L'Abbe, Ind.Chim.Belge, 33, 4051 (1968).

76. Treinin and Hayon, J.Chem.Phys., 50, 538 (1969).

77. Choi and Boutin, Acta Crystallogr., 25, 982 (1969).

78. Bonnemay, J.Chim.Phys., 40, 231 (1943).

79. Lister, U.S.Dept. Com. Office Tech Serv., P.B. Rept. 156, 460 (1962).

80. Mergerian and Marshall, Phys. Rev., 127, 2015 (1962).

81. Shida, Rika Gaku Kenkyusho Hokoku, 39, 385 (1963).

82. Burak and Treinin, J.Am.Chem.Soc., 87, 4031 (1965).

83. Ganilin and Dimova, Izv. Tomsk. Politekh. Inst., 162, 194 (1967).

84. Evans and Mitchell, Rep. on Bristol Conf. on Defects in Crystal Solids, Phys. Soc., London (1955).

85. Seitz, Solid State Physics, 2, 307 (1956).

86. Mitchell, J.Phot.Sci., 5, 49 (1957).

87. Bach and Bonhoeffer, Z.Physik.Chem., B23, 256 (1933).

88. Muller and Brons, J.Chem.Phys., 1, 482 (1933).

89. Andubert and Muraour, Compt.rend., 204, 431 (1937).

90. Mott and Gurney, Electronic Processes in Ionic Crystals, (Clarendon Press 1950).

91. Testa and Robinson, J.Chem.Phys., 55, 3056 (1971).

92. Dixon, Jenkins, and Waddington, Chem.Phys.Lett., 10, 600 (1971).

93. Iqbal, Garrett, Brown, and Mitra, J.Chem.Phys., 55, 4528 (1971).

94. Owens, J.Phys.Chem.Solids, 32, 2646 (1971).

95. Rao, Trevino, Prask,and Mical, Phys.Rev., B4, 4551 (1971).

96. Eggert, Proc. Roy. Soc., A 246, 216 (1958).

97. Boldyrev and Medvinskii, Kinet. i Katal., 6, 550 (1965).

98. Garner and Maggs, Proc. Roy. Soc. , A 172, 299 (1939).

99. Wischin, Proc. Roy. Soc. A 172, 314 (1939).

100. Gray, Quart.Rev.Chem.Soc., 17, 441 (1963).

101. Yoffe, "Developments in Inorganic Nitrogen Chemistry", C.B.

Colburn, Ed. Elsevier, New York, N.Y. (1966).

102. Krasner and Keating, PB Rept. 135 093 45 pp. from U.S.Govt. Research Repts., 31, 173 (1959).

103. Keating and Krasner, J.Phys.Chem.Solids, 20, 150 (1961).

104. Tompkins and Young, Trans. Faraday Soc., 61, 1470 (1965).

105. Pai Verneker and Maycock, J.Inorg. and Nucl. Chem., 29, 2723 (1967).

106. Prout and Moore, Nature, 203, 860 (1964).

107. Avrami, J.Chem.Phys., 7, 1103 (1939) : 8, 212 (1940) : 9, 177 (1941).

108. Erofevev, Acad.Sci. U.R.S.S., 52, 511 (1946).

109. Frenkel, Z.Phys., 35, 652 (1926).

110. Boldyrev, Eroshkin and Zakharov, Nauk. Dokl.Vysshikh. Shkolei, 3, (1959).